

Klinik und Poliklinik für Viszeral-, Thorax- und Gefäßchirurgie
Direktor: Prof. Dr. med. Jürgen Weitz

Analysis and modelling of gastric cancer subtypes by the use of patient derived and murine organoids as well as a stomach specific mouse model.

D i s s e r t a t i o n s s c h r i f t
zur Erlangung des akademischen Grades

Doctor rerum medicinalium
(Dr. rer. medic.)

vorgelegt
der Medizinischen Fakultät Carl Gustav Carus
der Technischen Universität Dresden

von

Therese Seidlitz M. Sc.

geboren am 27.10.1989
in Lauchhammer

Dresden 2020

1. Gutachter:

2. Gutachter:

Tag der mündlichen Verteidigung:

gez.: _____
Vorsitzender der Promotionskommission

Anmerkung:

Die Eintragung der Gutachter und Tag der mündlichen Prüfung (Verteidigung) erfolgt nach Festlegung von Seiten der Medizinischen Fakultät Carl Gustav Carus der TU Dresden. Sie wird durch die Promovenden nach der Verteidigung zwecks Übergabe der fünf Pflichtexemplare an die Zweigbibliothek Medizin in gedruckter Form oder handschriftlich vorgenommen.

List of content

Abbreviations	IV
Gene and protein notations	VII
1. Introduction	1
1.1. The stomach - an organ important for temporary food storage and digestion	1
1.1.1. Function and architecture	1
1.1.2. Stomach stem cells and their regulating role in homeostasis.....	3
1.2. Gastric cancer	4
1.2.1. Incidence and mortality	4
1.2.2. Tumor staging	4
1.2.3. Classification of gastric cancer based on histology or molecular rearrangements	5
1.2.4. Risk factors and pathogenesis	8
1.2.5. Treatment options for gastric cancer patients	9
1.3. Organoids - an <i>in vitro</i> model of mammalian development and disease	10
1.3.1. What are organoids?	10
1.3.2. History of organoid development	10
1.3.3. Organoid culture system in other tissues.....	11
1.3.4. Application of organoid technology.....	14
2. Aim of the study.....	16
3. Material and Methods	17
3.1. Material	17
3.1.1. Devices	17
3.1.2. Additional material and equipment	19
3.1.3. Fine chemicals	20
3.1.4. Biochemicals.....	22
3.1.5. Primary antibodies	23
3.1.6. Secondary antibodies.....	24
3.1.7. Nucleic acids.....	24

3.2.	Methods	26
3.2.1.	Cell culture	26
3.2.2.	Functional assays for analyzing proliferation and apoptosis	31
3.2.3.	Biochemical analysis	33
3.2.4.	DNA and RNA techniques	36
3.2.5.	Histology	40
3.2.6.	<i>In vivo</i> experiments	42
3.2.7.	Statistical analysis and graphical presentation	44
4.	Results	45
4.1.	Establishment and characterization of a human gastric cancer organoid biobank ..	45
4.1.1.	Human gastric cancer organoids with different phenotypes, proliferation rates and typical cancer characteristics	45
4.1.2.	Gastric cancer organoids show divergent response to cancer treatment	49
4.1.3.	Targeted therapy in gastric cancer organoids	51
4.2.	Mouse organoids allow cancer subtype modelling with a defined mutational spectrum	56
4.2.1.	Generation of mouse gastric tumor organoids	56
4.2.2.	Characterization of mouse gastric tumor organoids concerning morphology, pathway activity and treatment response	60
4.3.	Gastric cancer subtypes show different patterns of development, growth and dissemination in a gastric cancer mouse models	63
4.3.1.	Generation of a stomach specific mouse model	63
4.3.2.	Definition of characteristic gastric cancer subtype related alterations	65
4.3.3.	CIN subtype alterations in RTK/RAS, TP53 and TGF- β pathway led to the intestinal CIN model of gastric cancer	65
4.3.4.	GS subtype typical alterations in cell adhesion, RTK/RAS and TGF- β pathways result in poorly differentiated signet ring cell carcinoma	68
4.3.5.	Serrated adenomatous gastric cancer model characterized by tooth-like adenomatous tumor morphology	70
4.3.6.	Gastric cancer models showed a divergent drug response to classical chemotherapy and targeted therapy	72

5. Discussion.....	74
5.1. Patient derived cancer organoids - a model system allowing analysis of drug response and personalized cancer treatment.....	74
5.2. Gastric cancer subtype modelling using organoids with a defined genetic makeup	77
5.3. The stomach specific mouse line Anxa10-CreER ^{T2} represents a prime tool for gastric cancer research	78
Zusammenfassung	82
Summary	84
List of Figures.....	86
List of Tables.....	87
References.....	88
Acknowledgement	Fehler! Textmarke nicht definiert.
Appendix	107

Abbreviations

2D	two-dimensional
3D	three-dimensional
5-FU	5-fluoruracil
AEG	adenocarcinoma of esophagogastric junction
ATCC	American Type Culture Collection
BioGPS	Bio Gene Portal System
BSA	bovine serum albumin
bp	base pairs
CaCl ₂	calcium chloride
cDNA	complementary DNA
CIN	chromosomal instability
CuSO ₄	copper sulfate
CRISPR	clustered regularly interspaced short palindromic repeats
CT	computer tomography
dNTP	deoxynucleotide triphosphate
D-PBS	Dulbecco's phosphate buffered saline
dH ₂ O	distilled water
DMEM	Dulbecco's modified eagle medium
DNA	deoxyribonucleic acid
DMSO	dimethyl sulfoxide
EBV	Epstein-Barr virus
ECM	extracellular matrix
EDTA	ethylenediaminetetraacetic acid
EdU	5-ethynyl-2'-deoxyuridine
ER ^{T2}	tamoxifen-inducible estrogen receptor
ESC	embryonic stem cell
F12	Nutrient mixture F-12
FACS	fluorescence activated cell sorting
FAP	familial adenomatous polyposis
FCS	fetal calf serum
FITC	fluorescein isothiocyanate
FSC	forward scatter
GEO	Gene Expression Omnibus
GFP	green fluorescent protein
GOI	gene of interest

GS	genomically stable
GSK3	glycogen synthase kinase 3
GXD	Gene Expression Database
H ₂ O ₂	hydrogen peroxide
HCl	hydrochloric acid
HEPES	4-(2-hydroxyethyl)-1-piperazineethanesulfonic acid
HDGC	hereditary diffuse gastric cancer
HE	hematoxylin eosin
HGF	hepatocyte growth factor
HRP	horseradish peroxidase
IHC	immunohistochemistry
IMDM	Iscove's Modified Dulbecco's Media
i.e.	in example
i.p.	intraperitoneal
iPSC	induced pluripotent stem cell
KH ₂ PO ₄	monopotassium phosphate
KCl	potassium chloride
LN	lymph nodes
MgCl ₂	magnesium chloride
MSI	microsatellite instability
NCT MASTER	National Center for Tumor Diseases Molecularly Aided Stratification for Tumor Eradication
Na ₂ HPO ₄	disodium hydrogen phosphate
NaCl	sodium chloride
ON	over night
OS	overall survival
PAS	Periodic acid Schiff's reaction
PCR	polymerase chain reaction
PI	propidium iodide
p.i.	post induction
PS	phosphatidylserine
qRT-PCR	quantitative Real-Time PCR
RIPA	radioimmunoprecipitation assay
RPMI	Roswell Park Memorial Institute
RNA	ribonucleic acid
Rosa26	reverse oriented splice acceptor, clone 26
RT	reverse transcriptase

RTK	receptor tyrosine kinases
SDS	sodium dodecyl sulfate polyacrylamide gel electrophoresis
s.c.	subcutaneous
SCNA	somatic-copy number aberrations
SSC	sideward scatter
TAE	Tris acetate EDTA
TBS-T	Tris-buffered saline with tween 20
TCGA	The Cancer Genome Atlas
TNM	tumor node metastasis
Tris	tris (hydroxymethyl) aminomethane
UICC	Union for International Cancer Control
VUS	variant of unknown significance
WHO	World Health Organization

Gene and protein notations

In this work the official nomenclature for human and murine genes as well as proteins was used according to the Human Gene Nomenclature Committee. Human gene names are written in italic capital letters (i.e. *CDH1*). Mouse gene names are written in italic small letters. Only the first letter is large (i.e. *Cdh1*). Protein names of human and murine samples are written in non-italicized capital letters. To simplify gene and protein abbreviations in the list below the human nomenclature was used.

<i>ANXA10</i>	<i>annexin 10</i>
AKT	protein kinase B
<i>APC</i>	<i>Adenomatous polyposis coli</i>
<i>ARID1A</i>	<i>AT-rich interactive domain-containing protein 1A</i>
<i>ATP4B</i>	ATPase H ⁺ /K ⁺ transporting subunit beta
<i>BHLHA15, MIST1</i>	<i>basic helix-loop helix family member a15</i>
BMP	bone morphogenetic protein
<i>CADH17</i>	<i>cadherin 17</i>
CAPN8	calpain 8
CEA	carcinoembryonal antigen
<i>CCND1</i>	<i>cyclin D1</i>
<i>CDH1</i>	<i>cadherin 1</i>
CDK4/6	cyclin-dependent kinase 4/6
<i>CDKN2A</i>	<i>cyclin-dependent kinase inhibitor 2A</i>
CK7	cytokeratin 7
CK20	cytokeratin 20
<i>CTNNB1</i>	<i>β-catenin</i>
EGFR	epidermal growth factor receptor
<i>ERBB2</i>	<i>Erb-B2 receptor tyrosine kinase 2</i>
ERK1/2	extracellular-signal regulated kinase 1/2
FGFR	fibroblast growth factor receptor
<i>GAPDH</i>	<i>glyceraldehyde 3-phosphate dehydrogenase</i>
HER2/neu	human epidermal growth factor receptor
HGFR	hepatocyte growth factor receptor
<i>KRAS</i>	<i>Ki-ras2 Kirsten rat sarcoma viral oncogene homolog</i>
Krt19	keratin 19
LGR5	leucine-rich repeat-containing G-protein coupled receptor 5 positive

<i>LRIG</i>	<i>leucine-rich repeats and immunoglobulin-like domains protein 1</i>
MAPK	mitogen-activated protein kinase
MLH1	MutL homolog 1
<i>PIK3CA</i>	<i>phosphatidylinositol-4, 5-bisphosphate 3-kinase catalytic subunit alpha</i>
<i>PGC</i>	<i>progastricisin/ pepsinogen C</i>
PI3K	phosphoinositide 3-kinase
<i>PTEN</i>	<i>phosphatase and tensin homolog</i>
RAS	rat sarcoma
<i>RHOA</i>	<i>ras homolog family member A</i>
ROCK	Rho-associated, coiled-coil containing protein kinase
SOX2	<i>SRY (sex determining region Y)-box 2</i>
<i>STAT3</i>	<i>Signal transducer and activator of transcription 3</i>
TCF	T cell factor
TFF1	trefoil factor 1
TFF2	trefoil factor 2
TGF- β	transforming growth factor beta
<i>TNFRSF19, TROY</i>	<i>tumor necrosis factor receptor superfamily member 19</i>
<i>TP53</i>	<i>tumor protein 53</i>
VEGFR	vascular endothelial growth factor receptor

1. Introduction

1.1. The stomach - an organ important for temporary food storage and digestion

1.1.1. Function and architecture

The stomach is a muscular organ lying between the esophagus and intestine in the upper abdomen. With its characteristically curved portion it is present in all vertebrates that require food storage and enzymatic digestion in an acidic environment. The stomach is in permanent contact to nutrients, metabolites and resident bacteria, all of which compose a toxic microenvironment for the epithelium (Koelz, 1992). To ensure an intact and functional mucosal lining despite the constant damage a continuous self-renewal of the epithelium is required. The organ originates from the foregut endoderm and organizes itself during development. All three embryonic germ-layers including ectodermally derived nerves, mesodermally derived smooth muscle with mesenchymal cells and the endodermally derived epithelium are necessary for the stomach formation (Lawson et al., 1986; Tam and Beddington, 1987; Kwon et al., 2008).

The human stomach is divided into cardia, fundus, corpus (body) and antrum (pylorus) (Karam, 1999). The cardia connects to the esophagus and is the part where the food firstly enters the stomach. The fundus constitutes the upper part of the stomach, and shows substantial size and functional variations between different species. The corpus is the main part of the stomach secreting acid and digestive enzymes. The antrum secretes mucus and hormones. This part delivers the food to the intestine. The mouse adult stomach contains additionally a squamous-epithelium lined forestomach for storage and mechanical dissociation of food (Figure 1A, B) (Roman and Shivdasani, 2011; Kim and Shivdasani, 2016; Willet and Mills, 2016). The inner lining of the stomach is called Tunica mucosa, which consists of an epithelial lining, a connective tissue called Lamina propria and the Muscularis mucosae. Connective tissue called Tunica submucosa connects the Tunica mucosa with the outer smooth muscle layer Tunica muscularis propria. A thin layer called Tunica serosa forms the outer layer towards the abdominal cavity.

The stomach mucosa is composed of a single layer of epithelial cells organized into invaginating units called glands. They are divided in general into four regions from surface to bottom: pit, isthmus, neck and base. Stomach glands show substantial differences between different stomach parts. The corpus has short pits and long glands with pit and neck mucus cells, acid secreting parietal cells, hormone producing endocrine cells and Pepsinogen C (PGC) secreting chief cells (Karam and Leblond, 1992). In contrast, antral glands are shorter and consist only of pit and neck mucus cells, endocrine cells and a few basally located chief

cells (Lee et al., 1982) (Figure 1C). Unique to the antral gland are the gastrin-producing cells (Choi et al., 2014). The isthmus region shows a high cellular turnover and is proposed to be the location of (potentially quiescent) stem cells and their proliferating daughter cells (transit amplifying cells). Proliferating cells of the isthmus region bi-directly migrate to the top and the bottom of the gland (Bjerknes and Cheng, 2002). Mucus neck cells are found in the neck region, while chief cells are located at the base. Endocrine and parietal cells scatter throughout the whole gland (Figure 1C) (Karam and Leblond, 1993b; Karam and Leblond, 1993c; Karam and Leblond, 1993d; Karam and Leblond, 1993a).

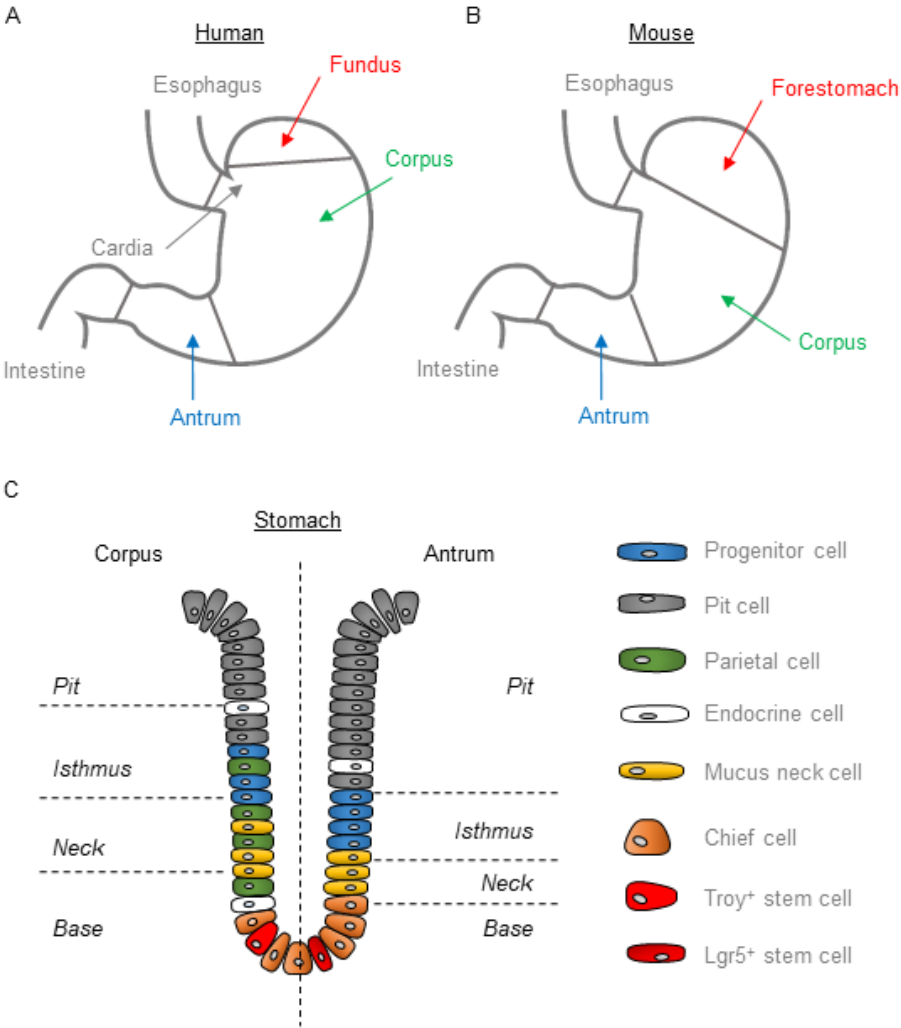


Figure 1: Morphology of the stomach and gland organization. (A) The adult human stomach is divided into cardia, fundus, corpus (body) and antrum (pylorus) (B) whereas the mouse stomach in addition exhibits a squamous-epithelium lined forestomach. (C) The adult gland consists of four regions: pit, isthmus, neck and base which differ in cell composition and localization between the corpus and antrum.

1.1.2. Stomach stem cells and their regulating role in homeostasis

Lifelong self-renewal of the stomach depends on the presence of stem cells. The intestinal stem cell marker leucine-rich repeat-containing G-protein coupled receptor 5 (LGR5) is found at the bottom of antral glands and these cells can differentiate to all other cells of the gastric antrum (Barker et al., 2010; Kim and Shivdasani, 2016) (Figure 1C). Notch signaling controls gastric epithelial homeostasis by regulating the stem cells in the antral gland. Therefore, signaling from the Notch receptor promotes overall stem cell proliferation in Lgr5⁺ stem cells (Demitrack et al., 2015). Interaction of Rspodin with the LGR5 receptor and Frizzled complex leads to activation of the WNT pathway resulting in proliferation, survival and self-renewal (de Lau et al., 2011; Schepers and Clevers, 2012).

Radiolabeling and electron microscopy suggest an undifferentiated 'granule free' cell as the undifferentiated stem cell in the corpus region of the stomach (Karam and Leblond, 1993a; Mills and Shivdasani, 2011). SRY (sex determining region Y)-box 2 (SOX2) positive cells have been proposed to constitute long-lived stem cells, whereas trefoil factor 2 (TFF2) positive cells are short-lived progenitors (Quante et al., 2010; Arnold et al., 2011). A recently published study describes that a subset of chief cells express the tumor necrosis factor receptor superfamily member 19 (TNFRSF19 or TROY) located at the gland base (Figure 1C). These cells are postulated to constitute a reserve stem cell population due to their slowly cycling nature but at the same time ability to differentiate into all cells of the corpus gland (Stange et al., 2013). A further quiescent stem cell is proposed to reside in the corpus in mature chief cells at the lower third of glands in the isthmus region. These cells are marked by the expression of the basic helix-loop helix family member a15 (BHLHA15 or MIST1) gene. Mist1⁺ stem cells give with a slow proliferation rate rise to all stomach epithelial lineages (Hayakawa et al., 2015). The Troy⁺ as well as the Mist1⁺ stem cells are both located exclusively in the corpus region and not in the antrum (Stange et al., 2013; Hayakawa et al., 2015).

The true nature of these cell populations are still under debate. Furthermore, no data is currently available that unravels the interaction between the proposed stem cell populations. Nevertheless, also not genetically unquestionably proven for the stomach, stem cells of the stomach are likely to be the origin of gastric cancer through aberrant self-renewal activity and further additional mutations in cell signaling pathways. At least for the intestine, the Lgr5⁺ stem cell population has been proven to constitute at least one of the origins of intestinal cancer (Barker et al., 2009; Schepers et al., 2012).

1.2. Gastric cancer

1.2.1. Incidence and mortality

Gastric cancer ranks the fifth most common malignancy after cancers of the lung, breast, colorectum and prostate. Incidence rates change since 1975 in which gastric cancer was the most prevalent neoplasm of the world (Parkin et al., 1988). Nevertheless, the disease remains the second leading cause of cancer related deaths worldwide (Global Burden of Disease Cancer Collaboration, 2015). In 2012 951 000 new cases of stomach cancer with 400 000 deaths per year are observed. Seventy percent (677 000) occurs in developing countries and most gastric cancer patients come from Eastern Asia. The highest mortality rates due to gastric cancer are found in Eastern Asia followed by Central and Eastern Europe as well as Central and Southern America. The lowest rate is found in Northern America. The incidence for gastric cancer is twofold-higher in men compared to women (Ferlay et al., 2015). Contrary to the overall trend, adenocarcinomas of the esophagogastric junction (AEG) constitute an entity with rising incidence rates and histological overlap with gastric cancer (McColl and Going, 2010; Arnold et al., 2015). The incidence for AEGs amounts to 52 000 patients per year worldwide. Most of the cases occur in Northern and Western Europe as well as Northern America and Oceania. The lowest rates are found in Eastern and South Eastern Asia. Similar to gastric cancer incidence for men is 4.4 fold higher to get AEG compared to women (Arnold et al., 2015).

1.2.2. Tumor staging

The Union for International Cancer Control (UICC) has developed a gastric cancer staging system according to the tumor node metastasis (TNM) classification consisting of five study groups (Figure 2). This staging system is either based on pathological findings (pTNM) or on imaging studies (cTNM). The cTNM classification plays an important role for the cancer treatment strategy. Within the TNM classification tumors are classified on the basis of three categories: primary tumor (T), regional lymph node metastases (N) and metastases at distant organs (M). The T status describes the invasion of tumor cells into the different tissue layers. In the stomach, these are: invasion into the Tunica mucosa/submucosa (T1), Tunica muscularis propria (T2), Tela subserosa (T3) and Tunica serosa (T4a) or adjacent structures (T4b). The N status is based on the number of regional lymph node metastases. The combination of T and N allows the classification in stages from I to III. In case of distant metastases patients are grouped in stage IV (Union for International Cancer Control, 1982; Union for International Cancer Control, 2017).

			M0					M1
Involved LN			<i>N0</i>	<i>N1</i>	<i>N2</i>	<i>N3a</i>	<i>N3b</i>	
			0	1-2	3-6	7-15	≥16	
M0	<i>T1</i>	Tunica mucosa, submucosa	IA	IB	IIA	IIB	IIB	IV
	<i>T2</i>	Tunica muscularis propria	IB	IIA	IIB	IIIA	IIIA	
	<i>T3</i>	Tela subserosa	IIA	IIB	IIIA	IIIB	IIIB	
	<i>T4a</i>	Tunica serosa	IIB	IIIA	IIIB	IIIC	IIIC	
	<i>T4b</i>	Adjacent structure	IIIB	IIIB	IIIC	IIIC	IIIC	
M1			IV	IV	IV	IV	IV	IV

Figure 2: TNM classification of gastric cancer. The staging system allows patient classification according to the primary tumor invasion (T), appearance of regional lymph node metastases (N) as well as distant metastases (M) (modified according to (Union for International Cancer Control, 1982; Union for International Cancer Control, 2017).

1.2.3. Classification of gastric cancer based on histology or molecular rearrangements

1.2.3.1. Histological classification according to Lauren or the WHO

The most common histologic classification of gastric cancer is based on the Lauren criteria. Lauren differentiates the intestinal, the diffuse and the indeterminate type (Lauren, 1965). More than 50 % of gastric carcinoma follow the intestinal type, 35 % diffuse and 15 % the indeterminate type (Polkowski et al., 1999). The intestinal type has a well differentiated architecture with a tendency to preferentially develop liver metastases whereas the diffuse type shows an undifferentiated mass of tumor cells preferentially metastasizing to the peritoneum.

The World Health Organization (WHO) proposes a classification of stomach cancer into four different histological subtypes: tubular, papillary, mucinous, poorly cohesive and uncommon histologic variants in 2010 (Bosman et al., 2010). The classification is based on the predominant histology within the carcinoma. The tubular adenocarcinoma shows irregular fused or branching tubules of various size with intraluminal mucus and inflammatory debris. Papillary adenocarcinoma are rare and more often found in older people with high prevalence for liver metastases and lymph node involvement. The carcinoma showing a central fibrovascular core. Mucinous adenocarcinoma represents 10 % of gastric cancer and contains a mucus amount greater than 50 % of the tumor volume. The tumor cells have a glandular form with irregular cell clusters. Throughout these clusters infiltration with signet ring cells is found. Signet ring cells contain large vacuoles and a nucleus, which is squeezed to the periphery due to the large amounts of mucus. The poorly cohesive adenocarcinoma is composed of a mixture of signet ring cells and non-signet ring cells (Hu et al., 2012). Papillary, tubular and mucinous adenocarcinoma overlap with the intestinal type according to the Lauren classification, whereas the poorly cohesive carcinoma follow the diffuse type morphology.

1.2.3.2. Molecular classification with deregulated stomach pathways

The Cancer Genome Atlas (TCGA) consortium has developed a robust molecular classification system for gastric adenocarcinomas based on the mutational signature. The consortium identifies deregulated pathways and candidate driver genes to optimize cancer treatment. Here, 295 patients with gastric cancer non-pretreated with radio- and/ or chemotherapy are analyzed. Samples are characterized and compared to healthy tissue using six different molecular platforms: array-based somatic copy number analysis, whole genome sequencing, array-based deoxyribonucleic acid (DNA) methylation profiling, messenger ribonucleic acid (RNA) sequencing, microRNA sequencing and reverse-phase protein assay. Four molecular subgroups of gastric cancer has been identified. The first group of tumors is significantly enriched for Epstein-Barr virus (EBV) infection and further named EBV-positive subtype. The second type shows a high frequency for microsatellite instability (MSI) representing the MSI subtype. The last two subgroups can be distinguished by the presence or absence of somatic-copy number aberrations (SCNA) and are termed genomically stable (GS) or chromosomal instability (CIN) subtype. From 295 patient samples 26 (9 %) belong to the EBV subtype and 64 samples (22 %) are MSI high. Fifty-eight cases (20 %) are classified as GS subtype and 147 (50 %) can be grouped into the CIN type (Figure 3).

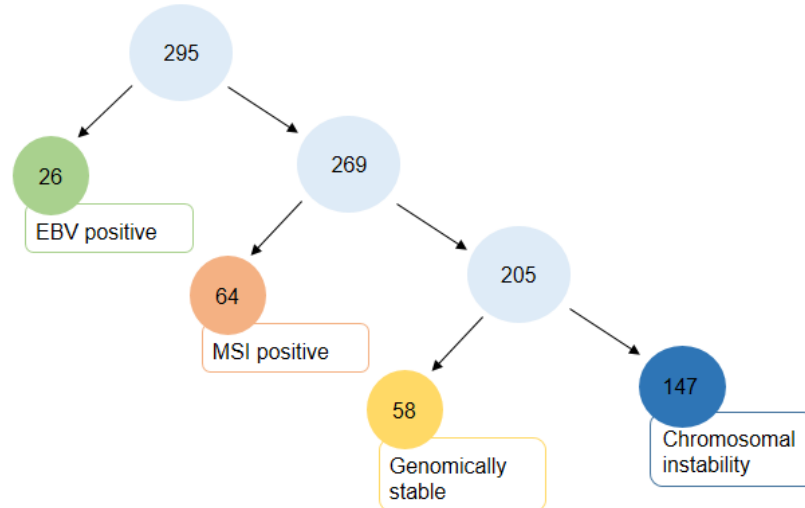


Figure 3: Flowchart of molecular classification of gastric adenocarcinoma into four subtypes. Classification into EBV positive (EBV), MSI high (MSI), genomically stable (GS) and chromosomal instability (CIN) subtype (modified according to The Cancer Genome Atlas Research Network 2014).

EBV positive gastric adenocarcinoma represent an enriched EBV burden. This subtype is often found in Asia and very rare in the western population. The EBV subtype represents a strong hypermethylation at DNA promoters especially of the tumor suppressor gene *cyclin-dependent kinase inhibitor 2A (CDKN2A)* with an accompanied silencing. No hypermethylation is observed at the MutL homolog 1 (MLH1) promotor. On top of that, EBV

positive tumors have a high rate of *phosphatidylinositol-4,5 bisphosphate 3-kinase catalytic subunit alpha (PIK3CA)* and *AT-rich interactive domain-containing protein 1A (ARID1A)* mutations. CIN tumors are frequently located at the gastric esophageal junction/ cardia and follow an intestinal histology with high SCNA. They often carry mutations in the *tumor protein 53 (TP53)* and genomic amplifications of receptor tyrosine kinases (RTK). The latter offer treatment possibilities using modern small molecules such as trametinib, cetuximab, imatinib and sorafenib. In contrast to the CIN subtype the GS tumors seldom show SCNA. They regularly present with a diffuse histology due to the loss of *cadherin 1 (CDH1)*. Further frequent mutations are found in the *ras homolog family member A (RHOA)* as well as *ARID1A*. GS tumors can be found throughout the whole stomach. Furthermore, patients are often diagnosed at an earlier age whereas MSI high patients are older at age of diagnosis. MSI positive patients tend to be female and tumors are found in the whole stomach. They show not only a high rate of MSI but also a hypermethylation of the *MLH1* promoter (The Cancer Genome Atlas Research Network, 2014). Important features of each subtype are shown in Figure 4.

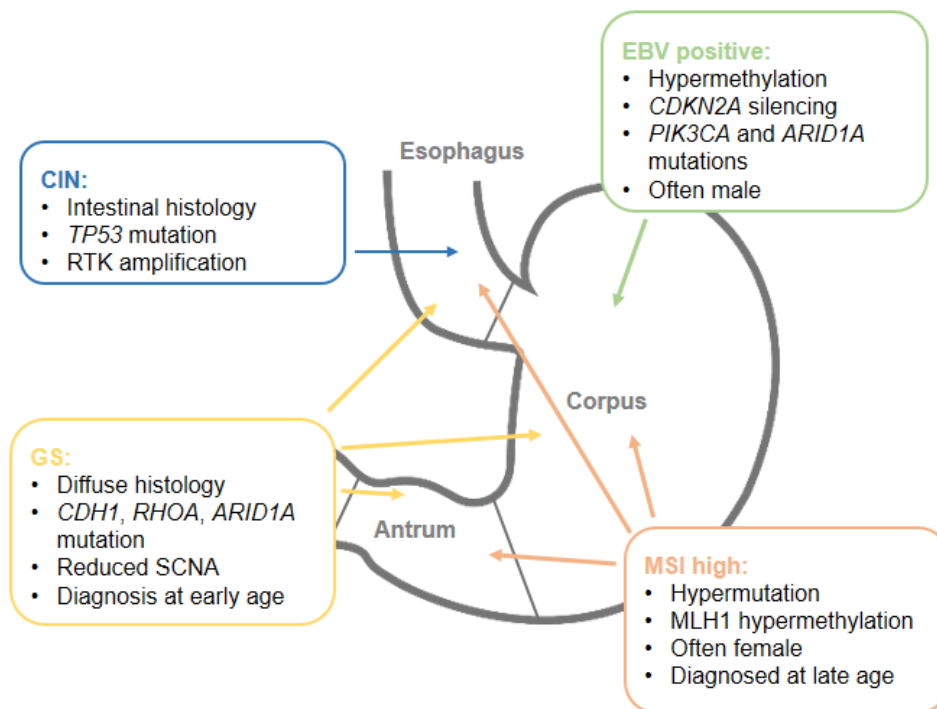


Figure 4: Key features of gastric cancer subtype. The boxes list the most important features of the four molecular subtypes. Color arrows representing the most frequent location of subtype tumors (modified after The Cancer Genome Atlas Research Network 2014).

1.2.4. Risk factors and pathogenesis

In general cancer develops through the occurrence of mutations leading to abnormalities like genomic instability, replicative immortality and apoptotic resistance. Additionally, metastases/invasion, angiogenesis and tumor supporting inflammation play an important role. A deregulation of the metabolism, immune system and inhibition of growth suppressors are also known tumor characteristics (Hanahan and Weinberg, 2000; Hanahan and Weinberg, 2011). However, for gastric cancer tumorigenesis not only genetic dispositions are necessary but also environmental factors. Risk factors are on the one hand infections with *Helicobacter pylori* (*H. pylori*) but on the other hand also high alcohol consume and smoking (Lochhead and El-Omar, 2008). Additionally, the obesity inducing general unhealthy lifestyle in well-developed industrial countries and the salted, nitrate containing food in the Asian population support the cancer development. Approximately 10-15 % arise in people who have a familiar predisposition like familial adenomatous polyposis (FAP), hereditary non-polyposis colon cancer as well as hereditary diffuse gastric cancer (HDGC). HDGC is often associated with mutations in *CDH1*, a high aggressiveness and a young age at diagnosis (Barber et al., 2006).

Intestinal gastric cancer develops through a multistep process involving gastritis, atrophy, intestinal metaplasia, dysplasia and gastric cancer (Figure 5). This long-term process depends not only on environmental factors but is also characterized by specific molecular events (Uemura et al., 2001). Chronic gastritis frequently develops in the setting of a *H. pylori* infection. *H. pylori* is recognized as a class I carcinogen for gastric cancer by the WHO. More than 50 % of world's population is infected with 1-2 % developing gastric cancer from chronic gastritis during their lifetime (Peleteiro et al., 2014). Additional factors need to be involved in the pathogenesis of intestinal cancer. Within the cancer progression gastric atrophy leads to the loss of chief and parietal cells from the antrum to the corpus (Satoki et al., 2015). Metaplasia is defined as a loss of normal stomach glandular structure and the epithelial replacement by intestinal differentiated goblet and mucin producing cells (Leushacke et al., 2013; Kinoshita et al., 2017). These alterations in the pathogenesis of gastric cancer lead to inflammation and genetic instability (Figure 5). The diffuse type of gastric cancer is thought to develop through independent mechanisms, specifically through the appearance of a number of mutations especially in genes with invasive properties.

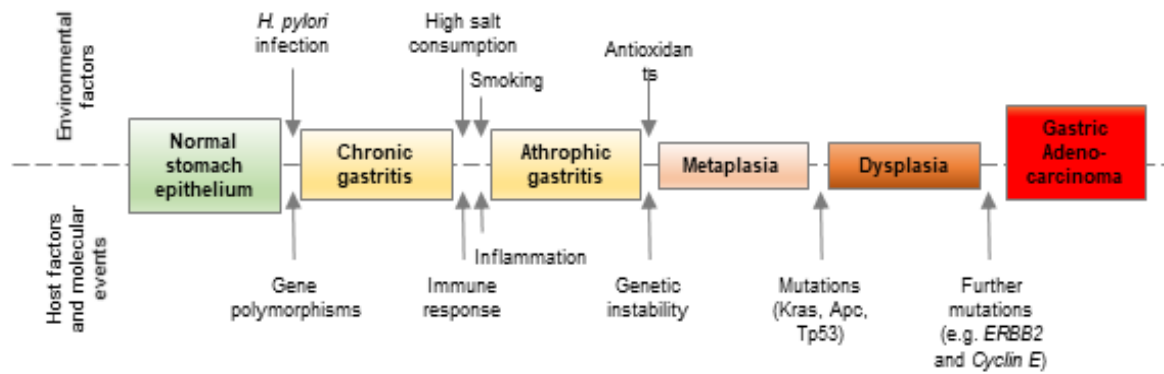


Figure 5: Pathogenesis of intestinal type gastric cancer. An overview of environmental factors as well as host factors and molecular events which lead to the development of intestinal gastric cancer (modified according to Tan and Yeoh 2015).

1.2.5. Treatment options for gastric cancer patients

Frequently the lack of clinical signs lead to a delayed diagnosis with three quarters of patients presenting with a non-curable advanced disease due to distant metastases (Hunt et al., 2015). In non-metastasized patients, surgery is the only curative option. Nevertheless, recent improvements in survival rates has been achieved through modern multimodal therapy approaches including neo-adjuvant and adjuvant chemotherapy (Cunningham et al., 2006; Ychou et al., 2011). The most commonly used chemotherapeutic drugs for gastric cancer are fluoropyrimidines (i.e. 5-fluoruracil (5-FU), capecitabine, S-1), platinum compounds (i.e. cisplatin, oxaliplatin), docetaxel and epirubicin (Cunningham et al., 2006; Ychou et al., 2011; Al-Batran et al., 2016). But not all patients show a tumor regression after chemotherapeutic treatment due to a resistance towards the cytotoxic agents. Therefore, genetic alterations found through whole genome sequencing represent new molecular targets for novel treatment options. At the moment the only approved targeted therapies are trastuzumab, a monoclonal antibody inhibiting the human epidermal growth factor receptor-2 (HER2/neu) and the anti-vascular endothelial growth factor receptor (VEGFR) antibody ramucirumab (Bang et al., 2010; Fuchs et al., 2014). HER2/neu is an oncogene encoded by the *Erb-B2 receptor tyrosine kinase 2 (ERBB2)* gene on chromosome 17 and often altered in patients with intestinal type of gastric cancer (Asioli et al., 2012). The efficacy of trastuzumab in gastric cancer patients is demonstrated in the ToGA study. In this randomized phase III trial 5-FU or capecitabine is administered with and without trastuzumab. Combining trastuzumab with chemotherapy lead to an increased overall survival (OS) (Bang et al., 2010). Angiogenesis is crucial for tumor growth and especially VEGF is overexpressed in 40 % of gastric cancer patients and correlates with aggressive and advanced disease (Vidal et al., 2009). Ramucirumab is a human IgG1 monoclonal antibody against VEGFR2. In the phase III trial

REGARD the antibody significantly improves OS with good tolerability in the patients (Fuchs et al., 2014). Other targeted therapeutics such as the anti-epidermal growth factor receptor (EGFR) antibodies cetuximab and panitumumab or the anti-VEGF antibody bevacizumab have failed to improve survival rates. One reason might be the missing availability of relevant biomarkers to direct targeted therapies to the right patients.

1.3. Organoids - an *in vitro* model of mammalian development and disease

1.3.1. What are organoids?

Organoids are a recently developed three-dimensional (3D) culture system derived from adult stem cells of primary tissue, embryonic stem cells (ESC), induced pluripotent stem cells (iPSC) or established cell lines (Shamir and Ewald, 2014). Through maintaining the stem cell niche they represent the ability of self-renewal, proliferation and self-organization. Organoids show a similar functionality as the organs they are derived from (reviewed in Merker et al., 2016; Werner et al., 2016). Through the cultivation of cells in an artificial laminin-rich extracellular matrix (ECM) organoids resemble the native tissue structure. The system represents a near-physiological model compared to standard two-dimensional (2D) cell cultures. Important differences exist between organoid cultures derived from adult stem cells as compared to ESC or iPSC derived cultures. While the latter also contain mesenchymal cells of the submucosa and muscle layers, adult stem cell derived organoids lack these structures. Immune and neural cells are missing in both organoid cultures, but co-culture protocols are currently established to allow also the analysis of these cellular compartments with the organoid cell culture technology (Chakrabarti et al., 2018; Dijkstra et al., 2018).

1.3.2. History of organoid development

The self-organizing capacity of mammalian cells is known for a long period of time. Evans *et al.* firstly created a primary rat adult intestinal crypt culture system. Hereby crypt epithelial cells adhere to collagen type I-coated culture vessels. Cells can be cultivated over a period of 1-2 weeks only with intact attached fibroblasts (Evans et al., 1992).

In 2009 two different 3D cultivation methods of intestinal organoids have been established. Ootani *et al.* have used an air-liquid system where neonatal intestine including mucosa and mesenchyme form long-lasting cell cultures (Ootani et al., 2009). The organoid culture system have been designed by combining the knowledge of growth requirements of intestinal epithelium to get a well-defined, robust and stable cell culture system for long-term growth (Sato et al., 2009). The self-renewing epithelium of the intestine is segmented into

crypts and villi (Bjerknes and Cheng, 2006). New cells are developed in the crypts and lost by apoptosis at the tip of the villi. Laminin ($\alpha 1$ and $\alpha 2$) is found to be enriched at the crypt base (Sasaki et al., 2002). Intestinal cell with no contact to an extracellular matrix will frequently undergo the programmed cell death anoikis (Hofmann et al., 2007). Therefore, isolated intestinal cells are cultivated in the laminin-rich Matrigel supporting the intestinal epithelial growth. Growth dependent required niche factors are WNT, R-spondin, EGF and Noggin. The WNT signaling is the key player for intestinal crypt proliferation (Korinek et al., 1998; Pinto et al., 2003; Kuhnert et al., 2004). R-spondin is implicated in the WNT pathway activation and produced by the intestinal stroma cells. Due to the absence of stroma cells in the organoid cultivation R-spondin is added to allow high efficiency cultivation (Kim et al., 2005). The EGFR signaling is activated by EGF supplementation important for the promotion of general cell proliferation (Dignass and Sturm, 2001). Additionally, the transforming growth factor beta (TGF- β)/bone morphogenetic protein (BMP) signaling is responsible for cell differentiation. Especially BMP originates in the mesenchyme and is necessary for morphogenesis as well as differentiation processes (Haramis et al., 2004; He et al., 2004; Zhang et al., 2009). As mentioned organoids are exclusively composed of epithelial cells and to allow long-term cultivation the BMP antagonist Noggin needs to be added to the culture medium. For organoid generation isolated mouse intestinal cells are mixed with Matrigel and overlaid by medium supplemented with the above mentioned niche factors (Sato et al., 2009). These intestinal organoids develop a central lumen lined by villus-like epithelium and several crypt-like domains. In that model dead cells are extruded from the renewing structure by filling the lumen with apoptotic cells. Expression analysis of organoids shows similar characteristics as for freshly isolated tissue with no induction of stress related genes open up new avenues for intestinal research (Sato et al., 2009).

1.3.3. Organoid culture system in other tissues

The intestinal organoid system was adapted to further mammalian tissues like colon, stomach, liver and pancreas (Figure 6). Different tissue of mice or human require different growth factors for long-term cultivation of organoids. These cultivation conditions are represented in Table 1.

Table 1: Organoid cultures derived from adult tissue (modified according to Clevers, 2016; Lancaster and Huch, 2019).

Organ	Derived from	Cultivation condition	Reference
Stomach	Mouse adult antrum stem cells Mouse adult corpus stem cells Human adult cancer/normal tissue	WNT, Rspodin, Egf, Noggin, Fgf10 WNT, Rspodin, Egf, Noggin, Fgf10 WNT, Rspodin, Egf, Noggin, Fgf10, TGF- β i	Barker et al. 2010 Stange et al. 2013 Bartfeld et al. 2015; Seidlitz et al. 2019a; Vlachogiannis et al. 2018; Nanki et al. 2018
Esophagus	Human adult esophageal cancer tissue	WNT, Rspodin, Egf, Noggin, Fgf10, RhoKi, TGF- β i	Li et al. 2018
Small intestine	Mouse adult stem cells	Rspodin, Egf, Noggin	Sato et al. 2009b
Colon	Human adult tissue	WNT, Rspodin, Egf, Noggin, TGF- β i, p38i	Jung et al. 2011; Sato, van Es, et al. 2011; Li, Nadauld, Ootani, David C. Corney, et al. 2014; Van De Wetering et al. 2015
Lung	Mouse adult stem cells Human adult cancer/normal tissue	Co-cultivation with endothelial cells + insulin-transferrin-selenium Rspodin, Fgf, Noggin, TGF- β i, p38i, RhoKi	Lee et al. 2014; Sachs et al. 2019
Liver	Mouse adult liver cancer/normal tissue Human adult liver cancer/normal tissue	Rspodin, Egf, Noggin, HGF, FSK, TGF- β i Rspodin, Egf, Noggin, HGF	Huch, Boj, et al. 2013; Peng et al. 2018; Hu et al. 2018; Cao et al. 2018 Huch et al. 2015; Hu et al. 2018; Broutier et al. 2017; Nuciforo et al. 2018
Pancreas	Mouse adult tissue Human adult cancer/normal tissue	Rspodin, Egf, Noggin, Fgf, WNT, Rspodin, Egf, Noggin, Fgf, TGF- β i	Huch, Bonfanti, et al. 2013 Boj et al. 2015; Seino et al. 2018; Boj et al. 2015
Prostate	Mouse adult cells, tissue Human adult cancer/normal tissue	Rspodin, Egf, Noggin, DHT, TGF- β i Rspodin, Egf, Fgf10, Fgf2, DHT, TGF- β i; p38ii	Xin et al. 2007; Karthaus et al. 2014 Karthaus et al. 2014; Gao et al. 2014
Fallopian tube	Human adult tissue	WNT, Rspodin, Egf, Noggin, Fgf	Kessler et al. 2015
Endometrium	Mouse adult tissue Human adult cancer/normal tissue	WNT, Rspodin, Egf, Noggin, Fgf10, TGF- β i, inulin-transferrin-selenium WNT, Rspodin, Egf, Noggin, Fgf10, TGF- β i, p38i, inulin-transferrin-selenium	Boretto et al. 2017 Boretto et al. 2017; Turco et al. 2017
Mammary Gland	Human adult cancer/normal tissue	Rspodin, Egf, Noggin, Fgf10, Fgf7, TGF- β i, neuregulin1	Linneman et al. 2015; Sachs et al. 2019

Salivary Gland	Mouse adult tissue	WNT, Rspodin, Egf, Fgf2, insulin, dexamethasone	Maimets et al. 2016
	Human adult tissue	WNT, Rspodin, Egf, Fgf2, insulin, dexamethasone	Pringle et al. 2016
Placenta	Human adult tissue	Rspodin, Egf, Fgf2, HGF, RhoKi, GSK3i	Turco et al. 2018
Bladder	Mouse adult tissue	Fgf10, Fgf7, TGF- β i	Mullenders et al. 2019
	Human adult cancer tissue	Fgf10, Fgf7, Fgf2, TGF- β i	Mullenders et al. 2019; S. H. Lee et al. 2018
Brain	Human adult cancer tissue	Neurobasal medium with Egf, Fgf	Hubert et al. 2016

Abbreviations: Tgf- β i: Tgf- β inhibitor, p38i: p38 inhibitor, RhoKi: Rho kinase inhibitor, GSK3i: GSK3: Glycogen synthase kinase 3 inhibitor, HGF: hepatocyte growth factor

1.3.3.1. Stomach organoids

The stomach contains two main parts namely corpus and antrum with their corresponding stem cells marked by LGR5 and TROY. Both murine stem cell compartments have the ability to form organoids when they are cultured in WNT3A, Rspodin, Noggin, Fgf10 and Egf (see Table 1) (Barker et al., 2010; Stange et al., 2013). By cultivation in differentiation medium through removal of Fgf10, Noggin and WNT, mouse organoids can develop differentiated cell lineages. However, differentiation into parietal cells as well as endocrine cells is inefficient with this model system (Stange et al., 2013). Co-cultivation of stomach organoids with immortalized stomach mesenchymal cells allow differentiation of parietal cells with acid production capacity (Schumacher et al., 2015). Human stomach organoids are established with similar culturing conditions as the mouse organoids (see Table 1). Infection of organoids with pathogens i.e. *H. pylori* allows analysis of host pathogen interactions (Bartfeld et al., 2015; Schlaermann et al., 2016; Pompaiah and Bartfeld, 2017). Also generation of patient derived gastric cancer organoids from tumor tissues and fine needle biopsies is possible. These tumor derived organoids allow detailed mechanistic studies in primary and living tumor material to better understand gastric cancer development and their molecular alterations (Gao et al., 2018; Nanki et al., 2018; Vlachogiannis et al., 2018; Yan et al., 2018; Seidlitz et al., 2019a). Stomach organoids can be also generated from ESCs or iPSCs if no access to primary tissue is feasible. Here, knowledge of signaling pathways involved in regulating early critical steps of stomach development are necessary (McCracken et al., 2014; Noguchi et al., 2015; Broda et al., 2019).

1.3.4. Application of organoid technology

The possibility of growing near-physiological and self-renewing organoids provides an excellent model system for a wide range of basic developmental as well as translational applications (Fatehullah et al., 2016). Due to the major advantage of fast expanding samples from small amounts of biopsies, in depth analyses of drug screenings, disease modelling as well as genetic screenings are possible. Figure 6 summarizes important applications of the organoid technology. Generation of organoids from human disease like cancer allow in depth analysis of the underlying pathobiology (Figure 6A). The process of embryonic development and tissue homeostasis can be studied using organoids derived from ESCs or iPSCs (Figure 6B) (McCracken et al., 2014; Noguchi et al., 2015). Large organoid collections of individual patient samples function as living human biobanks. Their usefulness has been demonstrated i.e. for colorectal cancer, gastric cancer, prostate cancer and pancreatic cancer (Figure 6C). Using these biobanks high-throughput drug screenings can be performed to individualize patient treatment and screen for novel therapeutics (Figure 6D). Genome,

transcriptome and proteome analyzes enable the detailed description of various signaling pathways and their alterations in disease (Figure 6E) (Dong Gao et al., 2014; Boj et al., 2015; Van De Wetering et al., 2015; Nanki et al., 2018; Tiriach et al., 2018; Vlachogiannis et al., 2018; Yan et al., 2018; Seidlitz et al., 2019a). Other studies use the clustered regularly interspaced short palindromic repeats (CRISPR)/Cas9 mediated gene editing technology in organoids to evaluate candidate genes for carcinogenesis or other disease (Figure 6F) (Li et al., 2014; Boj et al., 2015; Matano et al., 2015; Andersson-Rolf et al., 2017). Bacterial and viral infections can be studied by injecting infectious agents into the lumen of organoids (Figure 6G) (Bartfeld et al., 2015; Wroblewski et al., 2015; Schlaermann et al., 2016).

In summary, organoids represent a relevant model system to study the dynamics of stem cells, development, tissue homeostasis and disease. They can be easily amplified from several types of sources in a controlled environment. Through recapitulation of the original tissue composition they play an important role as a basic and translational research tool with a wide range of uses, i.e. for disease therapy in a personalized manner.

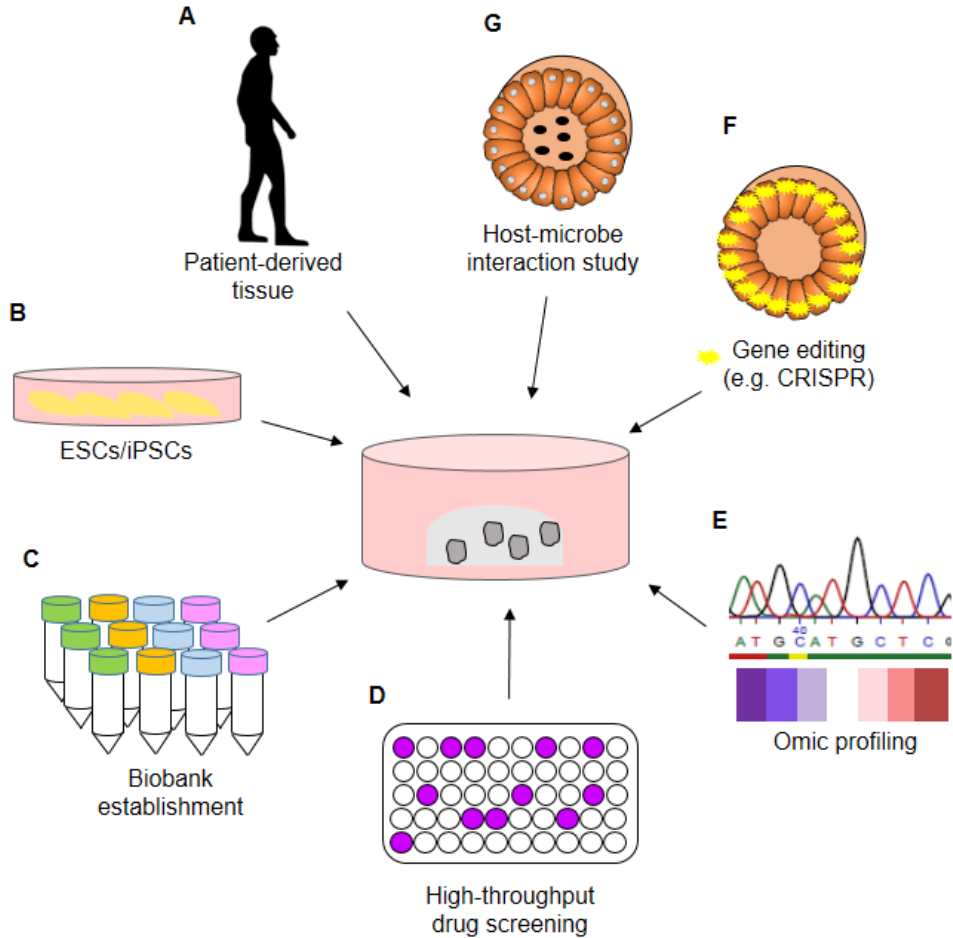


Figure 6: Applications of the organoid technology for studying development, homeostasis and disease (modified according to Fatehullah, Tan, and Barker 2016).

2. Aim of the study

Gastric cancer ranks the fifth most common malignancy and the second leading cause of cancer related deaths worldwide. Due to missing early clinically signs the prognosis of gastric cancer remains poor and three quarters of patients represent with non-curable disease. Additionally, the lack of potential biomarkers hampers the diagnosis as well as therapy strategy. Therefore, the main goal of this study was to basically deepen the understanding for gastric cancer and to identify possible therapy options for an increasing overall patient survival. The following three objectives were defined and addressed to investigate the mentioned goal.

In the first part of the story we aimed to establish patient derived gastric cancer organoids that can serve as living biomarkers to predict patients therapy response or resistance, thereby guiding personalised therapy approaches. Here, human tissues of diagnosed stomach adenocarcinoma or esophagus from surgical resection specimens were obtained and cancer organoids initiated. These generated organoid lines were further histologically and molecularly characterized. Additionally, the therapy response to classical chemotherapy as well as targeted drugs depending on the observed mutational pattern was addressed.

Human gastric cancer organoids allowed a detailed analysis of observed alterations for each individual patient. However, the high number of mutations affected the interpretation of targeted therapies. Thus, in the second part of the work murine tumor organoids with a defined mutational spectrum typically observed in the four gastric cancer subtypes were generated to further allow in depth characterization of pathway interference.

In the third part of the study we aimed to design gastric cancer specific mouse models. Here, the newly generated inducible stomach-specific Anxa10-CreER^{T2} mouse line was used to establish genetically engineered mouse models of the CIN and GS gastric cancer molecular subtypes as defined by the TCGA. A detailed characterization of gastric tumor progression with respect to histology, cell type composition and metastatic phenotype was conducted.

All in all, the observations and conclusions from the study can help to expand the knowledge for gastric cancer development, progression and therapy in the context of patients overall survival.

3. Material and Methods

3.1. Material

3.1.1. Devices

Table 2: For experiments used devices.

Device	Name	Company
-80 °C Freezer	Innova U725-G	Eppendor AG, Hamburg, Germany
-80 °C Freezer	Ultra-Low Temperature Freezer MDF-U76V	Panasonic, Kadoma, Japan
-20 °C Freezer	Comfort	LIEBHERR, Bulle FR, Switzerland
-20 °C Freezer	Premium NoFrost	LIEBHERR
Analytical balance	CP124S	Sartorius AG, Göttingen, Germany
Cell counter	TC20 Automated Cell Counter	BIO-RAD, Hercules, US
Centrifuge	MicroStar 17R	VWR, Darmstadt, Germany
Centrifuge	Centrifuge 5430	Eppendorf AG
Centrifuge	Rotanta 460R	Hettich, Tuttlich, Germany
Centrifuge	Centrifuge 5810R	Eppendorf AG
Centrifuge	Biofuge PrimoR	Heraeus, Hanau, Germany
Centrifuge	Megafuge 1.0R	Heraeus
Electrophoresis power supply	PowerPac 200	BIO RAD
Exhaust pump	Sicherheits-Absaugsystem AC 04	DITABIS AG, Pforzheim, Germany
Gel documentation system	G:Box	VWR
Incubator	BBD 6220 CO ₂ Inkubator	Thermo Fisher Scientific, Waltham, US
Fluorescence activated cell sorting (FACS)	LSRII	Becton Dickinson (BD), Franklin Lakes, US
Fluorescence microscope	DMI3000 B	Leica, Wetzlar, Germany

Laminar flow hood	Herasafe KS	Thermo Fisher Scientific
Liquid nitrogen tank	Biosafe MDß	Cryotherm, Kirchen (Sieg), Germany
Whole genome sequencing	HighSegXten	Illumina
Magnetic mixer	RH basic 2	IKA, Staufen, Germany
Microscope	EVOS FL Auto	Life Technologies, Carlsbad, US
Microplatereader	Genios	Tecan, Männedorf, Switzerland
Microscope	Axiovert 40C	Carl Zeiss AG, Oberkochen, Germany
Microtome	Leica RM2265	Leica
Microwave	MW 802	Exquisit, Kaarst, Germany
Multimode microplatereader	Varioskan LUX	Thermo Fisher Scientific
PCR cycler	Mastercycler egradient	Eppendorf AG
PCR cycler	Mastercycler	Eppendorf AG
PCR cycler	Mastercycler gradient	Eppendorf AG
PCR cycler	peqSTAR	VWR Life Science Competence, Erlangen, Germanx
pH meter	Five Easy Plus	METTLER Toledo, Columbus, US
Pipette controller	accu-jet pro	Sigma-Aldrich, St. Louis, US
Pipette controller	Easypet 3	Eppendorf AG
Precision balance	TE3102S	Sartorius AG
Quantitative Real Time PCR cycler	GeneAmp 5700 Step One Plus Cycler	Applied Biosystems
Quicksilver lamp	HXP R 120W/45C VIS	OSRAM, München, Germany
SDS PAGE power supply	E835 CONSORT	Sigma-Aldrich
Spectrophotometer	NanoVue Plus	GE Healthcare, Chicago, US
Thermoblock	Thermomixer comfort	Eppendorf AG
Tissue desrupter	TissueLyser II	Qiagen, Hilden, Germany
Tissue processor	Leica TP1020	Leica
Vortex mixer	MS2 Minishaker	IKA

Water bath	W12	Labortechnik-Medingen, Arnsdorf, Germany
------------	-----	---

3.1.2. Additional material and equipment

Table 3: Additional material, equipment and used kits.

Material	Name	Company
Adenovirus	FIVCMVCre-eGFPVSVG	Gene Transfer Vector Core facility, Boston, USA
Blocking kit	Streptavidin/Biotin Blocking Kit	Vector Laboratories, Detroit, US
cDNA kit	High Capacity cDNA Reverse Transcription Kit	Applied Biosystems, Foster City, US
Cell viability kit	Presto Blue Cell Viability Reagent	Thermo Fisher Scientific
DAB detection Kit	Imoact DAB (HRP) Substrate	Vector Laboratories
DNA polymerase	<i>GoTaq</i>	Promega, Madison, US
DNA quantification kit	Quant-iT PicoGreen dsDNA Reagent Kit	Invitrogen, Carlsbad, US
Electrophoresis chamber	EasyCast B2	Thermo Fisher Scientific
Electrophoresis system	Novex Mini-Cell	Invitrogen
Gel Western blot	NuPAGE 4-12 % Bis-Tris Gel (1.0 mm x 12 well)	Invitrogen
HRP substrate kit	Immobilon Western HRP substrate	Merck, Darmstadt, Germany
Mucus staining kit	Periodic Acid Schiff (PAS) Stain Kit	Abcam, Cambridge, UK
Nitrocellulose blotting membrane	Amersham Protran Premium 0.45 µM NC	GE Healthcare
Proliferation kit	Click-iT EdU BV421 Imaging Kit	Thermo Fisher Scientific
Protein quantification kit	Pierce BCA Protein Assay Kit	Thermo Fisher Scientific
qRT-PCR mix	Power SYBR Green PCR Master Mix	Life Technologies

RNA isolation kit	Nucleo Spin RNA II	Macherey-Nagel, Düren, Germany
Western blot detection kit	ECL Plus Western Blotting Detection Reagents	GE Healthcare

3.1.3. Fine chemicals

Table 4: Fine chemicals.

Fine chemical	Company
Agarose	Serva, Heidelberg, Germany
Alcoholic 1 % eosin solution	Clinic pharmacy UKD
AnnexinV-FITC (#556419)	BD
BlueJuice gel loading dye (10x)	Life Technologies
Bovine serum albumin	Carl Roth, Karlsruhe, Germany
Butanol	Clinic pharmacy UKD
Calcium chloride	Sigma-Aldrich
Calphostin C (#1626)	Tocris Bioscience, Bristol, UK
Chloroform	Carl Roth
Dimethyl sulfoxide (DMSO)	WAK-Chemie GmbH, Bad Homburg, Germany
DL-dithiothreitol	Sigma-Aldrich
dNTPs	Carl Roth
Docetaxel (24.8 µM)	Clinic pharmacy UKD
Entellan New	Merck
Ethanol	VWR
Ethylenediaminetetraacetic acid (EDTA)	Thermo Fisher Scientific
Epirubicin (3.7 µM)	Clinic pharmacy UKD
FACS-FLOW	BD
FACS-RINSE	BD
FACS-SAFE	BD
5-Fluorouracil (384 µM)	Clinic pharmacy UKD
Formaldehyde solution (4 %)	SAV Liquid Production GmbH, Flintsbach am Inn, Germany
Gel Loading Dye (6x), Blue	New England BioLabs, Frankfurt am Main, Germany
GelRed Nucleic Acid Stain (20,000x)	Biotium, Hayward, CA

Goat horse serum (#G9023)	Sigma-Aldrich
Halt Protease Inhibitor Single-use Cocktail (100x)	Thermos Fisher Scientific
Halt Phosphatase Inhibitor Single-use Cocktail (100x)	Thermo Fisher Scientific
Hematoxylin	Clin Tech, Guildford, UK
Hydrogen peroxide (30 %)	Merck
Irinotecan (34.1 μ M)	Clinic pharmacy UKD
Isopropanol	Merck
Magnesium chloride hexahydrate	Sigma-Aldrich
Methanol	VWR
Nonident P-40	US-Biological, Salem, US
NuPAGE Antioxidant	Life Technologies
NuPAGE LDS sample buffer (4x)	Life Technologies
NuPAGE MES SDS running buffer (20x)	Life Technologies
NuPAGE Sample reducing agent (10x)	Life Technologies
NuPAGE Transfer buffer (20x)	Life Technologies
Oxaliplatin (12.6 μ M)	Clinic pharmacy UKD
Palbociclib (#S1116)	Selleckchem, Eching, Germany
Phenol	Carl Roth
PonceauS	Sigma-Aldrich
Potassium chloride	Sigma-Aldrich
Potassium dihydrogenphosphate	Sigma-Aldrich
Precision Plus All Blue Protein™ Standard	Bio-Rad
Propidium iodide	Sigma-Aldrich
Proteinase K solution (680 mAnsonU/ml)	AppliChem
RNase A (50 mg/ml)	Sigma-Aldrich
Skim milk powder	AppliChem, Gatersleben, Germany
Sodium chloride	Carl Roth
Sodium deoxycholate	AppliChem
Sodium citrate tribasic dihydrate	Sigma-Aldrich
Sodium lauroyl sarcosinate	Sigma-Aldrich
Sodium phosphate dibasic	Sigma-Aldrich
Sorbitol	Sigma-Aldrich
Sucrose	Sigma-Aldrich
Surgipath Paraplast	Leica

Tamoxifen	Sigma-Aldrich
Trametinib	Selleckchem
Trastuzumab (Herceptin)	Roche, Basel, Switzerland
Tris	Sigma-Aldrich
TrisHCL (1 M)	Sigma-Aldrich
Tween 20	Carl Roth
Ultrapure distilled water (dH ₂ O)	Thermo Fisher Scientific
Xylene	VWR

3.1.4. Biochemicals

Table 5: Biochemicals.

Biochemical	Company
A83-01	Tocris Bioscience
B27	Invitrogen
Cell Recovery solution	Corning, New York, US
Collagenase XI	Sigma-Aldrich
Dispase II	Roche
Dulbecco`s Modified Eagle Medium (DMEM); 4,5 g/l glucose; 1,5 g/l sodiumbicarbonate, 2 mM GlutaMAX	Gibco, Thermo Fisher Scientific
Dulbecco`s phosphate buffered saline (D-PBS)	Gibco, Thermo Fisher Scientific
F12-K	Gibco, Thermo Fisher Scientific
Fetal calf serum (FCS)	PAA, Pasching, Austria
Gastrin	Sigma-Aldrich
GlutaMAX	GE Healthcare
hFgf10	Peprtech, Rocky Hill, US
HEPES	Thermo Fisher Scientific
IMDM	Gibco, Thermo Fisher Scientific
Matrigel	Corning
mEgf	Invitrogen
N2	Invitrogen
N-acetyl-L-cysteine	Sigma-Aldrich
Nicotinamide	Sigma-Aldrich
Noggin	Conditioned medium, own production

Penicilin/streptomycin	Gibco, Thermo Fisher Scientific
Primocin	Invitrogen
Recovery cell culture freezing medium	Thermo Fisher Scientific
RPMI-1640; 2 mM L-glutamine	Gibco, Thermo Fisher Scientific
Rspodin	Conditioned medium, own production
TrypLE	Gibco, Thermo Fisher Scientific
Trypsin	Gibco
Trypan Blue solution	Sigma-Aldrich
WNT3A	Conditioned medium, own production
Y-27632	Sigma-Aldrich

3.1.5. Primary antibodies

Table 6: Used primary antibody with usage dilution, blocking and secondary antibody.

Name	Usage	Dilution	Blocking	Secondary antibody	Company/ Cat.-No.
KI67 (SP6)	IHC	1:200 in 1 % BSA/D-PBS	5 % goat block	Anti-rabbit	Abcam (#16667)
PGC	IHC	1:2500 in 1 % BSA/D-PBS	5 % goat block	Anti-rabbit	Abcam (#180709)
CK20	IHC	1:1000 in 1 % BSA/D-PBS	5 % goat block	Anti-rabbit	Abcam (#97511)
ANXA10	IHC	1:2000 in 1 % BSA/D-PBS	5 % goat block	Anti-rabbit	Sigma (#HPA005469)
ERK1/2	Western Blot	1:100 in 5 % BSA/TBS-T	5 % milk	Anti-rabbit	Cell Signaling, Danvers, US (#9102S)
Phosphor- ERK1/2	Western Blot	1:100 in 5 % BSA/TBS-T	5 % milk	Anti-rabbit	Cell Signaling (#9101S)
GAPDH (14C10)	Western Blot	1:1000 in 5 % milk	5 % milk	Anti-rabbit	Cell Signaling (#2118S)

3.1.6. Secondary antibodies

Table 7: Used secondary antibody with usage and dilution.

Name	Usage	Dilution	Company/ Cat.-No.
ZyMAX Rabbit anti goat IgG (H+L)HRP-conjugate	IHC	1:500 in 1 % BSA/D-PBS	Invitrogen (#811620)
SignalStain Boost IHC Detection Reagent (HRP, rabbit)	IHC	1 drop per slide	Cell Signaling (#8114)
Anti-rabbit	Western blot	1: 1000 in 5 % milk	Cell Signaling (#7076S)

3.1.7. Nucleic acids

3.1.7.1. Polymerase chain reaction (PCR)

Table 8: Primer sequence for genotyping PCR reactions.

Gene	Label	Sequence (5'-3')
Murine		
<i>Apc</i> ^{fl/fl}	Apc_fwd Apc_rev Apc_Int14R4	GAG AAA CCC TGT CTC GAA AAA A AGT GCT GTT TCT ATG AGT CAA C TTG GCA GAC TGT GTA TAT AAG C
<i>Kras</i> ^{G12D/+}	KrasG12D_3 (LSL/For) KrasG12D_4 KrasG12D_5 (rev)	CTA GCC ACC ATG GCT TGA GT ATG TCT TTC CCC AGC ACA GT TCC GAA TTC AGT GAC TAC AGA TG
<i>p53</i> ^{R172H/+}	LSL_p53_for wt_p53_for wt_p53_rev	AGC TAG CCA CCA TGG CTT GAG TAA GTC TGC A CTG TTC GTT CCA TTC CGT TT AGC CAC ACT GAC AAT AGG AGG T
<i>Cdh1</i> ^{fl/fl}	Cdh1_fwd Cdh1_rev Cdh1_pl10as.3	GGG TCT CAC CGT AGT CCT CA GAT CTT TGG GAG AGC AGT CG TGA CAC ATG CCT TTA CTT TAG T
<i>Pik3ca</i> ^{H1047R/+}	Pik_E19_f1 Pik_WT_E20_r1	CAA GAG TAC ACC AAG ACC AGA GAG TT TGT CGT CCA TCC ACC ATG ATG T

	Pik_Mut_E20_r1	CAA GAG TAC ACC AAG ACC AGA GAG TT
<i>Arid1a^{fl/fl}</i>	mgArid1aF mgArid1aR	GTA ATG GGA AAG CGA CTA CTG GAG TGT TCA TTT TTG TGG CGG GAG
<i>Smad4^{fl/fl}</i>	gSmad4R2 gSmad4R1 gSmad4F	GAC CCA AAC GTC ACC TTC AG GGG CAG CGT AGC ATA TAA GA AAG AGC CAC AGG TCA AGC AG

3.1.7.2. Quantitative Real Time PCR (qRT-PCR)

Table 9: Primer sequence for qRT-PCRs.

Gene	Label	Sequence (5'-3')
Murine		
<i>Myc</i>	mMyc_for mMyc_rev	CTG TAC CTC GTC CGA TTC C GCT CTT CTT CAG AGT CGC T
<i>Ccnd1</i>	mCCND1_for mCCND1_rev	AGA CCA TTC CCT TGA CTG C AAG CAG TTC CAT TTG CAG C
<i>Ctnnb1</i>	mCTNNB1_for mCTNNB1_rev	CGC CTT CAT TAT GGA CTG C TCC AAC AGT TGC CTT TAT CAG
<i>GAPDH</i>	Mm_GAPDH_171_f Mm_GAPDH_171_r	AGC TTG TCA TCA ACG GCA AG CGG AGA TGA TGA CCC TTT G

3.2. Methods

3.2.1. Cell culture

All cell culture techniques were performed under sterile conditions. Cells were cultured at 37 °C and 5 % CO₂ with regular cell passaging or medium changes.

3.2.1.1. Human gastric cancer cell cultivation and chemotherapy treatment

Human gastric cancer cell lines AGS (CRL-1739), KatolIII (HTB-103), Snu1 (CRL-5971) or Snu5 (CRL-5973) were obtained from the American Type Culture Collection (ATCC) and cultured as described in the corresponding datasheet. The media composition of gastric cancer cell lines is shown in Table 10.

Table 10: Human gastric cancer 2D cell lines with the corresponding culture medium.

Cell line	Culture medium
AGS	F12-K, 10 % FCS
KatolIII	IMDM, 20 % FCS
Snu1	RPMI-1640, 10 % FCS
Snu5	IMDM, 20 % FCS

Long-term storage of cells was performed using cultivation medium supplemented with 5 % dimethyl sulfoxide (DMSO) and 10 % fetal calf serum (FCS). Therefore, 1x10⁶ cells were trypsinized, centrifuged (5 min, 300 g), resuspended in 1 ml freezing medium and pipetted in cryo reaction tubes. After overnight (ON) incubation at -80 °C the cryo vials were transferred to liquid nitrogen. For treatment experiments 1x10³ cells per well were seeded in 100 µl corresponding medium of a 96 well plate and incubated for 48 h prior treatment. Cancer cells were treated with 5-FU (0.001, 0.01, 0.05, 0.1, 0.15, 0.2, 2.0, 5.0, 10.0 µM), oxaliplatin (0.01, 0.025, 0.05, 0.075, 0.1, 0.5, 1.0, 1.5 µM), irinotecan (0.01, 0.05, 0.1, 0.5, 1.0, 2.0, 4.0, 8.0 µM), epirubicin (0.05, 0.1, 0.25, 0.5, 1.0, 1.25, 1.50, 2.0 µM) and docetaxel (0.0025, 0.005, 0.01, 0.025, 0.05, 0.1, 0.5, 1.0 µM) (Florou et al., 2013; Weinreich et al., 2014; Xu et al., 2015; Yuan et al., 2015; Alizadeh-Navaei et al., 2016). Predilutions were made in corresponding culture medium and cells analyzed after 24 h or 72 h (5-FU) incubation.

3.2.1.2. Human gastric cancer and normal organoid cultivation

3.2.1.2.1. *Isolation of gastric cancer and normal mucosa cells from biopsies*

Human gastric cancer and normal mucosa tissues were obtained from patients that underwent surgery at the Department of Visceral-, Thoracic- and Vascular Surgery (VTG) at the University Hospital Carl Gustav Carus TU Dresden. The study was approved by the ethical committee of the TU Dresden (EK451122014) and written consent was obtained from all patients. Clinical data of patients is presented in Appendix Table 1.

For cancer cell isolation approx. 1 cm³ of tumor was cut into small pieces and washed with basal Dulbecco's modified eagle medium (DMEM)/ nutrient mixture F-12 (F12) supplemented with penicillin, streptomycin, primocin, glutamax and 4-(2-hydroxyethyl)-1-piperazineethanesulfonic acid (HEPES) (DMEM/F12+++) until the supernatant was clear. The tissue was digested at 37 °C using 1 mg/ml dispase II and 0.1 mg/ml collagenase XI. Regular gentle inversion every 5 min and frequent observation of tumor disaggregation was performed until small tumor patches became visible. Time to disaggregation varied greatly between individual cancer patients. On average 150 tumor patches were picked under a stereomicroscope. These tumor patches were centrifuged (5 min, 200 g), resuspended in 20 µl Matrigel per well of a 48 well plate and overlaid with human stomach medium supplemented with 10 µM rho-associated, coiled-coil containing protein kinase (ROCK) inhibitor Y-27632. For normal organoid generation the tissue was cut in small pieces and washed with DMEM/F12+++ . The tissue pieces were incubated with 10 ml chelating buffer and 10 mM ethylenediaminetetraacetic acid (EDTA) while shaking at room temperature for 10 min. They were afterwards transferred to a petri dish and pressure was applied on the tissue, which results in the extrusion of stomach glands. The glands were washed with DMEM/F12+++ , plated in 20 µl Matrigel and overlaid with human stomach medium also supplemented with 10 µM Y-27632. Organoid growth was checked 24 h after seeding.

DMEM/F12+++	10 mM HEPES
	1x glutamax
	1x primocin
	1x penicillin/streptomycin
	ad 500 ml DMEM/F12

Chelating buffer: 5.6 mM Na₂HPO₄
8.0 mM KH₂PO₄
96.2 mM NaCl
1.6 mM KCl
43.4 mM sucrose
54.9 mM sorbitol
0.5 mM DL-dithiothreitol
ad 1 l dH₂O

Human stomach organoid medium: 26 % DMEM/F12+++
50 % WNT3A
10 % Rspodin
10 % Noggin
1x B27
1x N2
10 mM nicotinamide
1 mM N-acetyl-L-cysteine
200 ng/ml hFgf10
1x primocin
50 ng/ml mEgf
1 nM gastrin
2 µM A83-01

3.2.1.2.2. *Passaging of human organoids and treatment*

Human gastric cancer and normal organoids were cultured as described by Bartfeld *et al.* and passaged twice a week with a split ratio of 1:2/1:3 (Bartfeld *et al.*, 2015). Therefore, the organoids were mechanically dissociated using a glaspasteur pipette, centrifuged (300 g, 5 min), seeded in 20 µl Matrigel per well of a 48 well plate and overlaid with human stomach organoid medium. For long term storage four wells per organoid line were frozen in recovery cell culture freezing medium and stored in liquid nitrogen.

Treatment with chemotherapeutics was performed 24 h after seeding. One well of a 48 well plate was mechanically dissociated and seeded in 50 µl Matrigel in one well of a 96 well plate. The chemotherapeutic drugs were used at the following concentrations: 5-FU (0.1, 1.0, 10.0 µM), oxaliplatin (1.0, 1.5, 2.5 µM), irinotecan (1.0, 2.0, 4.0 µM), epirubicin (1.0, 1.5, 2.0 µM) and docetaxel (0.01, 0.1, 0.3 µM) (Florou *et al.*, 2013; Weinreich *et al.*, 2014; Xu *et al.*, 2015; Yuan *et al.*, 2015; Alizadeh-Navaei *et al.*, 2016). The drugs were prediluted in human

stomach organoid medium. Initial tests were performed using concentrations selected from the literature, but adaptation to higher concentrations for each drug was necessary to cover a broad response spectrum during organoid treatments. Selected cancer organoid lines were treated with the monoclonal antibody trastuzumab (0.1 μ M) and the inhibitor palbociclib (5 or 10 μ M). Trastuzumab treatment at concentrations of 0.01 or 0.1 μ M was also performed in combination with different 5-FU concentrations (0.1, 1.0, 10.0 μ M) and analyzed after 72 h incubation time.

3.2.1.3. Mouse gastric cancer and normal organoid cultivation

3.2.1.3.1. *Preparation and cultivation of gastric normal and cancer organoids*

Mouse gastric organoids were prepared and cultured as previously described (Stange et al., 2013; Bartfeld et al., 2015). The murine stomach was opened along the large curvature, washed in Dulbecco's phosphate buffered saline (D-PBS), spanned on cork and the corpus cut. The corpus tissue was incubated in chelating buffer (see 2.2.1.2.1) with 10 mM EDTA for 1 h at room temperature. Tissue pieces were afterwards transferred in a petri dish and pressure was applied to extrude healthy glands or cancer patches. Isolated glands or tumor patches were washed and centrifuged at 200 g for 5 min. After centrifugation glands or cancer cell patches were embedded in 20 μ l Matrigel per well of a 48 well plate and covered with corresponding mouse stomach organoid medium. Organoids were passaged 1:2 every three days and cultivated in mouse stomach organoid medium for over one year with no change in proliferation or phenotype. Freezing of organoids was similarly performed as described for human gastric cancer organoids (see 2.2.1.2.2).

Mouse stomach organoid medium: 25 % DMEM/F12+++
50 % WNT3A
10 % Rspodin
10 % Noggin
1x B27
1x N2
1 mM N-acetyl-L-cysteine
1x primocin
10 nM gastrin
100 ng/ml hFgf10
50 ng/ml mEgf

3.2.1.3.2. Adenoviral infection of normal mouse organoids to induce tumorigenic activation of oncogenes

To induce specific mutations in genes of interest, normal mouse gastric organoids were infected with a FIVCMVCre-eGFPVSVG adenovirus with a final virus titer of 12×10^6 . Cre expression in the organoids led to recombination of LoxP sides, resulting in an activation or deletion of the mutated alleles.

For infection 3-4 wells of a 48 well plate per organoid line were mechanically dissociated, incubated with the adenovirus in medium without any antibiotics for 1 h at 37 °C and spin infected for 5 min and 600 g. Successful virus infection was validated 24 h post infection by the viral mediated green fluorescence signal. Successfully infected organoids could be 72 h post infection selected by withdrawal of growth factors from the medium that activate the now mutated pathways (see Table 11). The selection process required around 7-14 days.

Table 11: Selection medium for adenoviral infected mouse organoids.

Organoid model	Pathway	Mutation	Selection
RTK/RAS activated	RTK/RAS, TP53	<i>Kras</i> ^{G12D/+} ; <i>Tp53</i> ^{R172H/+}	-Egf
Diffuse	WNT, Cell adhesion	<i>Apc</i> ^{fl/fl} ; <i>Cdh1</i> ^{fl/fl}	-WNT3A -Rspodin
WNT activated	WNT, TP53	<i>Apc</i> ^{fl/fl} ; <i>Tp53</i> ^{R172H/+}	-WNT3A -Rspodin
EBV associated	PI3K/AKT, Chromatin remodelling	<i>Pik3ca</i> ^{H1047R/+} ; <i>Arid1a</i> ^{fl/fl}	+Mek Inhibitor (PD0325901)

3.2.1.3.3. Mouse cancer organoid treatment

Murine cancer organoids were treated with the classical chemotherapeutics 5-FU (0.001, 0.01, 0.1, 1.0, 10.0, 50.0, 100.0 μ M), oxaliplatin (0.01, 0.05, 0.1, 0.5, 1.0, 1.5, 3.0 mM) and docetaxel (0.001, 0.005, 0.01, 0.05, 0.1, 0.5, 1.0 mM) for 24 h or 72 h (5-FU). Therefore, organoids were after mechanically dissociation seeded in 15 μ l Matrigel per well of a 384 well plate and covered with 50 μ l medium containing the diluted chemotherapeutic drugs. Organoids with an *adenomatous polyposis coli* (*Apc*) mutation were treated with 5 mM calphostin C for 48 h to inhibit the WNT signaling. Successful inhibition was analyzed by determining the expression of WNT pathway downstream targets (*Myc*, *cyclin D1* (*Ccnd1*) and β -*catenin* (*Ctnnb1*)). Organoids with mutations in *Ki-ras2 kirsten rat sarcoma viral oncogene*

homolog (Kras) were treated with trametinib (0.001, 0.01, 0.1, 1.0, 10.0, 50.0, 100.0 μM) for 72 h to block the EGFR signaling pathway. Successful inhibition was validated by analyzing the phosphorylation level of the downstream extracellular-signal regulated kinase 1/2 (ERK1/2) after 0.01 and 10.0 μM trametinib treatment.

3.2.2. Functional assays for analyzing proliferation and apoptosis

3.2.2.1. Viability assay

Viability was analyzed using the Presto Blue cell viability reagent kit which is a resazurin based non-fluorescent solution. Metabolic active cells rapidly reduce the blue solution to an intensely red-fluorescent dye. Organoids and gastric cancer cell lines were seeded in 96 well plates in 50 μl Matrigel covered by 100 μl corresponding organoid medium or in 15 μl Matrigel with 50 μl medium for analysis in 384 well plates. The organoids or cell lines were grown for 24-48 h, treated and viability analyzed after 24-72 h. Presto Blue reagent (final 1x) was added and organoids incubated for 2-3 h or gastric cancer cell lines for 10 min at 37 °C. Absorbance at 560/620 nm or fluorescence at 560/590 nm was measured to analyze metabolic activity of cells.

3.2.2.2. Proliferation assay

Cell proliferation was analyzed with the fluorescence based Click-iT™ EdU cell proliferation kit BV421 for flow cytometry assay. The assay is based on the integration of the thymidine analogue 5-ethynyl-2'-deoxyuridine (EdU) during cell synthesis. The incorporated EdU can be detected by a click reaction with a fluorescently labeled dye. For the assay, the organoids were seeded in 48 well plates incubated for 24 h and treated with 5 μM palbociclib for 24 h. Cells were incubated with 10 μM EdU for 2 h at 37 °C. A single cell suspension was prepared using TrypLE after incubation in Cell Recovery solution for 20 min on ice. Staining was performed according to the manufacturer's instructions. Therefore, the cells were fixed with the Click-iT fixative and permeabilized using the Click-iT saponin-based permeabilization buffer for 15 min. Cells were washed between fixation and permeabilization with 1 % bovine serum albumin (BSA)/D-PBS. Cell staining was performed using the Click-iT reaction cocktail for 30 min at room temperature and cells afterwards washed with permeabilization buffer. For flow cytometry analysis cells were dislodged in 300 μl D-PBS and analyzed using LSR II. The DIVA software was used to analyze the amount of proliferating cells (EdU positive) by excluding dead cells and doublets (Figure 7).

Click-iT saponin-based permeabilization: 10 % Component E
ad 25 ml 1% BSA/D-PBS

Click-iT reaction cocktail (1x): 438 μ l D-PBS
10 μ l CuSO_4
2.5 μ l fluorescent dye
10 μ l 1x reaction buffer additive
total 500 μ l

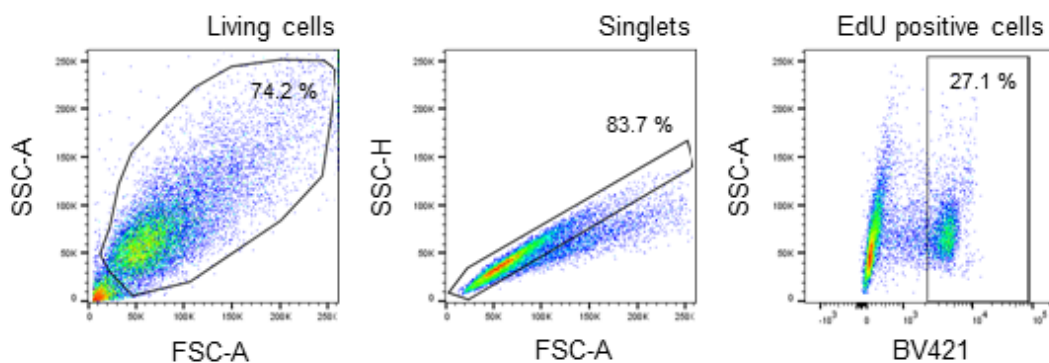


Figure 7: Exemplary gating strategy for the analysis of EdU positive cells. Proliferation assay was performed according to the instructions of the manufacturers and cells analyzed with the LSR II using the DIVA software. Firstly, living cells were determined according to their size (FSC-A) and granularity (FSC-H). Further, single cells were discriminated by plotting area of size (FSC-A) to height of granularity (SSC-H). Afterwards, EdU incorporated cells were distinguished by plotting BV421 against the area of granularity (SSC-A) (FSC- Forward Scatter, SSC-Sideward Scatter).

3.2.2.3. Apoptosis assay

In order to analyze cellular response after drug treatment the flow cytometry-based Annexin V-fluorescein isothiocyanate (FITC)/ propidium iodide (PI) assay was performed. Annexin V stains apoptotic cells by binding on membrane-bound phosphatidylserines (PS). Viable cells present the PSs at the inner cell membrane. During apoptosis the PSs translocate to the outer membrane layer allowing Annexin V binding at the cell surface. The amount of apoptotic cells can be determined by the FITC mediated green fluorescence signal. Contrary, the PI stain necrotic cells by allowing PI to enter the cell. Within the necrotic cell process the cell membrane loses its cell integrity and becomes leaky. For the assay organoids were seeded in 48 well plates, incubated for 24 h at 37°C and treated with 1 μ M 5-FU for 72 h. The organoids were isolated from Matrigel using Cell Recovery solution for 20 min on ice and single cells obtained by TrypLE incubation. The cells were stained with 5 μ l Annexin V-FITC and 50 μ g/ml PI for 30 min in 500 μ l FACS binding buffer, washed two times with FACS binding buffer and

dislodged in 300 μ l D-PBS. Samples were analyzed using the LSRII and the DIVA software. In Figure 9 an exemplary gating strategy is shown (Figure 8).

FACS binding buffer: 10 mM HEPES pH 7.4
 2.5 mM CaCl₂
 140 mM NaCl
 ad 1 l D-PBS

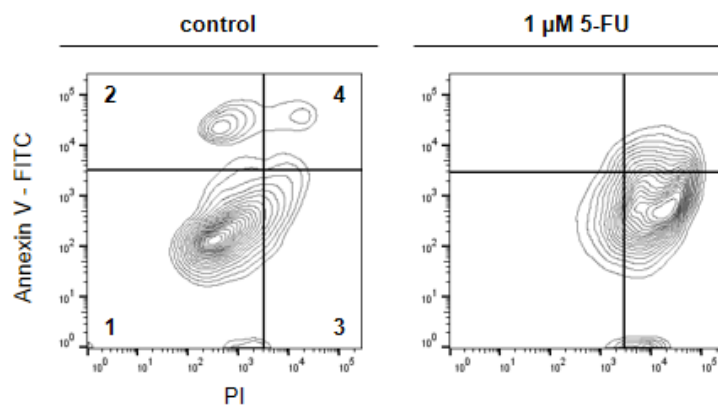


Figure 8: Exemplary Annexin V-FITC/ PI gating strategy. Cells were stained for apoptotic (Annexin V-FITC) and necrotic cells (PI). They were analyzed using the LSRII. Firstly, single cells were discriminated by plotting area of size (FSC-A) to height of granularity (SSC-H) (data not shown). Afterwards apoptotic and necrotic cells were distinguished by plotting Annexin V-FITC to PI. Double negative cells represented living cells (1); PI positive cells necrotic cells (2); Annexin V-FITC positive cells early apoptotic cells (3) and double positive cells late apoptotic cells (4). After 5-FU treat cells shifted from living to early and late apoptotic cells.

3.2.2.4. Single cell assay

To analyze the organoid formation efficiency of normal and cancer organoids, three wells per organoid line were incubated in TrypLE and mechanically dissociated to get a single cell suspension. Cells were counted using Trypan Blue and 100 cells seeded in a 48 well plate covered with 250 μ l corresponding medium. The ability of forming organoids from single cells was counted seven days post seeding.

3.2.3. Biochemical analysis

3.2.3.1. Protein extraction of organoids

Protein isolation of different human and murine gastric cancer organoid lines was performed for further pathway analysis. Therefore, 12 wells per sample were grown in 48 well plates and treated. The organoids were transferred to falcons with Cell Recovery solution and

incubated for 1 h on ice. A five times washing procedure with D-PBS followed to completely get rid of remaining Matrigel residuals. The pellet was lysed in 50-100 μ l radioimmunoprecipitation assay (RIPA) buffer with freshly added protease- and phosphatase inhibitors (each 1:100) for 30 min on ice. The organoid lysates were treated with ultrasound for 15 min and further centrifuged (20 min, 4°C, 11 000 g) to remove cell residuals. The protein solution was transferred in a new reaction tube and the protein amount determined using the Pierce BCA Protein Assay kit. The BCA assay is based on the protein reduction of Cu^{2+} to Cu^{1+} in an alkaline solution resulting in a purple color formation of bicinchoninic acid. Here, 2 μ l of organoid protein solution and 10 μ l of BSA standard were used. The reaction mix composed of solution A and B in a 1:50 ratio was added to the organoid sample or BSA standard and incubated for 30 min at 37°C. The absorbance at 560 nm was determined using the GENios spectrophotometer with the Magellan software. The assay was performed according the manufacturer's instructions and protein amount calculated by linear regression in Excel (Microsoft).

RIPA buffer: 50 mM Tris/HCl pH 8.0
 150 mM NaCl
 1 % Nonidet P-40
 0.5 % sodiumdeoxycholat
 0.1 % SDS
 ad 1 l dH₂O

3.2.3.2. SDS page and Western blot

The sodium dodecyl sulfate polyacrylamide gel electrophoresis (SDS page) was used to separate proteins according their molecular weight in acrylamide gels. Here, 10-20 μ g protein was diluted in 20 μ l D-PBS with 2 μ l sample reducing agent and 5 μ l 4x NUPAGE sample LDS buffer. Samples were incubated for 5 min at 90 °C and afterwards loaded on the polyacrylamide gel using the Xcell SureLock gel system. To allow determination according to molecular weight 10 μ l precision plus protein ladder was used. The gel was run in NUPAGE MES SDS running buffer for 50 min at 180 V. The separated proteins were blotted on nitrocellulose membrane by a wet-blot system. The blot was build up as described in Figure 9 and filled with NUPAGE transfer buffer.

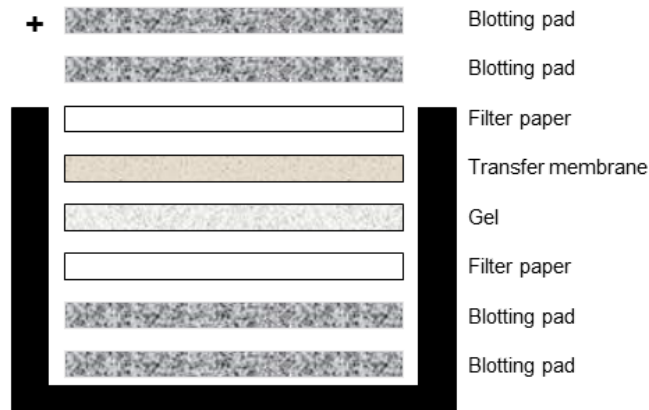


Figure 9: Wet-blot Western blot system. The blot was built up by 2x blotting pads, 1x filter paper, 1x gel, 1x nitrocellulose membrane and 2x blotting pads. Blotting was performed in NUPAGE transfer buffer for 1 h at 30 V.

The negative loaded proteins run at 30 V for 1 h to the positive loaded cathode and remained on the nitrocellulose membrane by hydrophobic interactions. The membrane was shortly stained with Ponceau S to control successful SDS page as well as blotting. The staining was removed by washing in 1x tris-buffered saline with tween 20 (TBS-T). To avoid unspecific binding the membrane was blocked ON in 5 % milk or 5 % BSA (each diluted in 1x TBS-T). The primary antibody was diluted in 5 % milk or 5 % BSA and incubated for 1 h at room temperature or ON at 4°C. The membrane was washed 3x times with 1x TBS-T for each 5 min and incubated with the secondary antibody for 1 h at room temperature. To remove unbound antibody the membrane was washed three times with 1x TBS-T. The secondary antibody recognized specific epitopes of the primary antibody and was linked to a horseradish peroxidase (HRP). This allowed the detection via chemiluminescence in the G:Box Chemi XT4 after a short incubation with the Immobilon Western chemiluminescent HRP substrate. Glyceraldehyde 3-phosphate dehydrogenase (GAPDH) was used as housekeeping gene to ensure similar protein load between different protein samples.

Running buffer: 5 % NUPAGE MES SDS running buffer (20x)
ad 1 l dH₂O

Transfer buffer: 5 % NUPAGE transfer buffer (20x)
ad 1 l dH₂O

TBS-T buffer: 1 M Tris/HCl ph 7.4
5 M NaCl
1 % Tween 20
ad 1 l dH₂O

Blocking buffer: 5 % BSA or 5 % skim milk powder
 in 1x TBS-T buffer

3.2.4. DNA and RNA techniques

3.2.4.1. DNA isolation of organoids and tissue

DNA was isolated from human and mouse gastric cancer organoids. Here, 10 wells of a 48 well plate per organoid line were used. The organoids were incubated for 30 min in Cell Recovery solution on ice, centrifuged (300 g, 5 min) and resuspended in 2 ml lysis buffer plus 1 mg/ml freshly added proteinase K. To allow lysis of cells the samples were shaken in a thermomixer at 56 °C for 1 h. The lysed organoids were heated to 80 °C for 30 min and afterwards cooled down to room temperature. To remove protein and RNA contaminations 450 µl phenol was added. The samples were vortexed and 450 µl chloroform added. The chloroform treatment led to the removal of phenol residuals. The samples were centrifuged for 1 min at 17 000 g and the upper aqueous phase was taken. A second chloroform treatment step followed and phases were again separated through centrifugation for 1 min at 17 000 g. The upper phase was taken and incubated for 1 h at 37 °C with 50 µg RNase A to remove RNA contaminations. DNA was precipitated through the addition of 900 µl isopropanol, pelleted by centrifugation for 10 min at 17 000 g and washed once with 70 % ethanol. The pellet was air dried for 10 min and diluted in 50-100 µl dH₂O. The concentration was determined using the NanoVue Plus.

For the isolation of DNA from human or mouse gastric cancer tissue and healthy mucosa 10 mg of tissue was cut in small pieces and transferred to 1 ml lysis buffer adding 1 mg/ml proteinase K. The addition of 5 mm steel balls to the samples allowed a lysis with the TissueLyser for 4 min at 30 Hz and 4 °C. The further DNA isolation was performed as described for the organoid lines.

Lysis buffer: 20 mM NaCl
 10 mM Tris/HCl pH 7.5
 10 mM EDTA pH 8
 0.5 % sodium lauroyl sarcosinate
 + 1 mg/ml Proteinase K (fresh each time)
 ad 50 ml dH₂O

3.2.4.2. PCR and gel electrophoresis

The polymerase chain reaction (PCR) allows the amplification of a specific DNA fragment from a given target. For the reaction a DNA polymerase synthesizing the new DNA strand as well as sequence complementary 3' and 5' primers are important to allow amplification of the gene of interest (GOI). The *GoTaq* polymerase was used for the GOI amplification running the following mix and program. The used primer sequences and annealing temperatures are written in Table 7.

Mix:	5 µl 5x <i>GoTaq</i> buffer	Run:	95 °C 2 min	
	2.5 µl MgCl ₂ (25 mM)		95 °C 1 min	} 30x
	0.5 µl dNTP mix (10 mM)		Temp 1 min	
	0.5 µl primer forward (10 µM)		72 °C 1 min	
	0.5 µl primer reverse (10 µM)		72 °C 5 min	
	0.25 µl <i>GoTaq</i> Flexi DNA polymerase		4 °C hold	
	x µl DNA (50 ng)			
	ad 25 µl dH ₂ O			

In order to prove successful DNA amplification, the PCR products were analyzed by agarose gel electrophoresis which separates DNA fragments according their length. Smaller fragments move faster through the agarose gel compared to larger ones. Agarose gels of 0.5-2 % were prepared in 1x tris acetate EDTA (TAE) buffer. The fluorescent, nucleic acid stain Gel Red (1:10 000) was added to the agarose mix prior polymerization and allowed PCR product visualization using the G:Box Chemi XT4. Loading buffer (final 1x) was added to the PCR mix to increase density and to allow successful DNA separation during the gel electrophoresis run. For correct PCR product size determination a ladder (100 bp, 1 kb) was also loaded on the gel. The gel was run for 1 h at 120 V.

TAE buffer (20x):	242.0 g Tris
	57.1 ml acetic acid
	0.5 M EDTA pH 8.0
	ad 1 l dH ₂ O, pH 8.3
TAE buffer (1x):	20 ml 20x TAE buffer
	ad 1 l dH ₂ O, pH 8.3

3.2.4.3. Pico Green DNA quantification and whole genome sequencing

For whole genome sequencing the DNA concentration was determined using the fluorescence based Quant-iT Pico Green dsDNA assay kit. This assay allows the ultrasensitive nucleic acid quantification of double stranded DNA. A λ DNA standard was prediluted to the following concentrations: 1, 0.1, 0.01 and 0.001 $\mu\text{g/ml}$. For the assay 100 μl 1:100 prediluted DNA samples and prepared standard were pipetted into a 96 well plate. Detection of DNA was achieved through addition of 100 μl 1:200 prediluted Pico Green fluorescent dye. The plate was incubated for 5 min in the dark and fluorescence analyzed at 480/520 nm at the plate reader Varioskan. The λ DNA standard allowed a linear regression and DNA quantification of the samples. The protocol was performed according to manufacturer's instructions. Whole genome sequencing was run in cooperation with the DKFZ Heidelberg. Therefore, 340 ng organoid DNA were used and analyzed with the HighSeqXten. Data were analyzed by Sebastian Merker (AG Stange, VTG, Dresden).

3.2.4.4. RNA isolation of eukaryotic organoids and tissues

The Nucleo Spin RNA II kit was used for RNA isolation. Organoid pellets of different lines were lysed in 350 μl RA1 buffer and centrifuged via the Nucleo spin filter (1 min, 11 000 g). Afterwards, 350 μl 70 % ethanol was added to the samples, vortexed and centrifuged using the Nucleo spin RNAII filter (1 min, 11 000 g). To desalt the bound RNA the filter was washed with 350 μl MDB buffer and centrifuged (1 min, 11 000 g). To remove genomic DNA the bound RNA was digested with 95 μl rDNase (10 μl rDNase + 90 μl rDNase reaction buffer) for 15 min at room temperature. The reaction was stopped by adding 350 μl RA2 (1 min, 11 000 g). The filter was washed two times with 700 μl RA3 (1 min, 11 000 g; 2 min, 11 000 g). RNA was eluted in 35 μl RNase free water and concentration determined using the NanoVue Plus.

For RNA isolation from tissues also the Nucleo Spin RNA II kit was used. Therefore, 10 mg tissue was cut in small pieces and transferred to 350 μl RA1 buffer. The tissues was lysed using the TissueLyser for 4 min at 30 Hz by addition of 5 mm steel balls. The further RNA isolation was performed as described for the organoid lines.

3.2.4.5. cDNA synthesis

To allow quantification of RNA expression the isolated RNA was transcribed to complementary DNA (cDNA) via the High Capacity cDNA Reverse Transcription kit. For synthesis 250 ng RNA was used running the following program.

Mix:	x μ l RNA	Run:	25 °C 10 min
	1 μ l 10x Reverse Transcriptase (RT) buffer		37 °C 120 min
	0.4 μ l 25x dNTP Mix (100 mM)		85 °C 5 min
	1 μ l 10x RT Random Primers		4 °C hold
	0.5 μ l MultiScribe RT		
	ad 10 μ l dH ₂ O		

3.2.4.6. quantitative Real-Time PCR

For quantitative Real-Time PCR (qRT-PCR) the power SYBR Green PCR Master Mix was used. Exon-spanning primer were designed and used to allow sequence specific quantification. Primer sequences of genes are presented in Table 8. The following mix and run was performed to allow quantification of mRNA expression.

Mix:	2 μ l cDNA	Run:	50 °C 2 min
	6.25 μ l SYBR Green PCR Master Mix		95 °C 10 min
	1.25 μ l Primer forward		95 °C 30 s
	1.25 μ l Primer reverse		60 °C 1 min
	ad 12.5 μ l with nuclease free dH ₂ O		95 °C 15 s
			60 °C 1 min

The qRT-PCR was performed using the GeneAmp 5700 Step One Plus Cyclers. During the run the SYBR Green dye bound to newly synthesized double stranded DNA and led to an increase of fluorescence intensity. This increase was measured based on the exponential growing amount of PCR products. In the process of amplification a linear threshold could be detected and the cycle on which this threshold exceeded defined the cycle of threshold (C_T -value). This C_T -value was determined for each analyzed sample and each specific DNA target. With the help of the $\Delta\Delta C_T$ logarithm the expression of the GOI was calculated after C_T -value normalization to a housekeeping gene (1) and subtraction to an untreated negative control (2). The expression was determined according to $2^{-\Delta\Delta C_T}$.

$$\Delta C_T = C_{T \text{ GOI}} - C_{T \text{ Housekeeping Gene}} \quad (1)$$

$$\Delta\Delta C_T = \Delta C_{T \text{ Treatment}} - \Delta C_{T \text{ Untreated control}} \quad (2)$$

3.2.5. Histology

3.2.5.1. Organoid and mice tissue embedding

For organoid histology 10-12 wells of a 48 well plate per organoid line were used. The organoids were transferred to Cell Recovery solution and incubated for 20 min on ice. Fixation of organoids was performed using 4 % formaldehyde for 5 min at room temperature. To get rid of the formaldehyde the organoids were washed two times with 10 ml D-PBS. Organoids were dehydrated by 3 min incubation with 25 %, 50 % and 70 % ethanol with a centrifugation step at 200 g for 1 min in between. To visualize organoids for embedding an incubation step with 1 % eosin in 2 ml 96 % ethanol for 5 min followed. Treatment with 96 % ethanol for two times each 3 min was performed. The organoids were incubated three times with 2 ml butanol for 3 min and resuspended in 500 µl liquid paraffin. The paraffin embedded organoids were transferred to cassettes and microtome sections of 2.5 µm prepared.

Mouse tissue was transferred during mice preparation in paraffin embedding cassettes, ON fixed in 4 % formaldehyde at room temperature and dehydrated. The dehydration was performed automatically using a standard protocol. The samples were embedded in paraffin and cut in 4 µm sections at the microtome.

3.2.5.2. Hematoxylin eosin staining

Hematoxylin eosin (HE) staining was performed for organoids and mouse tissue samples. They were deparaffinized in xylene and isopropanol for each 5 min. Incubation in 96 % and 70 % ethanol for 3 min allowed rehydration of samples. Nuclei of organoids were stained with hematoxylin for 2 min and respectively mice tissue slides for 6 min. After a short dip in dH₂O with hydrochloric acid the samples were blued for 10 min under warm running tap water. To stain the cytoplasm organoids slides were incubated in eosin for 3 min and mice tissue slides for 5 min. Dehydration by 2 min incubation in 70 % and 96 % ethanol followed. Finally, the slides were incubated for 5 min in isopropanol as well as xylene, mounted in entellan and analyzed using the EVOS FL Auto microscope.

3.2.5.3. Immunohistochemistry

Immunohistochemistry (IHC) was performed for mouse tissue as well as human and murine organoids. Samples were dewaxed for 10 min in xylene and rehydrated via a decreasing ethanol series of 95 %, 85 % and 70 % for 3 min each. The peroxidase quenching with 2.8 % H₂O₂/methanol for 20 min followed after a 10 min 1x TBS-T washing step. To retrieve

antigen binding sites samples were incubated in 0.01 M sodium citrate buffer pH 6.0 or pH 9.0 in a microwave. The tissue slides were heated for 5 min at 540 V, cooled down for 5 min and again heated for 10 min at 230 V. The organoid slides were first boiled three times at 540 V for 2 min with 2 min cooling down in between and then three times at 230 V for 2 min with 2 min cool down process. A wash step in 1x TBS-T for 10 min followed. To block unspecific binding of the primary antibody the slides were incubated for 1 h with 5 % goat block or 5 % BSA depending on the antibodies host. Afterwards an incubation with the primary antibody ON at 4°C or 1 h at room temperature followed. All used antibodies with dilution and blocking are written in Table 5. To get rid of the primary antibody a 1x TBS-T washing step for 10 min was performed. For detection the signal stain detection boost IHC/HRP rabbit/mouse or the HRP bound rabbit anti goat secondary antibody was used. The DAB chromogenic substrate recognized the HRP and allowed visualization of antibody binding. Counterstaining was performed with hematoxylin (preformed as described in the HE staining section 2.2.5.2). Slides were evaluated using the EVOS FL Auto microscope. IHC for cytokeratin 7 (CK7), cadherin 17 (CADH17), carcinoembryonal antigen (CEA) and Her2/neu was performed according to standard protocols by the Department of Pathology at the University Hospital Carl Gustav Carus TU Dresden.

H₂O₂/Methanol (fresh each time): 2.8 % 30 % H₂O₂ solution
ad 250 ml methanol

0.1 M Sodium citrate buffer: 14.9 g sodium citrate
ad 500 ml dH₂O

0.01 M Sodium citrate buffer: 10 % 0.1 M sodium citrate buffer
1 % Tween20
pH 6.0 or pH 9.0
ad 1 l dH₂O

5% goat block:
330 µl TrisHCl (1.5 M)
0.5 g MgCl₂
250 µl Tween 20
0.5 g BSA
2.5 ml goat serum
ad 50 ml D-PBS

5 % BSA block

5 g BSA
in 500 ml D-PBS

3.2.5.4. Periodic acid Schiff's reaction

Stomach mouse tissue sections were stained for Periodic Acid Schiff's reaction (PAS) using the corresponding stain kit to visualize mucus in the stomach epithelium. Slides were firstly deparaffinized via 5 min incubation in xylene and afterwards rehydrated for 2 min in 96 %, 70 % ethanol and aqua dest. The samples were treated for 3 min with periodic acid reaction mix, rinsed in aqua dest for 4 min and were further incubated for 10 min with Schiff's solution. The slides were rinsed for 3 min in running tap water, stained with haematoxylin for 3 min, again rinsed in tap water and finally incubated with the bluing reagent for 30 s. The samples were dehydrated via incubation time in 70 %, 96 % ethanol as well as xylene. After mounting imaging was performed using the EVOS FL Auto.

3.2.6. In vivo experiments

All experiments were performed regarding the terms of the local animal welfare commission. For all experiments eight weeks old mice of the animal facility Oncoray TU Dresden or Experimentelles Zentrum TU Dresden were used. They were kept under standard pathogen-free conditions with *ad libitum* access to water as well as food. All mouse experiments were approved by DD24.1-5131/394/44; TVV 41/2017. Table 12 shows the used mice lines.

Table 12: For in vivo experiments used mice strains.

Mouse line	Strain ID	Information	Usage	Literature
NMRI nude	NMRI Foxn1 ^{nu/nu}	Immunodeficient mice	Organoid transplantation	Isaacson and Cattanach 1962
Rosa26- FLPe	Gt(ROSA)2 6Sor tm1(FLP1) ^{Dym}	Knock in of a FLP recombinase under the Rosa26 promotor	Anxa10-CreER ^{T2} generation	Farley et al. 2000
Rosa26- LSL-LacZ	Gt(ROSA)2 6Sor/J	Knock in of the LacZ under the Rosa26 promotor	Anxa10-CreER ^{T2} functionality analysis	Friedrich and Soriano 1991
Anxa10-Cre ER ^{T2}	Anxa10-Cre ER ^{T2}	Knock in of an inducible Cre recombinase under the Anxa10 promotor	Stomach specific mouse model	(Seidlitz et al., 2019b)
Kras ^{LSL-G12D}	Kras ^{tm4Tvj}	Inducible Kras ^{G12D} mutation flanked by LoxP sites	Stomach specific gastric cancer mouse model,	Jackson et al. 2001

			organoid generation	
Tp53 ^{LSL-R172H}	Tp53 ^{tm2Tyj}	Inducible Tp53 ^{R172H} mutation flanked by LoxP sites	Stomach specific gastric cancer mouse model, organoid generation	Olive et al. 2004
Apc ^{fl/fl}	Apc ^{tm2Rak}	Exon 14 flanked by LoxP sites, truncated protein expression	Stomach specific gastric cancer mouse model, organoid generation	Kuraguchi et al. 2006
Cdh1 ^{fl/fl}	Cdh1 ^{tm2Kem}	Exon 6-10 flanked by LoxP sites, truncated protein expression	Stomach specific gastric cancer mouse model, organoid generation	Boussadia et al. 2002
Smad4 ^{fl/fl}	Smad4 ^{tm2.1Cxd}	Exon 8 flanked by LoxP sites, truncated protein expression	Stomach specific gastric cancer mouse model, organoid generation	Xiao et al. 2002
Arid1a ^{fl/fl}	Arid1a ^{tm1.1Zhw}	Exon 8 flanked by LoxP sites, truncated protein expression	Organoid generation	Gao et al. 2008
Pik3ca ^{H1047R}	Pik3ca ^{Lat-H1047R}	Latent Pik3ca ^{H1047R} mutation in Exon 20 downstream of Lox P site flanked wildtype Exon 20	Organoid generation	Tikoo et al. 2012

3.2.6.1. Subcutaneous human gastric cancer organoid transplantation

Gastric cancer organoids were subcutaneous (s.c.) injected into flanks of NMRI nude mice. For each organoid line four mice were used, each receiving unilateral 10 wells of organoids of a 48 well plate in 50 µl Matrigel. Mice behavior as wells as tumor size was checked two times per week. After reaching a tumor size of maximal 10x10 mm the mice were euthanized via cervical dislocation and xenograft tumors prepared, fixed and embedded for staining protocols. Mouse experiments were done in cooperation with Cläre von Neubeck (OncoRay, Dresden).

3.2.6.2. Anxa10-CreER^{T2} mice generation and characterization

In order to establish a stomach specific mouse model the Anxa10-CreER^{T2} line was generated by Ozgene Pty Ltd (Bentley WA, Australia). An IRES-CreER^{T2} was inserted in frame after the stop codon of the last exon (nr. 12) of the *Anxa10* gene plus a PGK-Neo cassette flanked by Frt sites. For creation the targeting construct was electroporated into a C57BL/6 ES cell line. Homologous recombinant ES clones were identified by Southern hybridization and

injected into blastocysts. Male chimeric mice were obtained and crossed to C57BL/6J females to establish heterozygous germline offspring on C57BL/6 background. The germline mice were crossed to a ubiquitous Rosa26-FLPe line to remove the FRT flanked selectable marker cassette. For further functionality analysis the mice was bred with the Rosa26-LSL-LacZ Cre reporter mouse. The generated Anxa10-CreER^{T2} line was used for gastric cancer subtype modelling. For a CIN subtype the Anxa10-CreER^{T2} line was combined with mice carrying the alleles *Kras*^{G12D/+}, *Tp53*^{R172H/+} and *Smad4*^{fl/fl}. Two different GS subtypes were generated. On the one hand the Anxa10-CreER^{T2} mouse was crossed with mice carrying the *Kras*^{G12D/+}, *Cdh1*^{fl/fl} and *Smad4*^{fl/fl} allele, and on the other hand with mice carrying the *Kras*^{G12D/+}, *Cdh1*^{fl/fl} and *Apc*^{fl/fl} alleles (information for mice see Table 12).

3.2.6.2.1. *Tamoxifen administration and mouse tissue preparation*

To induce Cre recombination 5 mg tamoxifen was injected intraperitoneal (i.p.) in 100 µl sunflower oil. Control mice received sunflower oil only. Mice were continuously monitored and sacrificed at different predetermined time points or immediately when showing signs of tumor burden. Lung, liver, spleen, lymph nodes and a half of the stomach were fixed ON in 4 % formaldehyde and then paraffin embedded. One quarter of the stomach was used for DNA isolation and organoid preparation. The other quarter was used for RNA isolation. Three to four mice were analyzed for each time period after induction of recombination.

3.2.7. Statistical analysis and graphical presentation

If not indicated the data are presented as mean ± standard deviation of three independent experiments (n=3). The level of significance was specified using Student's *t*-test of Microsoft Excel 2010. Repeated measures ANOVA using the R packages lme4 and emmeans was applied to analyze difference between cancer subtypes in the dose response curves by the help of the statistician Anna Klimova (Core Unit for Data Management and Analytics (CDMA), National Center for Tumor Diseases (NCT), Dresden). Results were defined statistically significant if a *p*-value of less than 0.05 (* < 0.05) was reached or high statistically significant with a *p*-level of less than 0.01 (** < 0.01). GraphPad Prism 4.0 was used for graphical presentation.

4. Results

4.1. Establishment and characterization of a human gastric cancer organoid biobank

4.1.1. Human gastric cancer organoids with different phenotypes, proliferation rates and typical cancer characteristics

Cancer tissue with diagnosed adenocarcinoma of the stomach or esophagus was obtained from surgical resection specimens (Figure 10A). Organoid lines were initiated in normal stomach medium after enzymatic digestion as described by Bartfeld and colleagues (Bartfeld et al. 2015). To increase the amount of cancer cells and minimize the outgrowth of normal organoids processing was optimized by picking 150 isolated tumor patches (see Material and Methods 2.2.1.2.1). Twenty different gastric cancer organoids could be established (see Appendix Table 1). The four organoid lines DD107, DD109, DD191 and DD282 were characterized in detail concerning their morphology, proliferation rate, and immunohistochemically features. These organoid lines were grown with no change in proliferation rate or phenotype over one year with a split ratio of 1:2 or 1:3 per week. In addition, freeze and thaw cycles also did not affect these growth characteristics (data not shown).

The obtained lines represented divergent morphologies indicating different subtypes of gastric cancer (Figure 10B). The DD107 originated from a stomach corpus carcinoma and had a cystic structure with a thickened epithelium. The DD109 from an AEGI had a non-coherent grape like growth pattern. The DD191 originated from an AEGII and DD282 from a stomach antrum carcinoma, and both showed a compact structure with no lumen. The DD282 was extremely resistant to mechanically dissociation. The normal organoids (DD320N, DD379N and DD392N) showed a different morphology as the cancer organoid lines. They had a cystic structure with a single layered epithelium (Figure 10B).

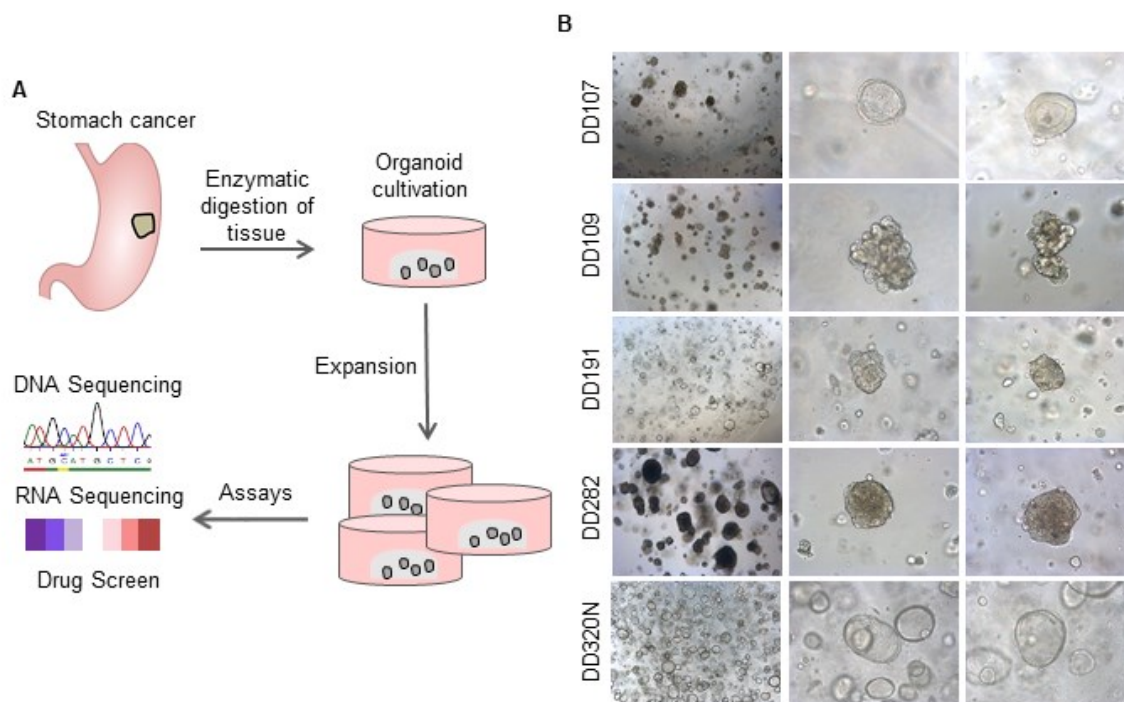


Figure 10: Human gastric cancer organoids. (A) Scheme of culture establishment and performed assays. (B) Representative overview of gastric cancer and normal organoids (scale bar 100 μm) (Seidlitz et al., 2019a).

Growth rate of organoids was analyzed using the EdU proliferation assay. A varying turnover rate was observed between the cancer and normal organoid lines. Especially, the DD107 and DD282 represented a significantly higher growth rate. The normal organoids showed the slowest proliferation (Figure 11A). In order to characterize growth factor dependency, we omitted one by one each relevant media compound for normal organoid growth (Figure 11B). The response differed widely between the cancer and normal organoid lines. Omission of A83-01, Fgf10 and WNT3A was without phenotypically impact on the cancer lines. Noggin, Egf and the combination of WNT3A plus Rspodin were important to varying degrees. However, the normal organoid lines just grew in the complete stomach medium (Figure 11B). In a xenograft experiment, the cancer organoid lines were s.c. injected into the hind legs of mice (Figure 11C). Tumor growth was observed for all lines (Figure 11D). Similar growth patterns of organoid xenografts were visible *in vivo* compared to *in vitro*. The xenograft tumors of the DD109 and DD282 organoids represented again the fastest growth whereas the DD191 showed the slowest (Figure 11D).

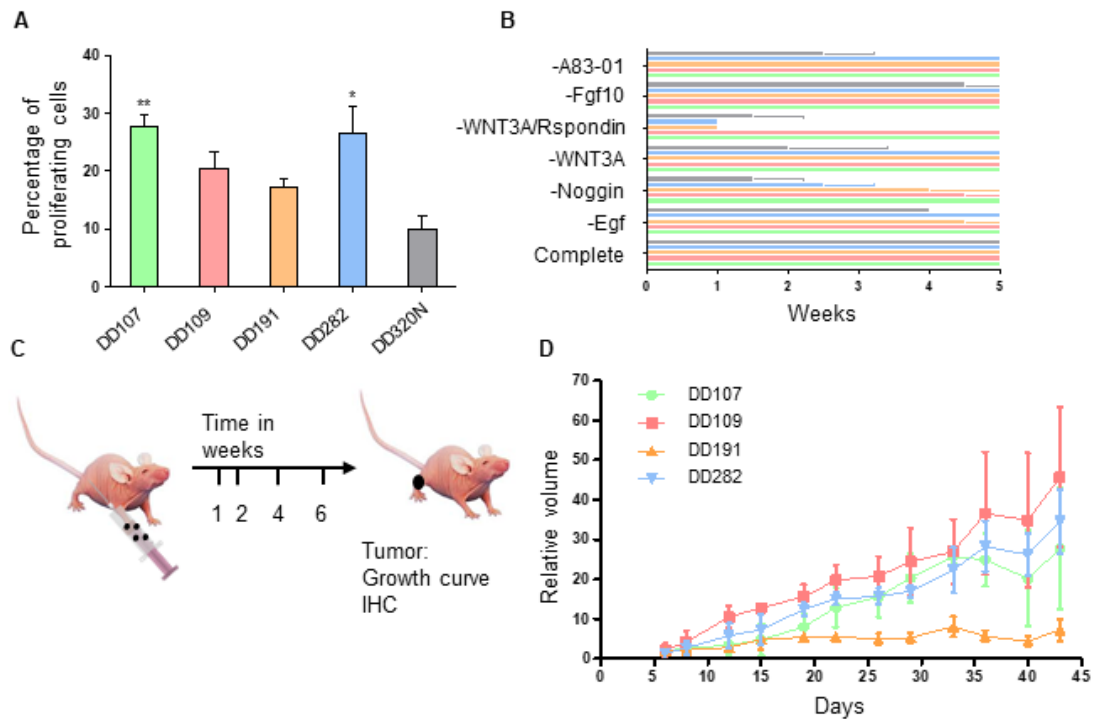


Figure 11: Cancer organoid characterization concerning proliferation. (A) Proliferation rate of gastric organoids analyzed by an EdU proliferation assay. Student's *t*-test cancer vs. normal; * < 0.5; ** < 0.01 (n=3) (B) Media component withdrawal. Each annotated component was omitted one by one from the complete medium and organoids followed over five weeks with two splits per week (n=2). (C) S.c. injection of gastric cancer organoids. (D) Growth curve of organoid xenografts (n=3 for each organoid line) (modified according Seidlitz et al., 2019a).

To analyze if organoids and xenograft tumors represented similar characteristics as the primary cancer tissue they were derived from, immunohistochemistry was performed. The gastric cancer marker cytokeratin 7 (CK7), cadherin 17 (CADH17), carcinoembryonal antigen (CEA) and PAS are routinely used by pathologists for gastric cancer diagnosis. We performed immunohistochemically stainings on these markers and showed that the organoids as well as xenograft tumors recapitulated similar characteristics as their primary cancer tissue (Figure 12A-D).

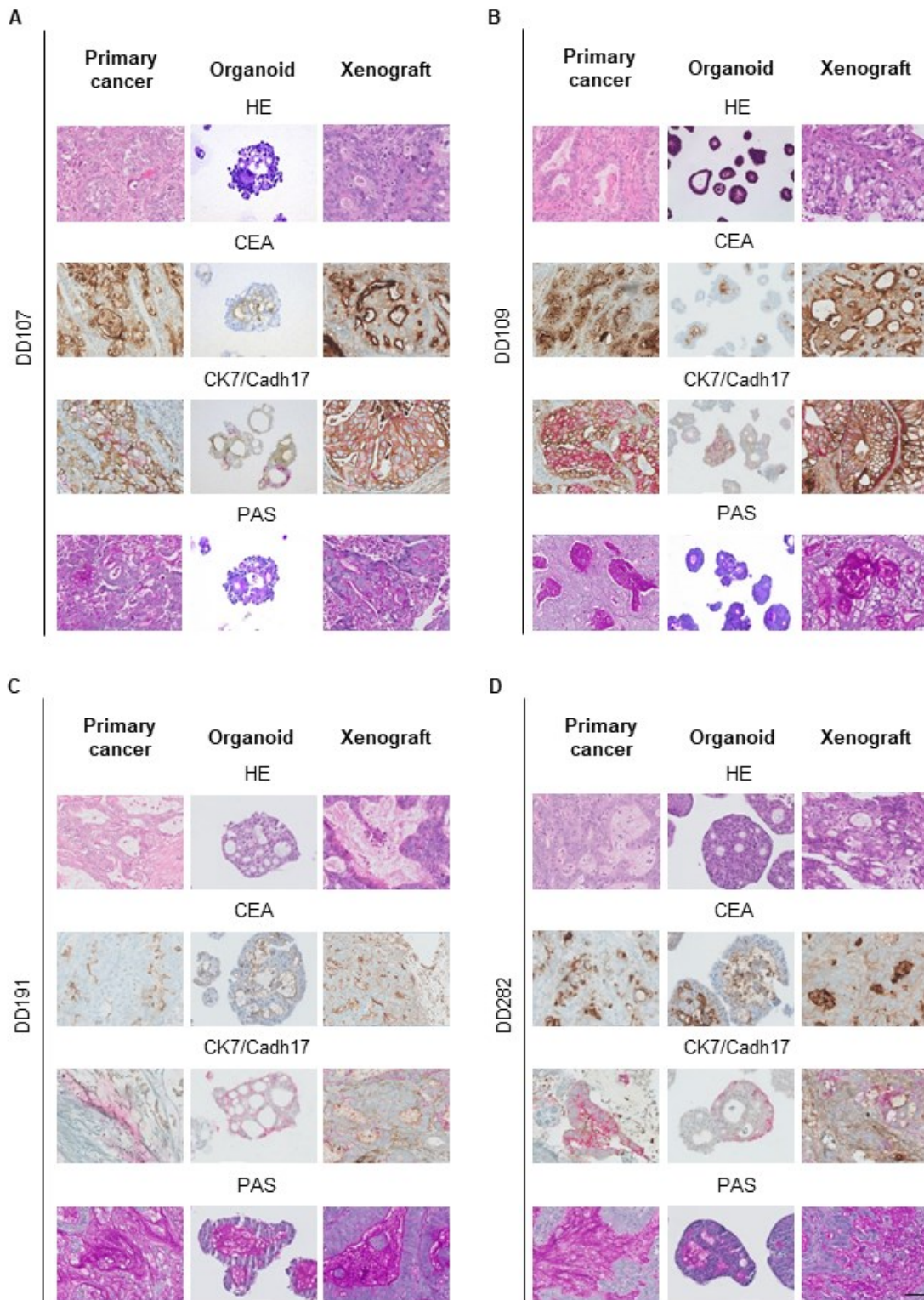


Figure 12: Immunohistochemistry comparison of gastric cancer organoids and derived xenograft tumors to primary cancer tissue. Staining for (A) DD107, (B) DD109, (C) DD191 and (D) DD282 using HE, carcinoembryonal antigen (CEA), cytokeratin 7 (CK7), cadherin 17 (CADH17), and periodic acid Schiff's reaction (PAS) of primary cancers, organoids and organoid derived xenograft tumors (scale bar 50 μ m) (Seidlitz et al., 2019a).

4.1.2. Gastric cancer organoids show divergent response to cancer treatment

The response of gastric cancer patients towards conventional chemotherapy can be categorized into different histological regression grades (Becker et al., 2011). To analyze if the obtained gastric cancer organoids also show a similar divergence in response, they were treated with conventional chemotherapeutic agents, especially 5-FU, irinotecan, oxaliplatin, docetaxel and epirubicin. The mentioned drugs are clinically used for gastric cancer treatment according the guidelines of stomach cancer

The organoids were treated with each mentioned drug at three different concentrations and incubated for 24 h or 72 h (5-FU). Afterwards, viability of organoids was analyzed using the Presto Blue viability assay. The results showed a divergent response of organoid lines to chemotherapeutics (Figure 13A-E). Especially, for 5-FU, epirubicin and irinotecan the response varied widely. In general, patterns of resistance could be documented, i.e. DD109 was relatively resistant to 5-FU and epirubicin, while DD191 responded well to the same drugs (Figure 13A, D). At the same time DD109 responded well to irinotecan treatment, while DD107 showed a response only at higher concentrations (Figure 13C). Normal gastric cancer organoids responded in a similar range as the gastric cancer organoids and displayed a differential response for 5-FU and oxaliplatin as it was also seen in the cancer organoids (see Appendix Figure 1).

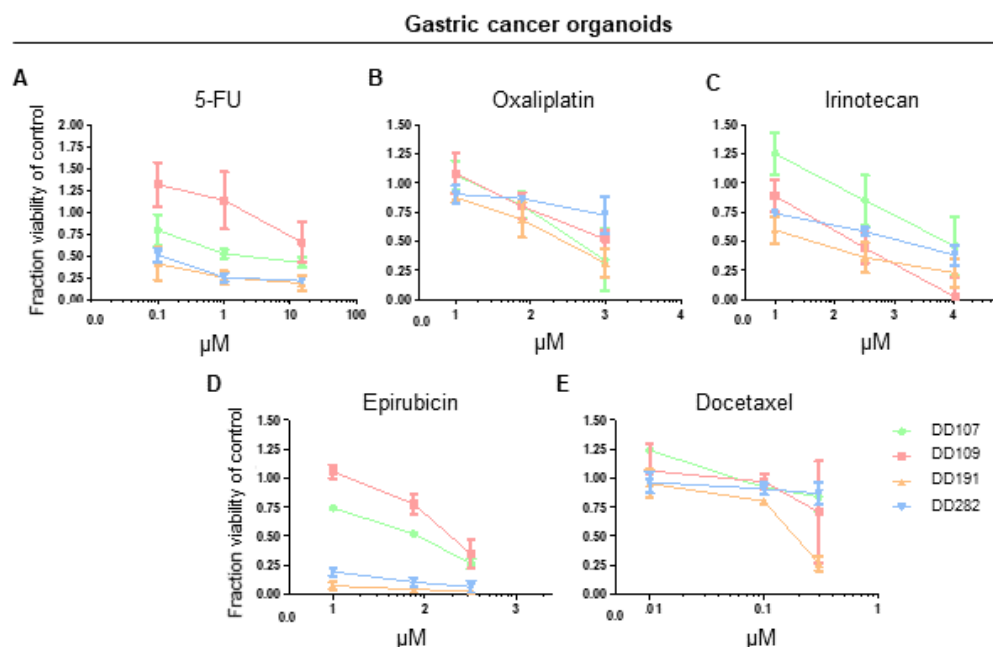


Figure 13: Gastric cancer organoids showed divergent response to conventional chemotherapy. (A-E) Viability assay after 5-FU, oxaliplatin, irinotecan, epirubicin and docetaxel treatment. Analysis for oxaliplatin, irinotecan, epirubicin and docetaxel was performed after 24 h incubation time and 5-FU was incubated for 72 h. Values were normalized to untreated control organoids of the same patient (n=3) (Seidlitz et al., 2019a).

To compare the human gastric cancer organoid chemotherapy response to typical 2D gastric cancer cell lines similar drug experiments were performed for the human cell lines AGS, KatoIII, Snu1 and Snu5 (Figure 14). The viability was analyzed as described above. In general the cell lines showed a similar response pattern as the gastric cancer organoid lines, especially for 5-FU, oxaliplatin and irinotecan (Figure 14A-C). The response of epirubicin and docetaxel varied between the used gastric cancer cell lines. The Snu1 cell line represented the strongest response to both chemotherapeutic drugs, whereas the Snu5 respond only at higher concentrations (Figure 14D-E). Compared to organoids the classically cultivated 2D cell lines were more sensitive to the treatment resulting in lower IC50 values. The organoid lines showed a tendency for higher resistance especially for oxaliplatin and irinotecan. The IC50 values for the cell lines and the organoids are presented in Table 13. Taken together, with the *in vitro* chemotherapy experiments we were able to define an active chemotherapeutic drug for each organoid line and additionally resistance patterns.

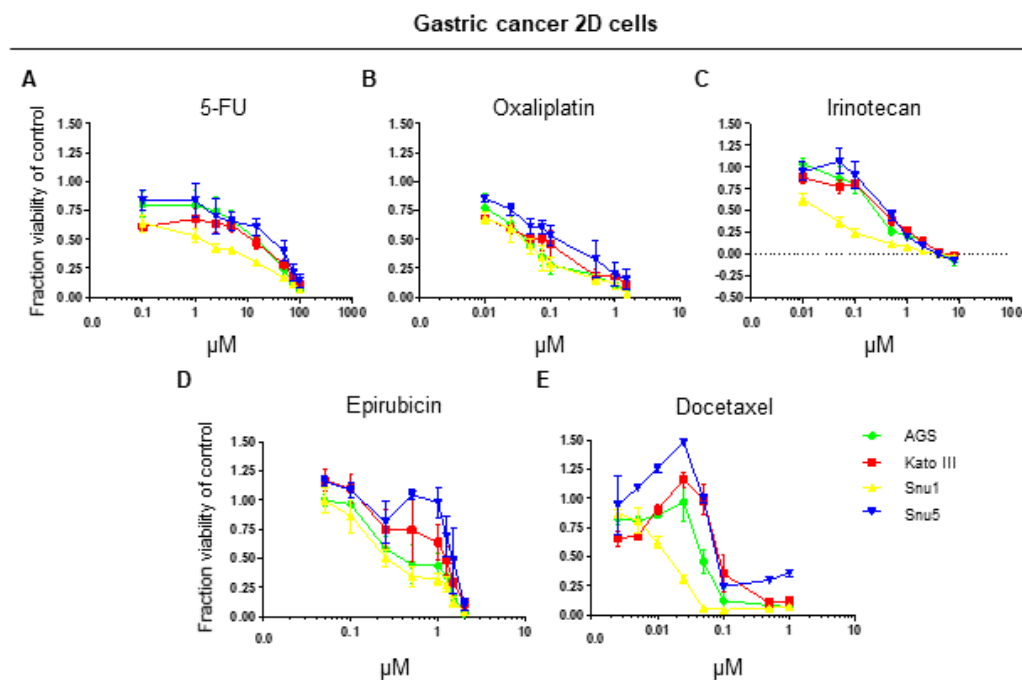


Figure 14: Chemotherapy of classical gastric cancer cell lines. (A-E) Viability assay of AGS, Kato III, Snu1 and Snu5 after 5-FU, oxaliplatin, irinotecan, epirubicin and docetaxel treatment. Analysis for oxaliplatin, irinotecan, epirubicin and docetaxel was performed after 24 h incubation time. The 5-FU was incubated for 72 h. Values were normalized to the untreated cell line (n=3) (Seidlitz et al., 2019a).

Table 13: IC50 calculation of gastric cancer organoids and cell lines (Seidlitz et al., 2019a).

Chemotherapeutics (μM)	Gastric cancer organoids				Gastric cancer cell lines			
	<i>DD107</i>	<i>DD109</i>	<i>DD191</i>	<i>DD282</i>	<i>AGS</i>	<i>Katoll3</i>	<i>Snu1</i>	<i>Snu5</i>
5-FU	0.19	2.90	0.02	0.06	0.73	3.53	0.11	0.50
Oxaliplatin	1.54	1.51	2.04	-*	0.03	0.12	0.04	0.11
Irinotecan	2.03	1.95	1.05	6.22	0.23	0.51	0.04	0.51
Epirubicin	2.93	1.53	0.11	0.43	0.30	2.72	0.18	-*
Docetaxel	-*	0.12	0.12	-*	0.06	0.22	0.01	0.06

*no IC50 calculation possible by GraphPad due to irregular curve shape or no response (see Figure 13 and 14)

4.1.3. Targeted therapy in gastric cancer organoids

Personalized anticancer treatment can increase patients response, improve overall survival and revolutionized in selected entities already current oncological treatments (Paterson et al., 2013). Nevertheless, for gastric cancer many approaches targeting the EGFR, hepatocyte growth factor receptor (HGFR) or fibroblast growth factor receptor (FGFR) pathway failed in the past by the lack of a promising potential biomarker (Lordick and Janjigian, 2016). To investigate if the newly established cancer organoids can function as living biomarkers for therapy response, mutations and activated pathways of each line were defined (Table 14). The gastric cancer organoid lines and the corresponding normal tissue were analyzed by whole genome sequencing. Results presented a broad mutational spectrum matching to typically detected gastric cancer features.

The DD107 displayed an activating mutation of the *ERBB2* gene by an amino acid change from serine to phenylalanine at position 310 (Ser310Phe). The mutation is located at the extracellular domain of the HER2/neu receptor and led to a pathway activation. It has been reported to be drug-sensitive (The Cancer Genome Atlas Research Network, 2014; Kavuri et al., 2015). Additionally, an amplification of the *ERBB2* gene in the DD109 line was found, which could be confirmed by immunohistochemistry (Figure 15A). Both lines and the DD282 with a variant of unknown significance (VUS) in the *ERBB2* gene (Gly201Asp) were used for HER2/neu targeting. The 0.1 μM treatment with the monoclonal antibody trastuzumab after 72 h resulted in a viability decrease to 70.6 % for DD107, to 79.2 % for DD109 and to 85.6 % for DD282 (Figure 15B). The VUS in DD282 might therefore indeed constitute an activating mutation. In the clinic trastuzumab is often applied in a combinatorial regime with 5-FU. Therefore, the two lines with known alterations in the HER2/neu pathway were treated with trastuzumab and additionally 5-FU (Figure 15C, D). An additive effect of 5-FU and trastuzumab was observed for both lines with a complete loss of the cultures at the highest concentration whereas 5-FU alone just led to a reduction of viability to maximally 40 %. To further characterize the specific effect of trastuzumab on the pathway we analyzed the RTK/RAS

pathway by determining the phosphorylation level ERK1/2 for the gastric cancer organoid lines DD107, DD109 and DD282 (Figure 15E, F). No change in phosphorylation level of DD107 and DD282 was observed. DD109 downregulated the phosphorylation of ERK1/2 after 0.1 μ M trastuzumab treatment to 55 %. All in all, DD107 with the activating mutation showed the highest response in the viability assay but signaled through a RTK/RAS independent way and DD109 with the ERBB2 amplification downregulated the RTK/RAS pathway upon trastuzumab treatment.

The DD109 organoid line harbored a bi-allelic loss of *CDKN2A*. *CDKN2A* encodes for the tumor suppressor p16 playing an important role in proliferation regulation by inhibiting the cyclin-dependent kinase 4/6 (CDK4/6) during the cell cycle. The DD109 with the bi-allelic loss, the DD191 with no *CDKN2A* mutation and the normal organoids DD320N were treated for 24 h with 5 μ M palbociclib. Palbociclib is a small molecule which inhibits the kinase activity of CDK4/6 and leads to cell cycle arrest. Successful inhibition was analyzed using the EdU proliferation assay (Figure 16A). The DD191 and DD320N showed a complete loss of proliferation after treatment. However, the DD109 displayed a strong decrease in proliferation with still 2 % proliferating cells. Long-term treatment with 10 μ M palbociclib including two times passaging resulted in a loss of the DD191 and DD320N cultures, indicating a complete inhibition of proliferation. DD109 organoids were still present and phenotypically unharmed (Figure 16B). We concluded that the loss of p16 in DD109 led to the survival of the line due to insufficient blockage of CDK4/6 by palbociclib.

Table 14: Targetable mutations found in DD107 and DD109 (Seidlitz et al., 2019a).

Patient ID	Mutation								Targeting	
	Gene (Homo sapiens)	Type	Location	Frequency / Zygosity	Nucleotide change	Amino acid change	Fold change	Pathway	Type	Name
DD107	<i>ERBB2</i>	SNV	Chromosome 17	100 % / Homozygous	C929T	S310F	-	Activating HER2 growth receptor signaling	Monoclonal antibody	Trastuzumab
DD109	<i>ERBB2</i>	CNV	Chromosome 17	-	-		+93x (Gain)	Increasing number of HER2 receptors	Monoclonal antibody	Trastuzumab
	<i>CDKN2A</i>	CNV	Chromosome 9	-	-		-77x (Loss)	Loss of cell cycle suppressor	Inhibitor	Palbociclib (PD-0332991)

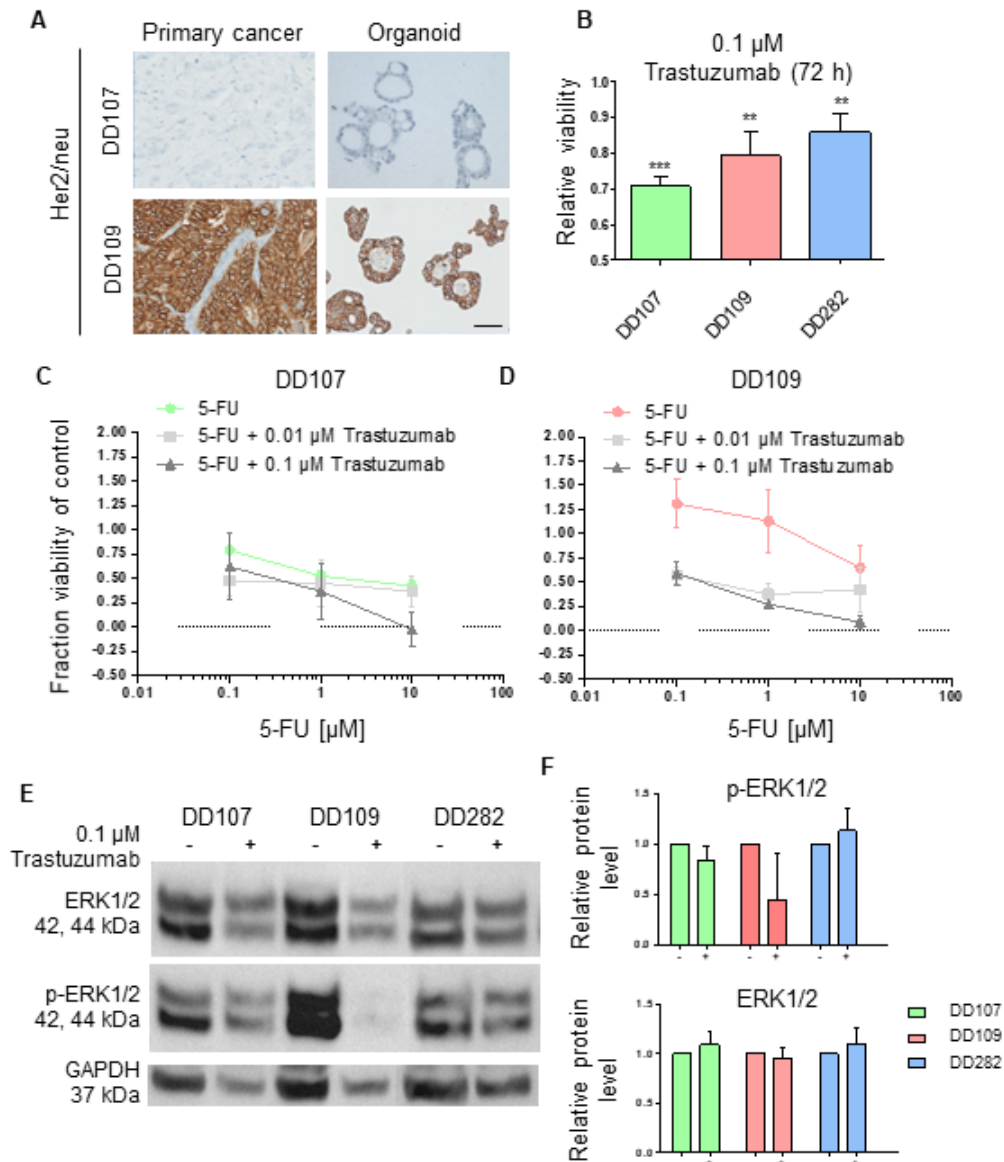


Figure 15: Targeting of HER2/neu receptor pathway using trastuzumab. (A) IHC for ERBB2 of DD107 and DD109 (scale bar 50 μ m). (B) Cell viability measurement after 72 h 0.1 μ M trastuzumab treatment (Student's *t*-test treated vs. untreated; ** < 0.01; *** < 0.001; n=3). (C+D) Cell viability assay after combined chemotherapy regimen 5-FU plus trastuzumab for DD107 and DD109. Values were normalized to untreated control (n=3). (E+F) Western blot and densitometric analysis of phosphor-ERK1/2 after 72 h 0.1 μ M trastuzumab treatment (n=3) (modified according Seidlitz et al., 2019a).

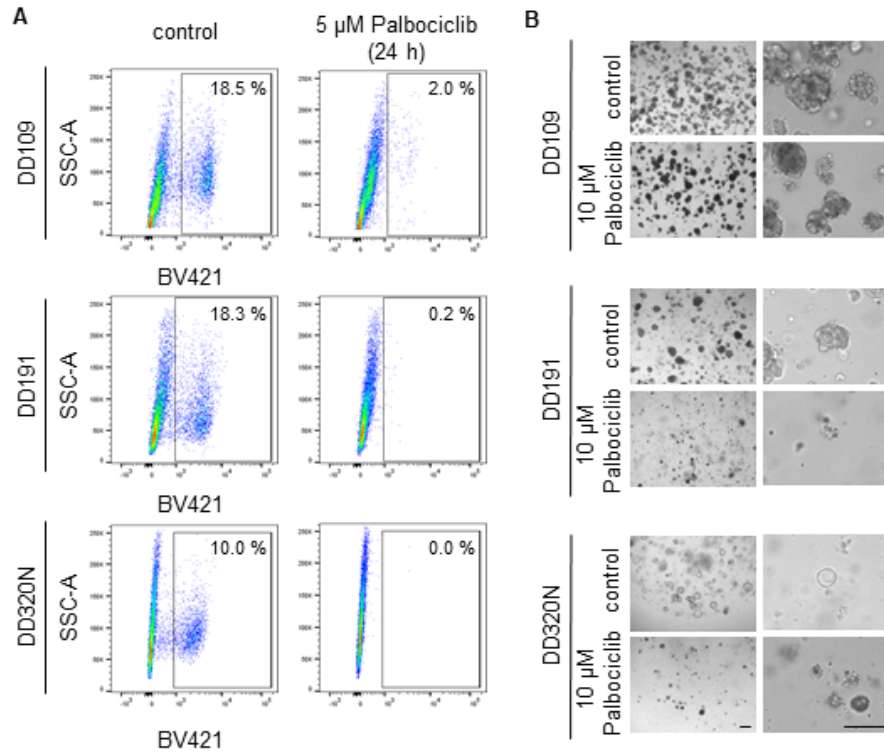


Figure 16: Cell cycle arresting by small molecule targeting. (A) Targeting of CDK4/6 in DD109 (bi-allelic loss of CDKN2A) and DD191 (no CDKN2A alteration) as well as DD320N (normal control) using 10 μ M palbociclib. Proliferation was analyzed after 24 h of treatment using an EdU proliferation assay (n=3). (B) Long-term palbociclib treatment with 5 μ M (11 days, 2 splits) (modified according Seidlitz et al., 2019a)..

4.2. Mouse organoids allow cancer subtype modelling with a defined mutational spectrum

4.2.1. Generation of mouse gastric tumor organoids

Human gastric cancer organoids allowed a detailed analysis of observed alterations for each individual patient. However, the high number of mutations affected the interpretation of targeted therapies, as the result of such a treatment needs to be interpreted taking into account the whole mutation spectrum of each specific organoid line. In order to establish organoids with a defined mutational spectrum for in depth analysis of pathway interference, we decided to cross mice with inducible alleles of frequently mutated genes in subtypes of gastric cancer and generate organoids from these mice. In order to define relevant genes, we explored the TCGA dataset and used the cBio portal to define altered pathways for each subtype of gastric cancer (Cerami et al., 2014; Jianjiong Gao et al., 2014). For each pathway we next defined inducible alleles that would allow us to manipulate the pathway. To analyze the CIN subtype with mutations related to the RTK/RAS pathway and TP53 signaling we combined the inducible mutated alleles *Kras*^{G12D/+} and *Tp53*^{R172H/+} (named RTK/RAS activated tumor model). In order to characterize the GS subtype typically harboring mutations in the WNT pathway and genes relevant for cell adhesion, a combination of the floxed *Apc*^{fl/fl} and *Cdh1*^{fl/fl} alleles was used (named diffuse tumor model). To model gastric cancers showing mutations in the WNT and TP53 signaling pathways we combined the floxed *Apc*^{fl/fl} and inducible *Tp53*^{R172H/+} alleles (named WNT activated tumor model). A fourth model models the TCGA classified EBV subtype, which is characterized by mutations in the phosphoinositide 3-kinase (PI3K)/ protein kinase B (AKT) pathway and genes involved in chromatin remodeling. We therefore combined the inducible *Pik3ca*^{H1047R/+} mutation and the floxed *Arida*^{fl/fl} allele (named EBV associated tumor model) (see also Material and Methods Table 11). Oncogenic driver mutations are preceded by floxed stop sequences, while for the other genes floxed alleles were used.

Mice containing the relevant alleles were crossed, and genotypes for each model confirmed by PCR. Next, mouse organoids were prepared as described in the literature and procedure is figured out in Figure 17 (Stange et al., 2013; Bartfeld et al., 2015). The stomach was opened along the large curvature, washed in D-PBS, stretched out on cork. The corpus region was isolated and cut in small pieces. Tissue pieces were incubated in chelating buffer with 10 mM EDTA for 1 h at room temperature and pressure was applied on the tissue, which results in the extrusion of stomach glands. The glands were embedded in Matrigel and covered with corresponding normal murine stomach medium (Figure 17A). After 48-72 h round cystic organoids with a thin epithelial layer were visible. The uninduced stomach organoids of each subtype displayed a similar morphology (Figure 17B).

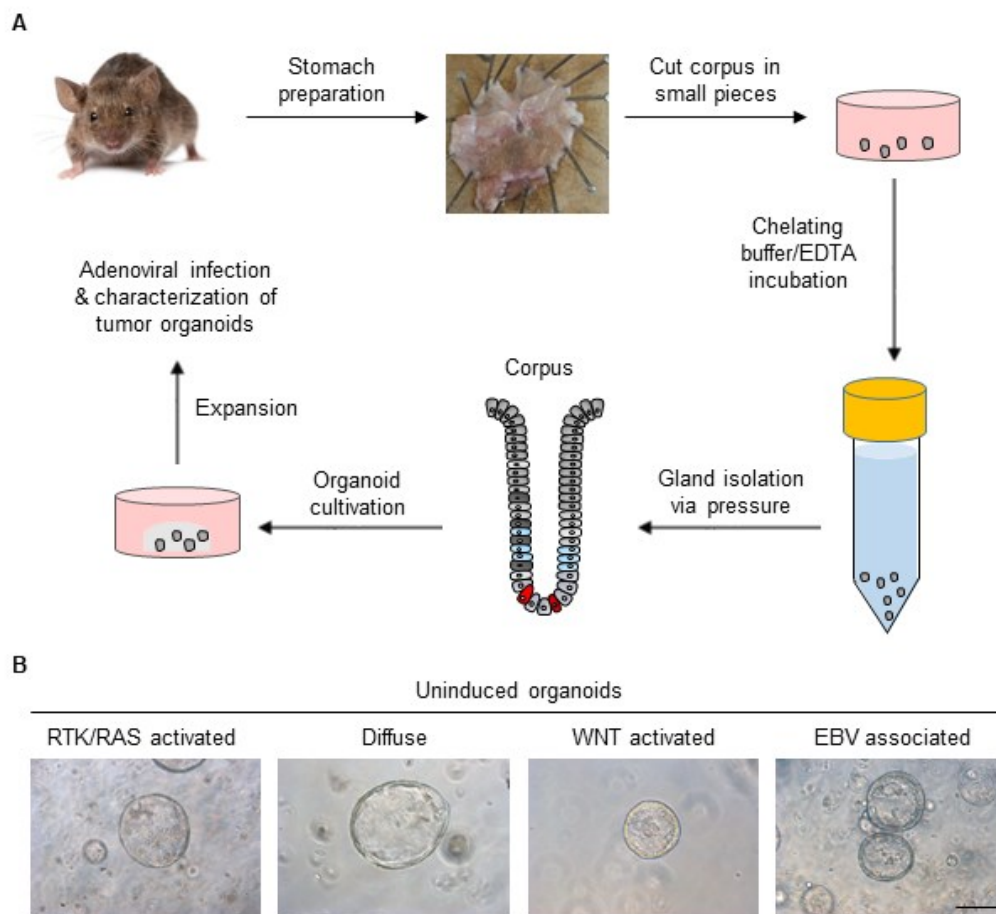


Figure 17: Process of mouse gastric organoid generation. (A) Experimental setup of organoid generation. (B) Morphology of uninduced organoids representing a cystic structure with a thin epithelium (scale bar 100 μ m).

Gastric cancer was generated by infecting the uninduced organoids with a Cre expressing adenovirus, which also expresses the green fluorescent protein (GFP). Cre expression in the organoids led to recombination of LoxP sides, resulting in an activation or deletion of the mutated alleles, respectively. Thus, organoids were mechanically dissociated, resuspended in medium without any antibiotics containing the virus and spin infected. After an incubation for 1 h at 37°C organoids were embedded in Matrigel (Figure 18A). Successful infection was verified by a positive GFP signal 24 h post infection (Figure 18B). Seventy-two hours after infection selection for recombined genes started. The selection was performed by withdrawal of growth factors from the medium that activate the now mutated pathways (see Material and Methods Table 11). Successfully mutated organoids grew independent of the respective growth factors, resulting in the death of non-recombined organoids. The RTK/RAS activated tumor model had an activating mutation in the *Kras* gene resulting in an active EGFR signaling. In this case, Egf was released from the medium. The diffuse and the WNT activated tumor models each contained a floxed *Apc* allele resulting in WNT pathway activation. The loss of

Apc allowed a withdrawal of WNT3A plus Rspodin from culture medium to enrich the recombined tumorigenic organoids. The EBV associated tumor model contained a mutation in the PI3K/AKT pathway and allowed selection by addition of 50 nM Mek inhibitor to block *Pik3ca* signaling (see Material and Methods Table 11) (Matano et al., 2015). After selection for approximately 7-14 days, DNA was extracted and analyzed for successful recombination via PCR with further gel electrophoresis (Figure 18C-F). Generated tumor organoids were used for further gastric cancer characterization.

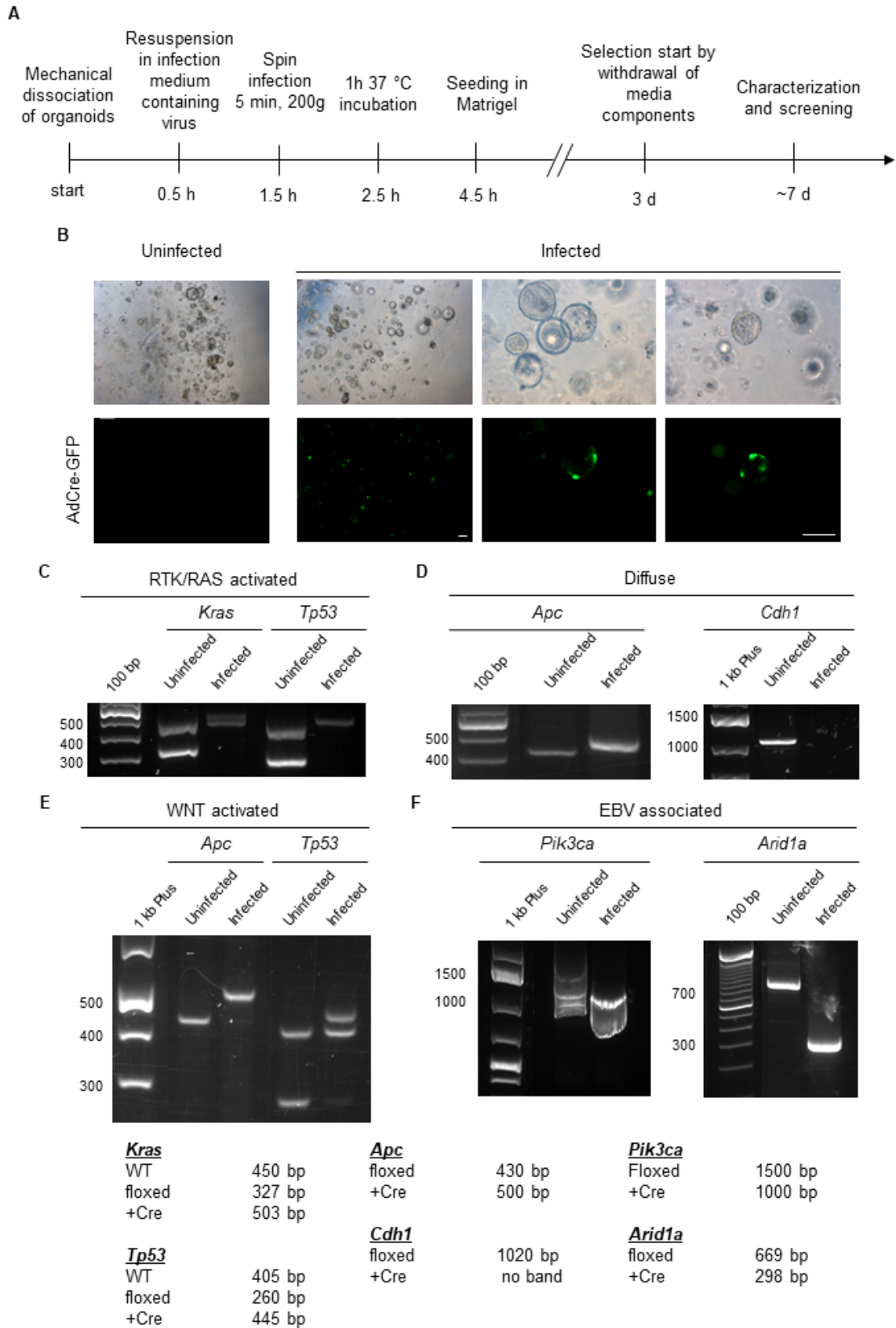


Figure 18: Adenoviral infection of normal organoids to generate gastric tumor mouse organoids. (A) Experimental procedure of adenovirus infection. (B) Fluorescence microscopy of successful viral infection 24 h post infection (scale bar 100 μ m). (C-F) Genotyping PCR's of infected organoids of each subtype to proof activation of mutations post infection.

4.2.2. Characterization of mouse gastric tumor organoids concerning morphology, pathway activity and treatment response

Generated mouse gastric tumor organoids showed a divergent morphology. The uninduced stomach organoids had a cystic structure with a thin single layered homogenous lumen. The organoids of the RTK/RAS activated tumor model showed a thickened irregular epithelium, which was partly multi-layered. The *Cdh1* mutation in the diffuse tumor model resulted in a complete structural alteration towards a grape-like form with no lumen compared to normal organoids, induced by the loss of *Cdh1*/E-cadherin mediated cell-cell connections. The WNT activated tumor model was characterized by an irregular thin layered epithelial structure with smaller organoids in size compared to the RTK/RAS activated model. In contrast, the EBV associated model had a compact organoid morphology with a cystic structure and a thick epithelial lumen (Figure 19).

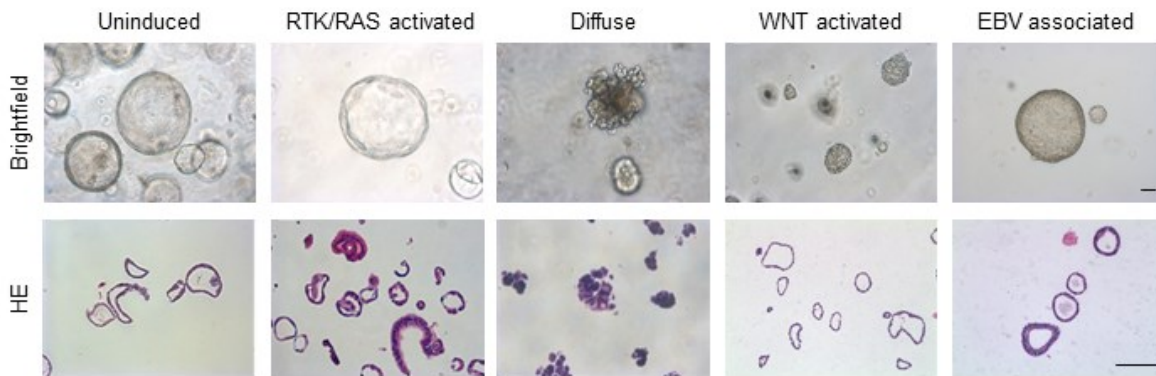


Figure 19: Morphologic characterization of mouse gastric tumor organoids. The organoids of the gastric tumor subtypes represented different morphologies by brightfield imaging as well as HE staining (scale bar 100 μ m).

Further characterization concerning niche independency, proliferation and organoid formation efficiency was performed using the RTK/RAS activated as well as the diffuse gastric tumor model. For analyzing the independency of growth factors necessary for the growth of normal organoids (niche independency) of generated tumor organoids, a medium withdrawal experiment was performed. Egf, Noggin, Rspodin, Rspodin plus WNT3A as well as Fgf10 was each omitted from the culturing medium. The tumor organoids of both models were completely unharmed whereas the uninduced organoid line was lost at different time points during withdrawal. After 2-3 weeks uninduced organoids were not proliferating in any medium with an omitted component (Figure 20A). To further test the ability of the tumor organoids to generate new organoids from single cells, organoids were dissociated to single cell level and 100 single cells were plated in a well of a 48 well plate. Organoids were counted after seven days of culturing. An increase in organoid formation efficiency was observed especially for the diffuse gastric cancer model compared to the normal organoids. Approximately 30 single cells

formed organoids in the case of the diffuse tumor model, whereas the RTK/RAS activated tumor model formed around 15 and the uninduced organoid line less than 10 (Figure 20B).

Personalized cancer treatment becomes more and more important. Nevertheless, to understand and improve the effect of targeted therapies, relevant model systems need to be established. These model systems need to have an activation of relevant signaling pathways, while at the same time showing a defined mutational spectrum to allow clear interpretations. To test if our generated mouse gastric tumor organoids are useful for such analyses, we first targeted the altered pathways in each model. The RTK/RAS activated tumor model contained an activating *Kras*^{G12D} mutation. Organoids of this model were treated with 10 μ M trametinib for 72 h. Trametinib is a small molecule that inhibits the EGFR signaling pathway downstream of KRAS the ERK1/2 kinase. This resulted in a block of proliferation and differentiation. A successful inhibition was analyzed by performing Western blot to detect the phosphorylation level of ERK1/2. Uninduced as well as tumor organoids showed a decrease in phosphorylated ERK1/2 (Figure 20C). The uninduced organoid culture was supplemented with Egf to keep the line alive and explained the observed targeting response. However, the EGFR signaling pathway of the RTK/RAS activated tumor model was completely blocked by trametinib treatment (Figure 20C).

By floxing out *Apc*, the diffuse tumor model contains a non-functional destruction complex activating the translocation of β -catenin into the nucleus and dimerization with the T cell factor (TCF), resulting in the activation of WNT signalling. This led to an increase in expression of the WNT signature genes *Axin2* and *Ccnd1*. Treatment of the diffuse tumor model with calphostin C, a potent inhibitor of the dimerization of the β -catenin/TCF complex, reduced downstream WNT target gene expression of *Axin2* and *Ccnd1* compared to normal organoids (Figure 20D).

As mentioned above the treatment of aberrantly altered pathways within the generated human gastric cancer organoid lines is often difficult to interpret, as additional mutations interfere with the inhibited pathway. To have a clean system for therapy testing we generated the described four different mouse tumor organoid lines. Activation of just two known cancer driver genes resulted in a robust transformation of organoids with different phenotypes. The RTK/RAS activated tumor model constitutes a cellular system to test the effect of drugs downstream of mutated *Kras*, while the diffuse gastric tumor model can be used to test WNT inhibitors downstream of the *Apc* complex. Taken together, the models can be used in the future to test therapeutic interventions in a defined genetic background.

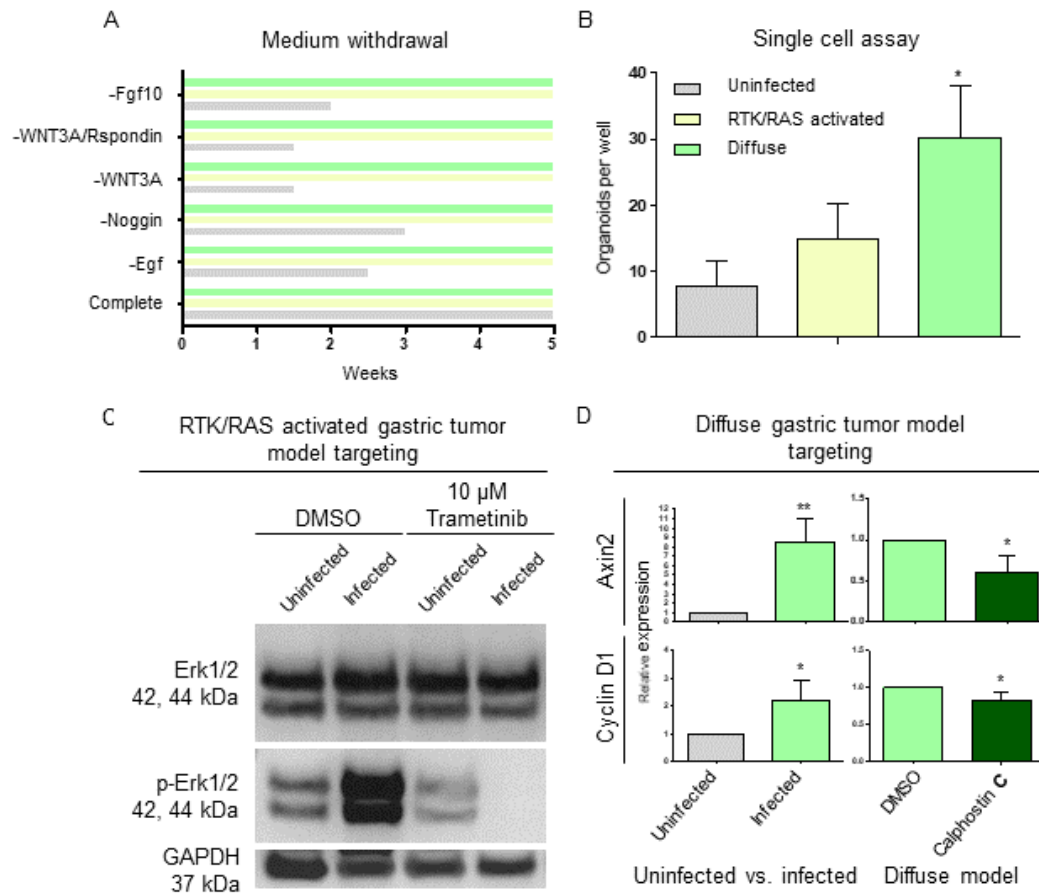


Figure 20: Gastric cancer characterization of the RTK/RAS activated and diffuse gastric tumor model. (A) Medium withdrawal experiment to finally check full organoid transformation. (B) Determination of organoid formation efficiency by plating single cells (Student's *t*-test uninfected vs. tumor model; * < 0.05; n=3). (C) RTK/RAS activated gastric tumor model targeting by 10 μM trametinib treatment for 72 h. Western blot experiment for ERK and phospho-ERK1/2 before and after treatment of uninduced and gastric tumor organoids. (D) Diffuse gastric tumor model targeting with 5 mM calphostin C treatment for 24 h (Student's *t*-test uninfected vs. infected and DMSO vs. calphostin C; * < 0.05; ** < 0.01; n=3).

4.3. Gastric cancer subtypes show different patterns of development, growth and dissemination in a gastric cancer mouse models

4.3.1. Generation of a stomach specific mouse model

For manipulation of different gastric cancer subtypes a tamoxifen-inducible (ER^{T2}) expressing Cre mouse line was needed with expression uniquely in the stomach epithelium. There are several mouse lines used for modelling of gastric cancer but they are either not stomach specific (i.e. keratin 19 (KRT19)-Cre, Tff1-Cre) or specific for a certain cell type (i.e. ATPase H⁺/K⁺ transporting subunit beta (Atp4b)-Cre, Calpain 8 (Capn8)-Cre) (Zhao et al., 2009; Zhao et al., 2010; Zhao et al., 2017; Kinoshita et al., 2018). Screenings of mouse gene expression databases (i.e. Gene Expression Omnibus (GEO), Gene Expression Database (GXD) and Bio Gene Portal System (BioGPS)) for stomach specific expression resulted in limited number of candidates. Further literature analysis identified the *Annexin10* (*Anxa10*) gene as a potential candidate. ANXA10 is a calcium-dependent phospholipid-binding protein expressed by all cells of the stomach corpus epithelium. A clear function of the protein has not yet been determined. IHC for ANXA10 showed a strong expression in the whole stomach gland. All other tissues were negative, except a slight but clear positivity within the glomerular capsule and the convoluted tubes of the kidney (Figure 21A).

Using classical homologous ESC recombination an internal ribosomal entry site (IRES)-CreER^{T2} cassette was inserted in frame downstream of the last *Anxa10* exon to generate the *Anxa10*-CreER^{T2} mouse line (Figure 21B). Functionality was analyzed by crossing the *Anxa10*-CreER^{T2} line with the Cre reporter line Rosa26-LSL-LacZ. The Rosa 26 (reverse oriented splice acceptor, clone 26) locus is a constitutive and ubiquitous expressed locus which is a frequently used targeting locus for expression of genes of interest. After tamoxifen i.p. application, the *Anxa10* driven Cre recombined the Lox-Stop-Lox sequence, resulting in the expression a β -galactosidase. LacZ staining was performed to visualize β -galactosidase activity. Among all tissues only the antrum and corpus of the stomach stained positive. The expression was patchy, but could be seen throughout the whole gland. The observed patchiness is most likely a result of the relative low expression of the *Anxa10* gene within the stomach. This is in contrast to i.e. the Cre activity in the Villin-CreERT2 line, which is based on the extremely high expression of the gene villin in the intestine. All other tissues including the kidney were negative for LacZ (Figure 21C). The patchiness of the mouse model is of benefit in case of the generation of gastric cancer models, where a widespread induction is not desirable but rather a restricted induction in a few loci (Seidlitz et al., 2019b).

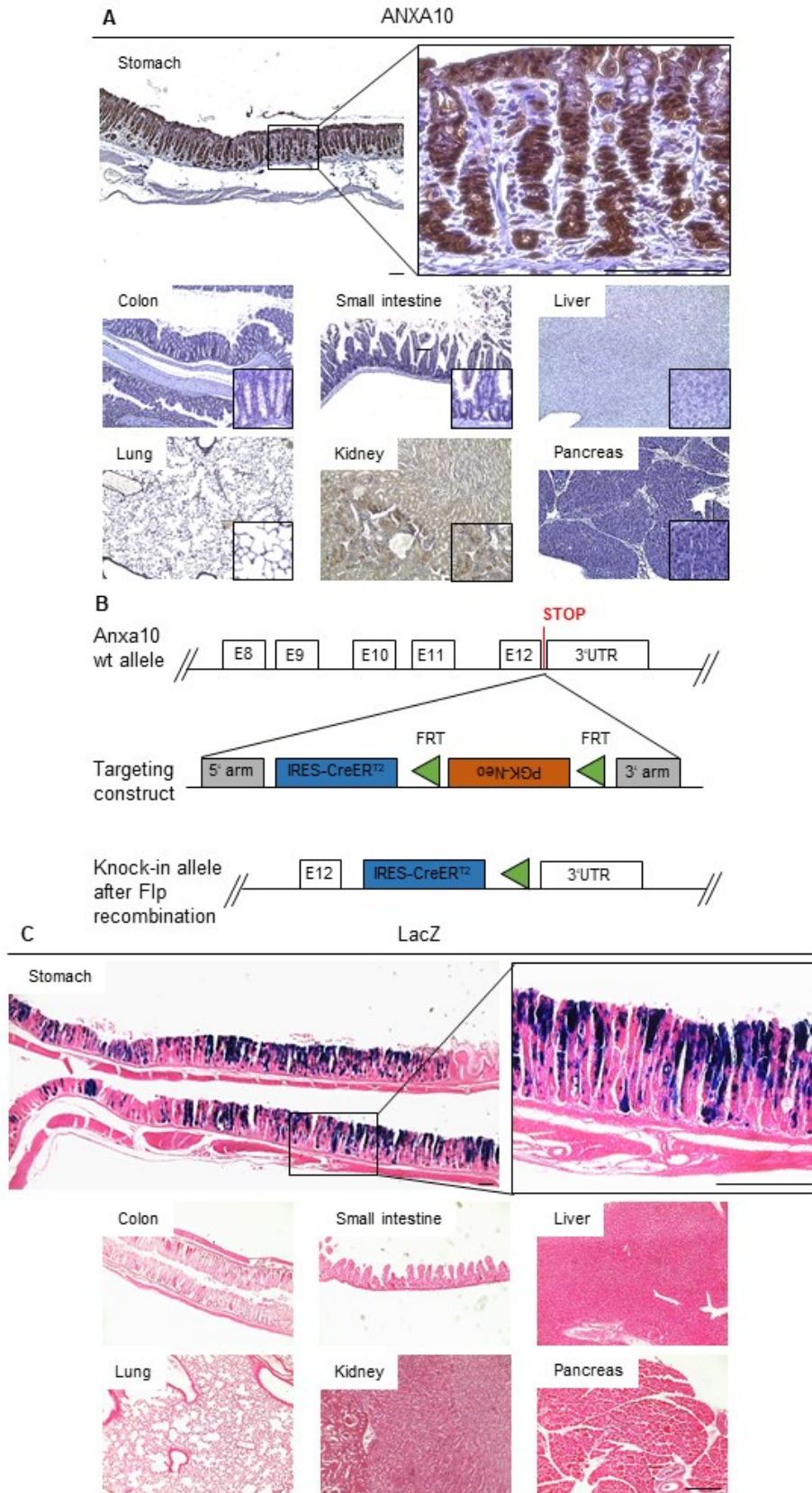


Figure 21 Anxa10-CreER^{T2} mouse-a stomach specific mouse model. (A) ANXA10 IHC of stomach, colon, small intestine, liver, lung, kidney and pancreas. (B) Knock-in construct of the inducible Anxa10-CreER^{T2} mouse. IRES-CreER^{T2} was inserted downstream of exon 12 via homologous recombination. (C) Expression of Rosa26-LacZ in Anxa10⁺ cells in stomach, colon, small intestine, liver, lung, kidney and pancreas tissue 48 h after 5 mg tamoxifen application (scale bar 100 μ m) (modified according Seidlitz et al., 2019b).

4.3.2. Definition of characteristic gastric cancer subtype related alterations

To generate subtype specific gastric cancer mouse models the TCGA database was used to define characteristic mutations and altered pathways. Frequent mutations or genomic alterations were found in genes belonging to the RTK/RAS, PI3K/AKT, WNT, TP53, TGF- β , cell adhesion and chromatin remodelling pathway. We focused on the CIN and GS subtype by defining a set with frequently altered genes and calculated the percentage of patients with altered pathway per molecular subtype. The CIN subtype is characterized by a high percentage of patients with TP53 pathway alterations as well as activated RTK/RAS pathway. In addition, we found the TGF- β , WNT and PI3K/AKT to be frequently affected. The CIN pathway was therefore modeled by combining as a basis alleles of the TP53 ($Tp53^{R172H/+}$) and the RTK/RAS ($Kras^{G12D/+}$) pathway plus TGF- β by adding a $Smad4^{fl/fl}$ allele (Table 15). The GS subtype is characterized by a high percentage of mutations in $Cdh1$ and $RhoA$, both genes being associated with cell adhesion. In addition, the next top three pathways were TGF- β , RTK/RAS and WNT. We chose to add to a $Cdh1^{fl/fl}$ allele as the basic mutations in the RTK/RAS plus TGF- β and RTK/RAS plus WNT pathway: GS1 ($Cdh1^{fl/fl}$; $Kras^{G12D/+}$; $Smad4^{fl/fl}$) and GS2 ($Cdh1^{fl/fl}$; $Kras^{G12D/+}$; $Apc^{fl/fl}$) (Table 15).

Table 15: Gastric cancer subtype modelling using the Anxa10-CreER^{T2} stomach specific mouse.

Subtype	Mutations
CIN subtype	$Kras^{G12D/+}$; $Smad4^{fl/fl}$; $Tp53^{R172H/+}$
GS1 subtype	$Kras^{G12D/+}$; $Smad4^{fl/fl}$; $Cdh1^{fl/fl}$
GS2 subtype	$Kras^{G12D/+}$; $Apc^{fl/fl}$; $Cdh1^{fl/fl}$

4.3.3. CIN subtype alterations in RTK/RAS, TP53 and TGF- β pathway led to the intestinal CIN model of gastric cancer

As described above we combined the $Kras^{G12D/+}$, $Tp53^{R172H/+}$ as well as $Smad4^{fl/fl}$ lines with the Anxa10-CreER^{T2} line to model the CIN subtype (Table 15). Tamoxifen was applied i.p. and mice analyzed after different time points. Mice could be observed over a period of 12 weeks p.i., a longer monitoring was not possible due to the tumor burden. Up to three weeks mice represented a dysplastic transformation of stomach epithelium (Figure 22A, B2). Early cancer of T1/T2 with invading the submucosa and later the muscularis propria developed between week 2 and 8 p.i. (Figure 22A, B3). Invasion of subserosa was observed between week 8 and 10 while reaching T3/T4 (Figure 22A, B4). Metastases in the liver and lung were firstly found at week 10 p.i. (Figure 22A, B5).

Detailed analysis of stomach specific cell types revealed pronounced changes in the normal glandular distribution of cell types. In the dysplastic stomach the proliferating Ki67⁺ cells shifted down to the gland bottom and presented a similar localization as the Pgc⁺ chief cell like cells (Figure 22B7, B17). A strong increase in mucus within the stomach gland was documented in PAS staining (Figure 22B12). Interestingly, a complete loss of parietal cells was observed 2 weeks p.i. (data not shown). The early cancer T1/T2 displayed a well differentiated glandular morphology of tumor cells, with Pgc⁺ chief cell like cells remaining at gland bottoms, while parietal continued to be not detectable (Figure 22B18). Proliferating cells were found throughout the whole tumor (Figure 22B8). The tumors became clear visible by PAS staining as they were mucus deprived compared to the surrounding dysplastic glands (Figure 22B13). At 8 to 12 weeks, advanced cancer T3/T4 developed showing an invasion and in some cases penetration of the subserosa (Figure 22B4, B5). While some tumor regions remained a well differentiated glandular structure, others developed into poorly differentiated cancer. The cell lineage composition and distribution remained comparable with that described for early cancer (Figure 22B9-10, B14-15, and B19-20). Of note, the differentiated cell type of Pgc⁺ chief cell like cells remained to be present in advanced tumors even in poorly differentiated areas (Figure 22B19). The advanced tumors T4 represented metastatic spread to the lung and liver (Figure 22C). The metastases showed a glandular solid growth pattern with a similar tumor morphology as the primary cancer. Expression of cytokeratin 20 (CK20), a marker of gastrointestinal tissue normally not expressed in liver and lung, as well as ANXA10, a specific gastric-epithelial marker, was detected in lung and liver metastases (Figure 22C).

In summary, the used genetic alterations as described in the TCGA for the CIN recapitulated the main features of the described intestinal gastric cancer subtype according to Lauren classification (Lauren, 1965). We therefore refer to this mouse model as the “intestinal CIN model”.

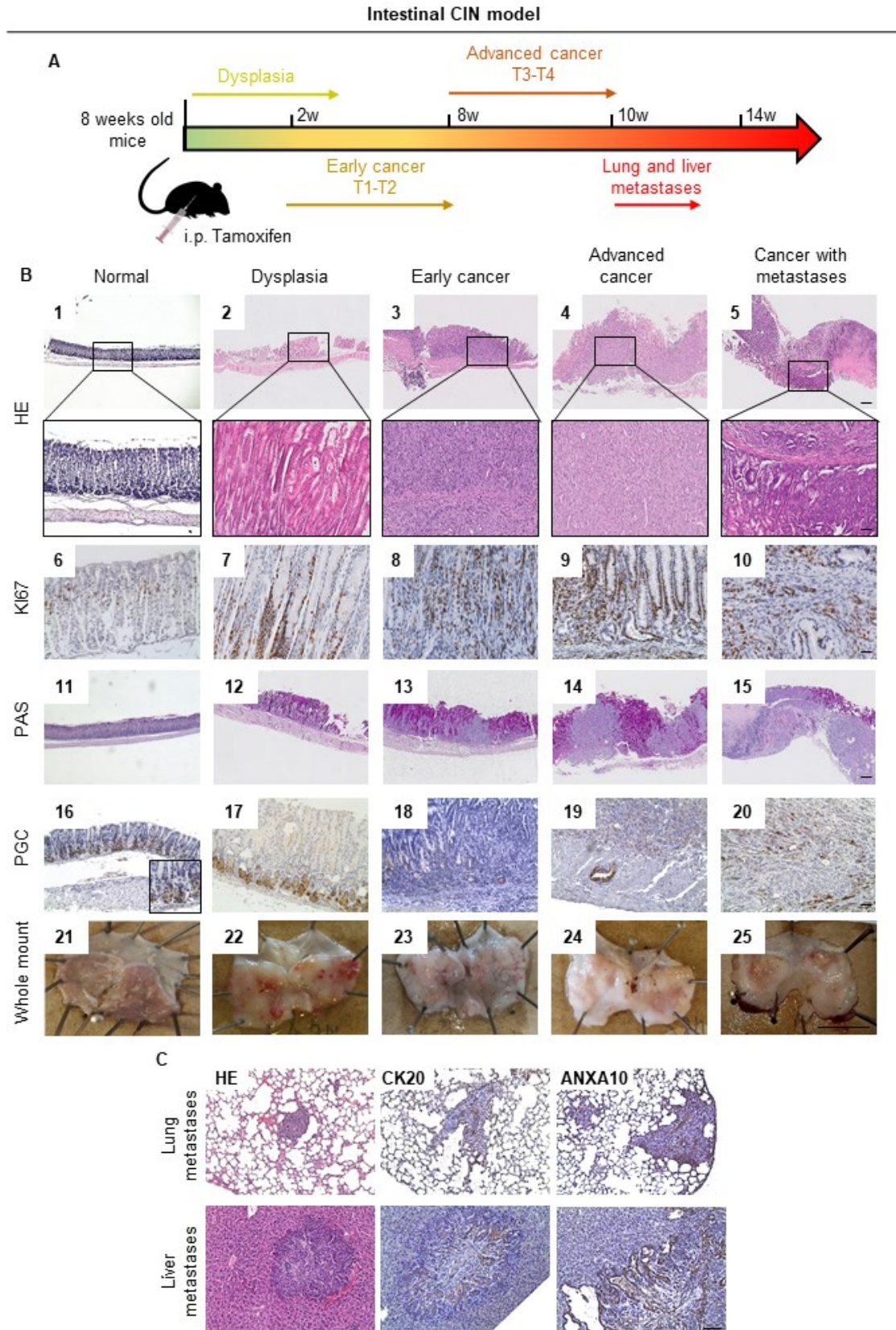


Figure 22: Intestinal CIN model. (A) Timeline of the intestinal CIN gastric cancer model (*Anxa10-CreER^{T2}; Kras^{G12D/+}; Tp53^{R172H/+}; Smad4^{fl/fl}*). (B) HE, Ki67, PAS and PGC staining at different stages of gastric cancer development (scale bar: 1-5, 11-15 500 μ m; 6-10, 16-20 50 μ m; zoom in 1-5 25 μ m). (C) HE, CK20, ANXA10 staining of liver and lung metastases (scale bar 50 μ m) (modified according Seidlitz et al., 2019b).

4.3.4. GS subtype typical alterations in cell adhesion, RTK/RAS and TGF- β pathways result in poorly differentiated signet ring cell carcinoma

For modelling GS gastric cancer, we crossed a *Cdh1^{fl/fl}* allele as a basic mutation in the Anxa10-CreER^{T2} mice. In the first GS model, *Kras^{G12D/+}* and *Smad4^{fl/fl}* alleles were added due to frequent mutations in the RTK/RAS and TGF- β pathway (Table 15). Tamoxifen was applied i.p. and mice analyzed at different time points over a period of maximally 28 weeks p.i. A longer observation was not possible due to food refusal and weight loss (Figure 23A). Already one week after tamoxifen application early cancerous lesions of T1 were observed, followed by progression to T2 till week 8 (Figure 23B2). Advanced cancer T3/T4 was found afterwards and metastases were first visible from week 16 p.i. onwards (Figure 23B3-4). The mutational setup of *Cdh1^{fl/fl}*, *Kras^{G12D/+}* and *Smad4^{fl/fl}* within the Anxa10-CreER^{T2} led to lung metastases and peritoneal carcinomatosis (Figure 23C).

Early cancer invading the muscularis propria represented a poorly differentiated tumor with signet ring cells. In addition, multiple *in situ* lesions with signet ring cells could be observed (Figure 23B2). An increase in the number of Ki67⁺ tumor cells was seen (Figure 23B6). Additionally, a strong mucus production within the stomach gland was documented by PAS staining. However tumors lost mucus production and could be therefore distinguished from non-cancerous lesions (Figure 23B10). The advanced tumor represented an invasion into subserosa and serosa with a strong increase in Ki67⁺ tumor cells (Figure 23B7-8). The diffuse morphology was maintained with characteristic signet ring cells. Some glandular structures were however found in the tumor mass (Figure 23B3-4). The increase of mucus as described for early cancer remained also for advanced cancer (Figure 23B11-12). Nevertheless, observed signet ring cells within the tumor mass could be distinguished by representing large PAS positive vacuoles. Of note, Pgc⁺ chief cell like cells remained in early and advanced cancers and could be found in patches of tumor cells in invasive tumor parts (Figure 23B14-16). The advanced cancers showed metastases in lung tissue and additionally peritoneal carcinomatosis with multi-focal infiltration of signet ring cells and a diffuse morphology of tumor cells. The gastric origin was again confirmed by CK20 and ANXA10 staining (Figure 23C).

To summarize, we observed histologically in the GS model a poorly differentiated invasive and metastatic cancer with characteristic signet ring cells, which shows remarkable similarities to the diffuse type cancer according to the Lauren classification (Lauren, 1965). Thus, this mouse model is named “diffuse GS model”.

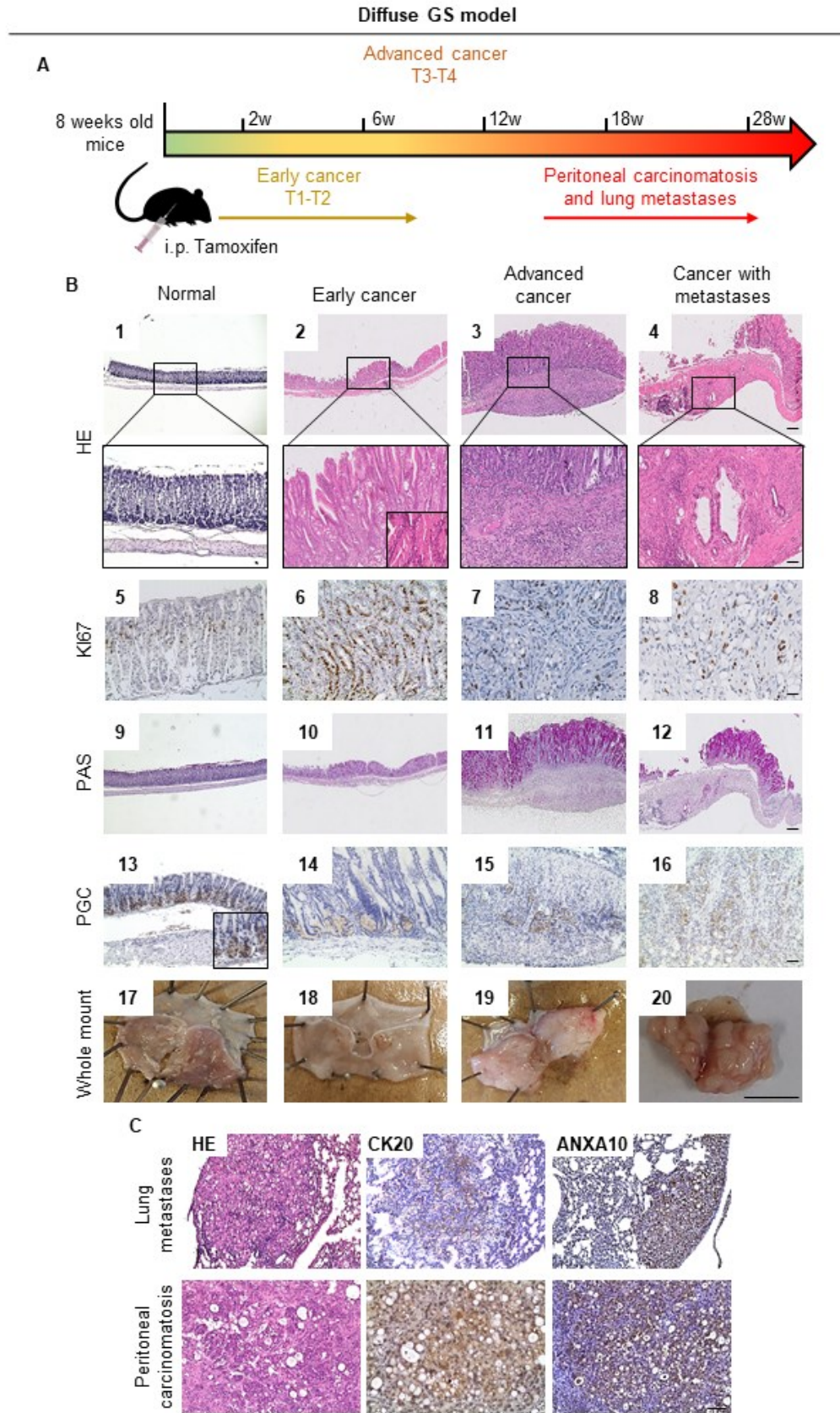


Figure 23: Diffuse GS model. (A) Timeline of the diffuse GS gastric cancer model (*Anxa10-CreER^{T2}*; *Cdh1^{fl/fl}*; *Kras^{G12D/+}*; *Smad4^{fl/fl}*). (B) HE, KI67, PAS and PGC at different stages of gastric cancer development (scale bar: 1-4, 9-12 500 μ m; 5-8, 13-16 50 μ m; zoom in 1-4 25 μ m). (C) HE, CK20, ANXA10 staining of lung metastases and peritoneal carcinomatosis (scale bar 50 μ m) (modified according Seidlitz et al., 2019b).

4.3.5. Serrated adenomatous gastric cancer model characterized by tooth-like adenomatous tumor morphology

For the second GS model the Anxa10-CreER^{T2} line was combined with *Cdh1^{fl/fl}*, *Kras^{G12D/+}* and *Apc^{fl/fl}* alleles. Mice could be observed over a period of 25 weeks p.i.. Longer monitoring was not possible due to large tumor formations inside of the stomach lumen leading to obstruction and cessation of food intake (Figure 24A). To week four a dysplastic stomach was observed (Figure 24B2). Early cancer with T1a and T1b was found from 4 weeks p.i. onward (Figure 24B3-4).

As in the intestinal CIN and diffuse GS model the dysplastic stomach represented a shift of Ki67⁺ cells down to the gland bottom and Pgc⁺ chief cell like cells remained unchanged (Figure 24B6, B14). In contrast to the other both models parietal cells were still present (data not shown). Here, a weak increase in mucus was observed compared to the normal epithelium (Figure 24B10). For that model only early cancer was observed within the analyzable time of 25 weeks p.i. with invasion into the lamina propria (T1a) and a maximum to the submucosa (T1b) (Figure 24B3-4). Instead of further invasion into the muscularis propria, tumors started to form macroscopically large tumor masses inside of the stomach lumen. Microscopically tumors formed adenomatous cancer with tooth-like structures. For that case the whole epithelium was transformed contrasting to the other two tumor models where clearly distinguishable structures within surrounding dysplastic epithelium could be observed. The presence of Ki67⁺ cells was observed throughout the whole tumor (Figure 24B7-8). Similar observations were made for Pgc⁺ chief cell like cells (Figure 24B15-16) while parietal cells were lost in the cancerous structure (data not shown). The production of low amount of mucus remained in early cancer (Figure 24B11-12).

Due to the characteristic morphologic observations this model resembles the relatively new histological subtype of serrated adenomatous gastric cancer (Rubio, 2001). We therefore refer to this mouse line as the “serrated adenomatous GS” model.

Serrated adenomatous GS model

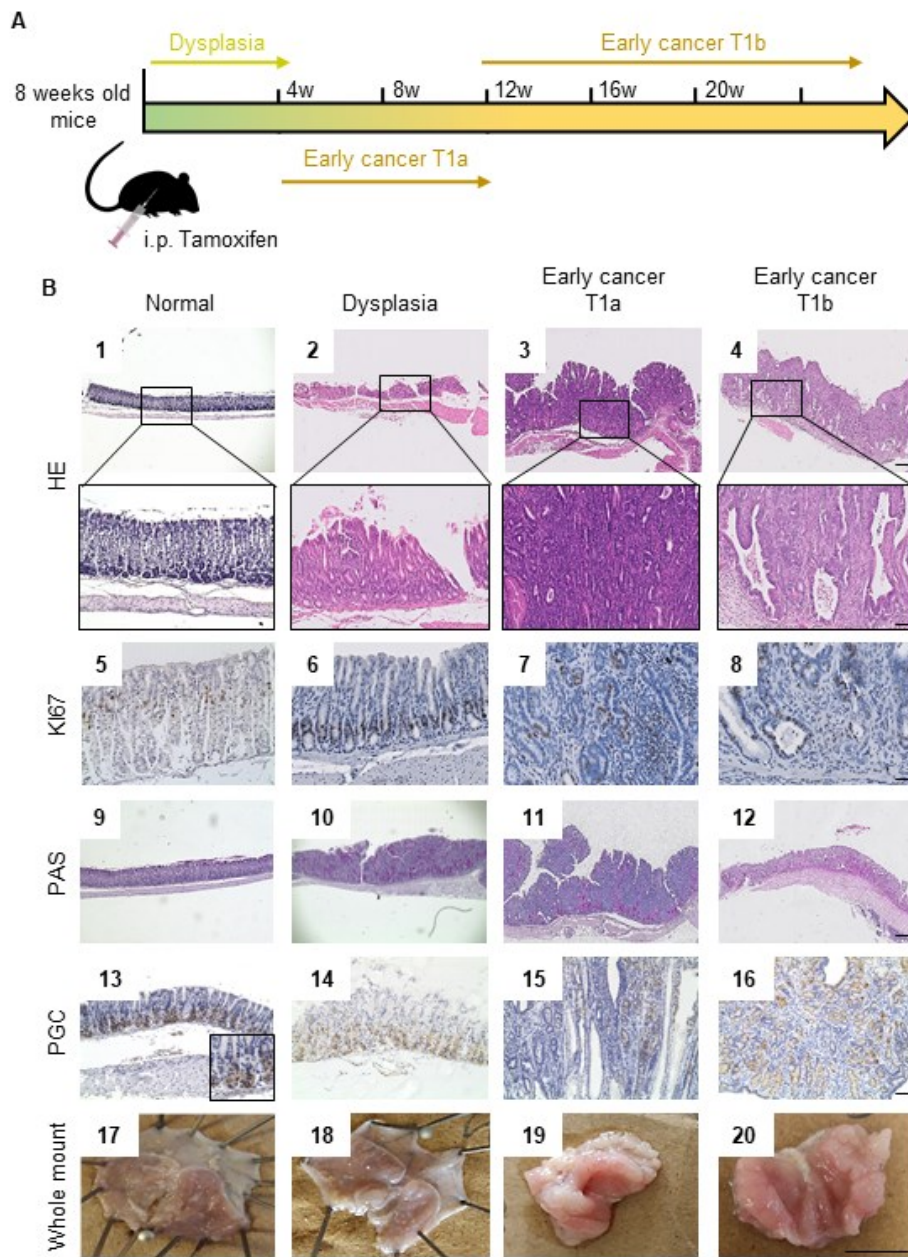


Figure 24: Serrated adenomatous GS model. (A) Timeline of the serrated adenomatous GS gastric cancer model (*Anxa10-CreER^{T2}; Cdh1^{fl/fl}; Kras^{G12D/+}; Apc^{fl/fl}*). (B) HE, KI67, PAS and PGC at different stages of gastric cancer development (scale bar: 1-4, 9-12 500 μ m; 5-8, 13-16 50 μ m; zoom in 1-4 25 μ m) (modified according Seidlitz et al., 2019b).

4.3.6. Gastric cancer models showed a divergent drug response to classical chemotherapy and targeted therapy

Tumor organoids were generated from each mouse model and selected via removal of medium compounds depending on the altered pathway. The intestinal CIN model showed cystic organoids with a thin lumen (Figure 25A1, A4). Contrary, the diffuse GS model represented a non-coherent grape like growth pattern (Figure 25A2, A5), while the serrated adenomatous GS organoids had an irregular compact morphology with no lumen (Figure 25A3, A6).

To analyze how the different gastric cancer subtypes reacted on treatment with classical used chemotherapy, they were treated with these routinely used drugs, i.e. 5-FU, oxaliplatin and docetaxel (Figure 25B). No significantly difference was seen in drug response. However, a trend of intestinal CIN model sensitivity compared to the diffuse GS and serrated adenomatous model could be observed for docetaxel treatment ($p= 0.13$ and 0.17). Response of both GS models did not drop down under 50 % of cell metabolic activity, while the intestinal model decreased down to 20 % (Figure 25B).

In order to perform targeted therapy experiments we choose to analyze the EGFR pathway by treating the organoids with trametinib. All cancer organoid subtypes showed an altered pathway due to the inducible *Kras*^{G12D} allele. The blockage led to a significantly higher response of the diffuse GS compared to the intestinal CIN model ($p= 0.007$) (Figure 25C). To validate the treatment phosphorylation level of ERK1/2 was analyzed. All three models showed a downregulation of the ERK1/2 phosphorylation post trametinib treatment (Figure 25C). A significantly increased apoptosis was observed for the serrated adenomatous GS model, whereas the intestinal CIN and diffuse GS model did not respond with a significantly change (Figure 25C). We observed inhibition of the EGFR pathway in all three models, only the diffuse GS responded to the targeting. Interestingly, the sensitivity of the diffuse GS is not a result of increased cell death, while this is the case for the serrated adenomatous GS model.

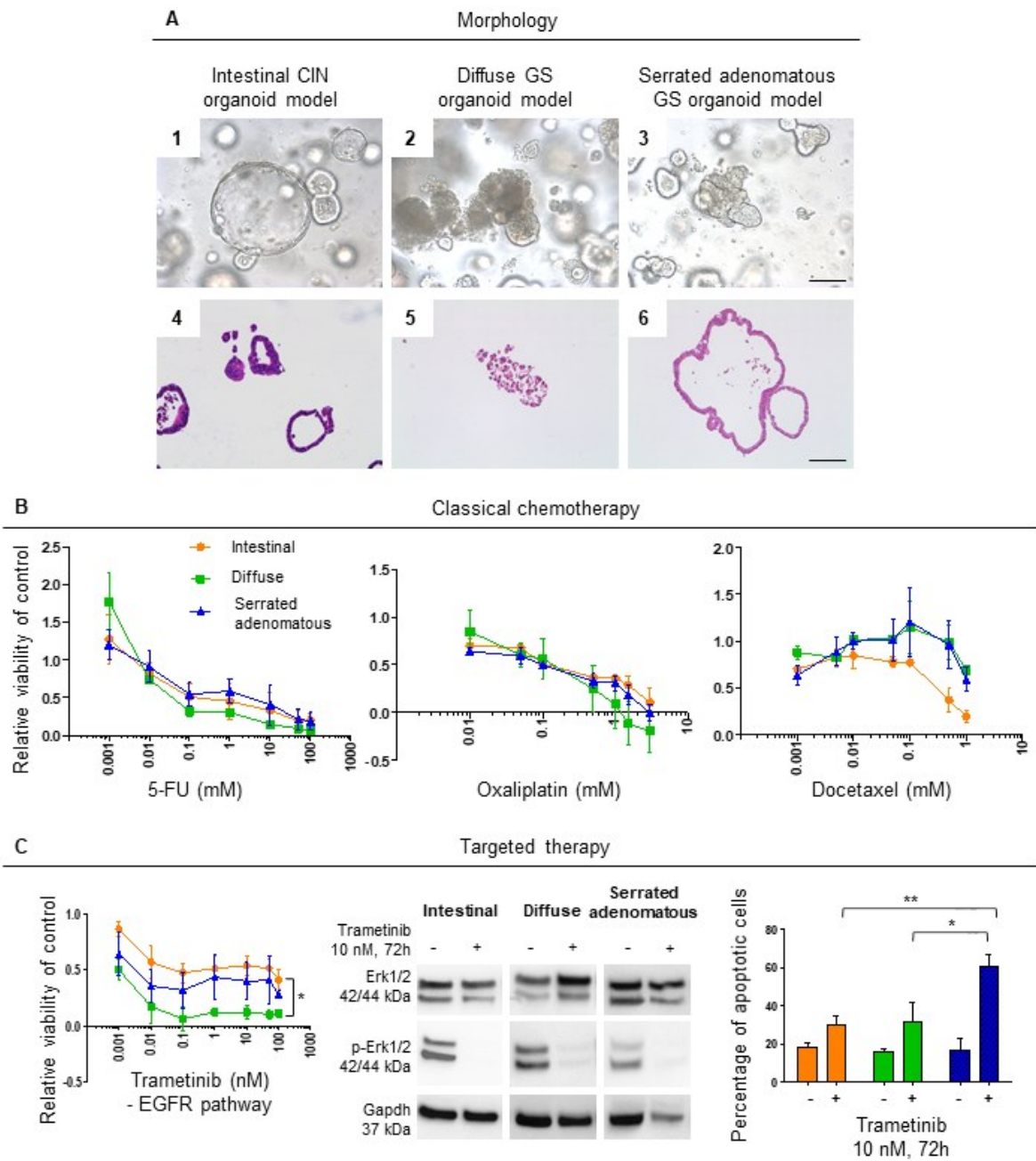


Figure 25 Gastric cancer organoid models characterized by different morphology and drug response. (A1-3) Gastric cancer organoid morphology of three subtypes: intestinal CIN, diffuse GS and serrated adenomatous GS organoid model. (A4-6) HE staining of gastric cancer organoid lines (scale bar 100 μ m). (B) Dose response curves of organoids treated with classical chemotherapy (5-FU, oxaliplatin, docetaxel). Statistical analysis of dose response curves by repeated measures ANOVA. (C) Targeting of EGFR signaling pathway with trametinib. Dose response curve after 72 h trametinib treatment. Statistical analysis by repeated measures ANOVA (* < 0.05). Western Blot of ERK1/2 and phosphor-ERK1/2 levels of the three models after 10 nM trametinib treatment for 72 h. Amount of apoptotic cells (FITC Annexin V+/PI+ and FITC Annexin V+/PI- cells) after 10 nM and 72 h trametinib treatment. Statistical analysis of the percentage of apoptotic cells by Student's t Test (* < 0.05, ** < 0.01) (modified according Seidlitz et al., 2019b).

5. Discussion

5.1. Patient derived cancer organoids - a model system allowing analysis of drug response and personalized cancer treatment

In the first part of the work, a human gastric cancer biobank consisting of 20 different organoid cultures was established. While for other cancer entities like colorectal, prostate and pancreatic cancer large biobanks of patient derived organoids have been reported, such a biobank for gastric cancer was still missing (Dong Gao et al., 2014; Boj et al., 2015; Van De Wetering et al., 2015). Focusing on four different gastric cancer organoid lines representing different morphologies, we firstly analyzed their growth pattern and phenotype using immunohistochemical stainings typically performed by the pathology to diagnose gastric cancer. The organoids as well as their derived xenografts phenocopied the architecture of the primary cancer they were derived from. In the next step we studied the response of organoids to classical chemotherapeutics selected by the currently used clinical treatment strategies (Cunningham et al., 2006; Ychou et al., 2011; Al-Batran et al., 2016). The organoid lines were exposed to 5-FU, oxaliplatin, irinotecan, docetaxel and epirubicin and a divergent response could be observed. For example, DD191 and DD282 responded to 5-FU at low concentrations whereas the DD109 only at high concentration. Similar observations were made for the other drugs. In summary, a divergent response to classical chemotherapeutics could be observed in gastric cancer organoids while for each line an active chemotherapeutic drug could be defined.

Using whole genome sequencing we searched for targetable mutations in each organoid line. We found an activating drug-sensitive mutation of the *ERBB2* gene in the DD107 line. Additionally, an amplification of the *ERBB2* gene in the DD109 line was recognized. This amplification was firstly confirmed by IHC staining using an antibody against ERBB2. Amplifications of *ERBB2* are found in gastric cancer in up to 22 % of cases and can be successfully targeted with trastuzumab, an antibody binding to the HER2/neu receptor, showing a significant overall survival benefit in the clinical setting (Bang et al., 2010). Both lines were treated with trastuzumab and a response observed. In the clinic, trastuzumab is often administered in combination with 5-FU (Bang et al., 2010). Therefore, the two lines were also targeted with trastuzumab plus 5-FU in combination. Pathway specificity was analyzed by analyzing the phosphorylation level of ERK1/2. No change in phosphorylation level of DD107 was observed. DD109 downregulated the phosphorylation of ERK1/2 after 0.1 μ M trastuzumab treatment. It seemed that DD107, carrying the activating mutation and which showed the highest response, signaled through a RAS/RAF independent way. Of note, gastric cancers are routinely tested only by IHC for a HER2/neu amplification. The activating mutation of DD107 would have been missed, and thus the patient would have not been considered a candidate

for trastuzumab. Thus, in this case, molecular analyses together with *in vitro* response testing provided strong evidence for a potential targetable pathway in this patient. In the future, such cases should be discussed in molecular tumorboards, where the information of the genetic setup could be merged with functional data.

The DD109 harbored additionally a bi-allelic loss of *CDKN2A*. DD109, DD191 and DD320N were treated with palbociclib, a FDA approved inhibitor, targeting the kinase activity of CDK4/6. *CDKN2A* plays an important role in cell cycle progression and is frequently mutated in gastric cancer (The Cancer Genome Atlas Research Network, 2014). Palbociclib treatment resulted in a complete cell cycle arrest in DD191 and DD320N, whereas DD109 had still a small fraction (2 %) of proliferating cells. Long-term treatment with 10 μ M palbociclib including two times passaging resulted in a loss of the DD191 and DD320N cultures, indicating a complete inhibition of proliferation. DD109 organoids were still present and phenotypically unharmed. A potential explanation is the dual inhibition of the cell cycle by palbociclib and a functional CDK4/6 in the control lines, while in DD109 the loss of *CDKN2A* resulted in an incomplete suppression of the cell cycle (Huang et al., 2015).

In this work we demonstrated the usefulness of patient derived gastric cancer organoids as an *ex vivo* model system that faithfully recapitulates many aspects of the *in vivo* tumor. All in all we generated 20 different lines and characterized in detail four concerning similarities to the primary cancer, molecular alterations by state-of-the-art sequencing methods as well as drug sensitivity (Figure 26). In the meantime two further studies dealing with patient derived gastric cancer organoids were published (Nanki et al., 2018; Vlachogiannis et al., 2018). Nanki and colleagues reported a gastric cancer biobank consisting of 37 cancer organoid lines by including samples from surgical resection, endoscopic biopsy and ascites puncture (Nanki et al., 2018). Vlachogiannis and colleagues described a biobank consisting of 50 cancer organoid lines derived from metastatic colorectal cancer tissue, metastatic gastro-esophageal cancer tissue and metastatic cholangiocarcinoma. The samples were taken from ultrasound, computed tomography guided- or endoscopic biopsies (Vlachogiannis et al., 2018). In contrast, our generated biobank only originated from surgical resection specimens. There were slight variances for initiating and growth of organoid cultures. For example, Nanki and colleagues optimized the organoid establishment efficiency by directly selecting the tumor organoids to circumvent the overgrowth with normal ones. Therefore, organoids were selected based on pathways dysregulated in gastric cancer like TP53, RHOA, TGF- β and RTK/RAS by media withdrawal or specific inhibitor addition (Nanki et al., 2018). All three studies have in common, that they showed phenotypic, genotypic and drug response similarities of the different generated gastric organoid lines to the cancer they are derived from (Nanki et al., 2018; Vlachogiannis et al., 2018; Seidlitz et al., 2019a). In one study, organoids were further genetically modified. Nanki *et al.* performed mammalian gene editing by using the

CRISPR/Cas9 technique to further modify the patient derived gastric cancer organoids. Here, knockouts of *CDH1* as well as *RHOA* were performed verifying that the *CDH1* loss is important for the diffuse morphology of gastric cancer whereas the *RHOA* loss maintained normal glandular morphology (Nanki et al., 2018). Similar experiments were also performed for other patient derived cancer organoids of entities like pancreas (Lee et al., 2017; Seino et al., 2018), colorectum (Drost et al., 2015; Matano et al., 2015; Fumagalli et al., 2017) and breast (Dekkers et al., 2019).

Taken together, the human cancer organoids allow response prediction to classical chemotherapeutics as well as targeted drugs in a living system (Figure 26). With the knowledge of altered pathways, predictions can be made on the potential effectiveness of a given drug. Nevertheless, the response represents the result of the concurrence of all present mutations of an individual patient. This response can only be predicted bioinformatically in about 30-40 % of cases, as i.e. shown by the ongoing National Center for Tumor Diseases Molecularly Aided Stratification for Tumor Eradication (NCT MASTER) study. Response testing in patient derived model systems might therefore improve personalized cancer treatment. One drawback of the organoid cultivation method is, that it consists only of the epithelial compartment of the tumor. Mesenchymal cells, blood vessels or surrounding immune cells are not included. This has to be kept in mind, as drugs targeting the microenvironment or immune system cannot be assessed. Taken together, patient derived cancer organoids simulate cancer behavior *ex vivo* and can be used for functional analyses and drug response evaluation.

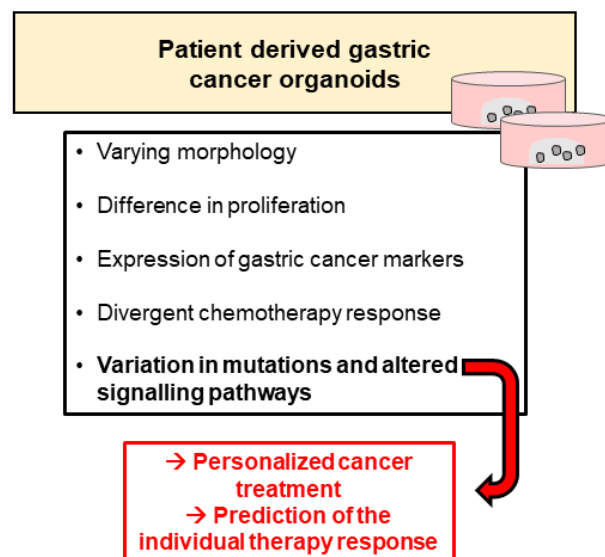


Figure 26: Characteristics of the generated human gastric cancer biobank. Organoids represented differences in morphology, proliferation, drug response and mutational pattern. The knowledge of mutations and altered pathways allow the personalized cancer treatment not only for gastric cancer but also for other cancer entities. Together with organoid based response prediction, these new techniques allow the selection of possibly active drugs and the prediction of their efficacy

5.2. Gastric cancer subtype modelling using organoids with a defined genetic makeup

The analysis of interference into a specific signalling pathway can be affected by cross talk from other aberrantly activated signalling pathways. Therefore, working with human cancer organoids that usually carry depending on the subtype between a few hundred to several thousand mutations, often results in difficult to interpret data. We therefore set out in the second part of this work to generate mouse organoid models with a defined mutational load according to described molecular subtypes. To achieve this, we used mice with the Cre/Lox system to activate mutations or delete tumor suppressor genes. Selection of mutations were made according the TCGA study that described typical mutations for each of the subtypes (The Cancer Genome Atlas Research Network, 2014). The RTK/RAS activated tumor model was modelled by combining an activating hotspot mutation of *Kras*^{G12D/+} as well as the hotspot mutation *Tp53*^{R172H/+}. The second model combined a mutated WNT pathway (*Apc*^{fl/fl}) as well as an alteration in the cell adhesion gene *Cdh1*^{fl/fl} (named diffuse tumor model). The third subtype combined a hotspot mutation in *Tp53*^{R172H/+} as well as an activated WNT pathway (*Apc*^{fl/fl}) (named WNT activated tumor model). The last model is associated to the TCGA classified EBV subtype representing mutations in the PI3K/AKT pathway and chromatin remodeling. We therefore combined the *Pik3ca*^{H1047R/+} mutation and a loss of *Arida*^{fl/fl}. This model was named EBV associated tumor model. Corresponding mice were crossed and generation of organoids was performed as previously described (Stange et al., 2013). An *in vivo* induction of the Cre/Lox system was not possible, as a stomach specific Cre-recombinase did not exist at that time. The generated organoids were infected *in vitro* with an adenoviral system carrying the Cre recombinase to activate floxed alleles. The different gastric tumor organoid cultures developed different morphologies. Especially, the *Cdh1* mutation in the diffuse gastric cancer model resulted in a complete structural alteration towards a grape like form with no lumen compared to normal organoids, induced by the loss of cell-cell connections. The RTK/RAS activated and WNT activated tumor models represented a cystic structure with a thick lumen, whereas the EBV associated tumor model was more compact compared to the other ones.

The *Kras* activation in the RTK/RAS activated tumor model resulted in an increased ERK1/2 phosphorylation indicating an active mitogen-activated protein kinase (MAPK) signaling. Similar observations were also made by Li *et al.* using a collagen-based air-liquid model of neonatal mouse cells directly transformed by adenovirus Cre upon initiation of culture (Li et al., 2014). Targeting the EGFR pathway with trametinib, a small molecule inhibiting ERK1/2, led to a complete inhibition of signaling through this pathway. The diffuse tumor model resembled due to the described grape-like morphology the classical diffuse type of gastric

cancer according to the Lauren classification (Lauren, 1965). The concomitant loss of *Apc* led to an increased expression of WNT target genes, which could be partly reversed by calphostin C treatment. Calphostin C is a small molecule inhibiting the colocalization of β -catenin with the T cell factor (TCF) within the WNT pathway.

Taken together, the adenoviral established organoid tumor model lines represent an easy to use and elegant model system with a defined mutational pattern showing typical characteristics and altered pathways of the known gastric cancer subtypes by just altering two genes. These generated organoid lines will be useful models to perform functional tests that require a well characterized genetic makeup. In the future, new therapeutic interventions can be firstly tested with the help of this organoid model lines to give a first clue concerning stability, efficacy and response before performing experiments *in vivo* or going into clinical trials. Alternatively, frequently mutated genes in gastric cancer with unknown function could be additionally genetically manipulated using CRISPR/Cas9 in these models to analyze their relevance in cancer biology.

5.3. The stomach specific mouse line Anxa10-CreER^{T2} represents a prime tool for gastric cancer research

In order to analyze gastric cancer *in vivo* a stomach specific mouse model was necessary. As described above, a Cre recombinase mouse line that is specifically active only in the stomach epithelium has not been established. Several Cre mouse lines with recombination in the stomach have been described and also used for gastric cancer analysis, i.e. Krt19-CreER^T, Mist1-CreER^{T2}, Lgr5-CreER^{T2}, Tff2-CreER^{T2} or Lrig-CreER^{T2} (Lee et al., 2005; Means et al., 2008; Barker et al., 2010; Quante et al., 2010; Hayakawa et al., 2015; Schweiger et al., 2018). However, all these lines are not restricted to the stomach. KRT19 is widely and highly expressed in several organs including the intestine, colon, lung or mammary gland; MIST1 is additionally highly expressed in salivary and lacrimal glands, prostate and pancreas; LGR5 is also abundant in the intestine, epidermis and prostate; TFF2 is additionally present in the pancreas and the Leucine-rich repeats and immunoglobulin-like domains protein 1 (LRIG) is also highly expressed in the intestine, colon and epidermis. Due to the Cre expression in multiple organs their usage for cancer analysis is restricted. As an example, the use of the Lgr5-CreER^{T2} mouse to analyze gastric cancer development resulted only in the formation of small adenomas in the antrum. A further analysis was not possible due to concomitant very fast tumor formation in the intestine (Barker et al., 2010). The described Tff1-Cre mouse line represented recombination events mostly in the antral glands but also in the small intestine and colon. However, TFF1 is only expressed in mucus producing cells and recombination is therefore restricted to this specific cell line. Combining this line with either *Kras* activation,

phosphatase and tensin homolog (Pten) or *Cdh1* deletion led to the observation of different metaplastic phenotypes, but no cancerous lesions developed (Kinoshita et al., 2018). A second inducible Tff1-CreER^{T2} line has been described as a stomach specific mouse model (Thiem et al., 2016). Combining this line with *Kras* and *signal transducer and activator of transcription 3 (Stat3)* led to gastric adenoma development in the antrum but not in the main body of the stomach. Both transgenic Tff1 mouse lines thereof mostly recombine in the antrum of the stomach with just few events in the main body of the stomach.

Thus, due to the absence of a stomach specific mouse model showing recombination events in the main body of the stomach, we set out to generate such a mouse line. Therefore, literature search and data mining analysis was performed. This resulted in the identification of ANXA10 as a stomach specific protein, which at the same time is expressed in all different cell types of the stomach epithelium. The generated *Anxa10-CreER^{T2}* line faithfully recapitulated the endogenous ANXA10 expression, showing only stomach specific recombination events and no restriction to a specific cell type. Nevertheless, activation of Cre results in a patchy recombination pattern throughout the whole gland and not a uniform deletion in all cells. Due to this patchy expression, the mouse line is an optimal tool for cancer models, where a complete transformation of an organ is not desired (Seidlitz et al., 2019b).

This newly stomach-specific mouse line was used for modelling gastric cancer subtypes *in vivo*. Therefore, the TCGA database was used to define frequently altered pathways and hotspot mutations of each cancer subtype, similarly to what we performed before to generate the defined organoid models. Alterations were mainly found in the following pathways: RTK/RAS, PI3K/AKT, WNT, TGF- β , cell adhesion and chromatin remodelling. As described above three different subtypes were generated and analyzed in depth. In this work, we focused on one CIN model and two GS models. To our knowledge these three models are the first to exclusively initiate tumor formation in the stomach corpus. Furthermore, the different models mimic very closely the histology of known human gastric cancer subtypes. The intestinal CIN model represented formation of tumor cells into glandular and tubular structures showing morphologies of human intestinal type gastric cancer (Lauren, 1965). This mouse model over time developed liver and lung metastases. The human GS subtype often shows a loss of adhesion molecules. This is modelled in our GS model by a *Cdh1* loss as the main characteristic. The first GS model was further combined with *Kras* and *Smad4* resulting in a diffuse cancer morphology with the presence of typical signet ring cells. Advanced cancers developed peritoneal carcinomatosis as the main metastatic side with additionally lung metastases. Of note, the divergent metastatic patterns found in the intestinal CIN model and diffuse GS model find its correlation in the clinical course of patients depending on the Lauren subtype. Intestinal tumors mostly metastasize to the liver, while the diffuse type frequently metastasizes to the peritoneum and the lung (Jun H Lee et al., 2018). A complete other

morphology was seen for the second GS model harboring a WNT pathway activation. Here, an adenomatous tooth-like gastric cancer morphology was observed. While no metastases were found, large tumor formations inside the lumen of the stomach were detected, resulting in a luminal occlusion prohibiting food passage. The characteristic tooth-like structures are reminiscent of the histology of serrated adenomas of the colon (Longacre and Fenoglio-Preiser, 1990). This type of adenoma has also been described in gastric lesions (Rubio, 2001). The features of each generated model are summarized in Figure 27.

Despite advances in understanding the molecular basis of gastric cancer, treatment of cancer patients is still based mainly on classical chemotherapy. Trastuzumab and ramucirumab as targeted therapies are the only exceptions in gastric cancer treatment. We and others have recently shown that gastric cancer organoids are a useful tool between classical 2D cultures and the *in vivo* situation to model gastric cancer (Nanki et al., 2018; Vlachogiannis et al., 2018; Yan et al., 2018; Seidlitz et al., 2019a). We therefore analyzed the therapeutic response of organoids established from the different gastric cancer models towards frequently used chemotherapies. No significant differences were observed in the response to the classical chemotherapeutic drugs. The EGFR inhibitor trametinib resulted in a varying response. The generated organoids represented therefore an innovative molecular subtype specific model system to analyze individualized treatment regimes.

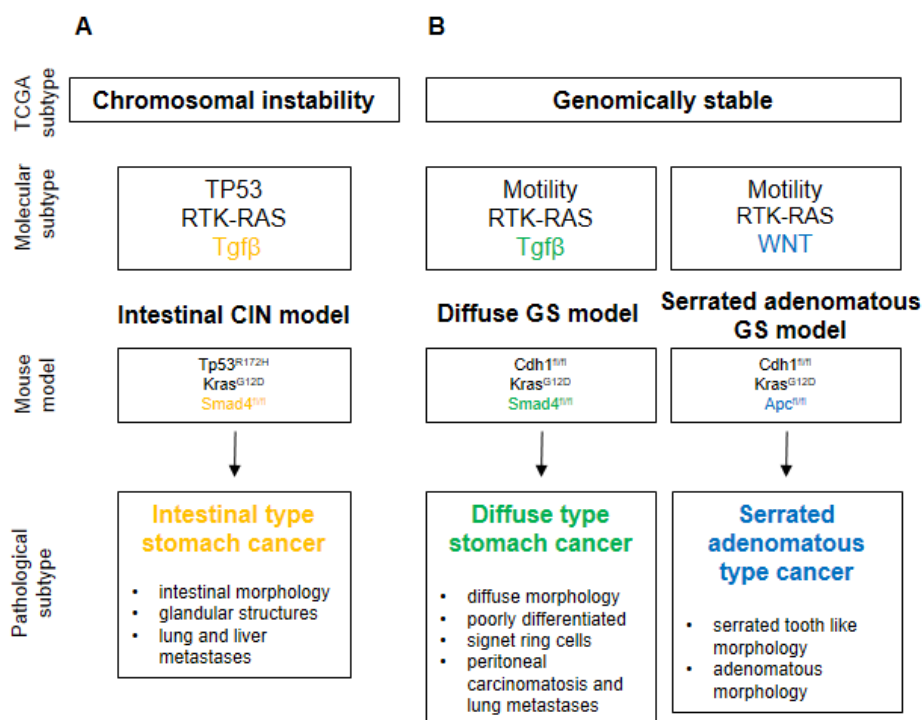


Figure 27: Characteristically features of each gastric cancer subtype. (A) Molecular as well as pathological features of the chromosomal instability subtype. (B) Molecular as well as pathological features of the genomically stable subtype. Two different molecular pattern were used representing different pathological features (Seidlitz et al., 2019b).

Taken together, the generation of the Anxa10-CreER^{T2} mouse line allowed us to model for the first time different known gastric cancer subtypes (Seidlitz et al., 2019b). The created models show similar characteristics as their human counterparts including a divergent metastatic pattern. Furthermore, the models give the opportunity of cancer analysis at different stages, helping us to understand the molecular development and progression of gastric cancer. In the future, the biology behind the divergent metastatic spread and the properties of circulating tumor cells within stomach cancer models can be investigated in depth. For the first time *in vivo* monitoring of drug responses in stomach cancer mouse models that closely mimic different human stomach cancers becomes possible before going into clinical trials. On top of that, the organoids established from the gastric cancer mouse models represent an easy to use, elegant *in vitro* tool to further analyze gastric cancer related signaling pathways. Organoid lines from primary stomach cancer as well as their metastases can be established, allowing large scale screenings of anti-cancer drugs. Generated organoid lines can be genetically manipulated by i.e. the CRISPR/Cas9 system. Using this system, observed genes for gastric cancer progression as well as metastases can be activated or silenced, organoids orthotopically re-implanted into mouse stomach and analyzed for their potential role in cancer progression. All in all, this Anxa10-CreER^{T2} mouse represents a prime tool for future gastric cancer research.

Zusammenfassung

Karzinome des Magens stellen die zweithäufigste krebisbedingte Todesursache und die fünfhäufigste bösartige Erkrankung weltweit dar. Die Diagnose erfolgt meist erst in späten Stadien, wodurch neoadjuvante und adjuvante Chemotherapien eine zunehmend wichtige Rolle spielen um im Zusammenspiel mit der Chirurgie kurative Therapiekonzepte zu ermöglichen. Personalisierte mutationsspezifische Therapieoptionen erweitern hierbei das Spektrum der Behandlungsmöglichkeiten wobei jedoch ihre Wirksamkeit häufig schwer vorherzusagen ist. Aufgrund von fehlenden spezifischen Biomarkern konnten viele Studien mit gezielten Therapieansätzen beim Magenkarzinom keinen Überlebensvorteil zeigen.

Organoide stellen ein drei-dimensionales (3D) *in vitro* Zellkultursystem dar, welches aus verschiedenen Ressourcen etabliert werden können. Hierzu zählen adulte Stammzellen, embryonale Stammzellen (ESC) und induzierte pluripotente Stammzellen (iPSC). Während ESC und iPSC Organoide eine Nische beinhalten, welche die Stammzellpopulation aufrechterhalten, weisen Organoide aus adulten Stammzellen keine solche Nische auf. Aufgrund der vorhandenen Kenntnisse bezüglich der Stammzellnische und deren Wachstumsfaktoren können *in vitro* Bedingungen geschaffen werden, die die Selbsterneuerung und Proliferation auch von adulten Stammzellen ermöglichen. Die Organoide zeigen ähnliche Funktionen wie die Organe von denen sie abgeleitet sind. Aufgrund der beschriebenen Charakteristika bieten sie eine hervorragende Möglichkeit Krankheiten auf patientenbezogener Ebene zu untersuchen.

In dieser Arbeit wurde Magenkrebs mit Hilfe von humanen als auch murinen Organoidlinien analysiert und charakterisiert. Zunächst wurde eine Patienten-abgeleitete humane Magenkrebs Organoid Biobank etabliert. Die generierten Linien wurden hinsichtlich ihres molekularem Profils charakterisiert und mit klassischen Chemotherapeutika behandelt. Des Weiteren ermöglichten gefundene molekulare Alterationen die signalwegspezifische Behandlung. Unterschiede in Morphologie, Proliferationsrate als auch in den notwendigen Kultivierungsbedingungen konnten in den einzelnen Organoidlinien aufgezeigt werden. Immunhistochemisch sowie molekularpathologisch wiesen die Organoide ähnliche Charakteristika wie das korrespondierende Primärgewebe auf. Ein divergentes Ansprechen der unterschiedlichen Organoidlinien auf Chemotherapeutika wurde detektiert. Aufgrund der Komplexität der vorhandenen Mutationen in den humanen Organoidlinien muss jede Patienten-abgeleitete Organoidlinie hinsichtlich des Therapieansprechens für sich interpretiert werden. Um ein Modellsystem zur Verfügung zu haben, welches erlaubt eine Interferenz mit einem Signalweg im Detail zu analysieren, haben wir murine Organoidmodelle mit definierten induzierbaren Alterationen generiert. Diese Alterationen aktivieren oder depletieren Signalwege welche für das Magenkarzinom beschrieben sind. Die Linien wurden hinsichtlich

ihrer Morphologie, Funktionalität als auch mutationsspezifisches Therapieansprechen analysiert.

Um die Analyse des Magenkrebses *in vivo* zu ermöglichen wurde ein Magen-spezifisches Mausmodell generiert. Literatur- und Datenbankrecherchen identifizierten *Annexin10* (*Anxa10*) als ein vielversprechendes Gen, welches gleichzeitig in allen Zelltypen des Magenepithels exprimiert wird. Daraufhin erzeugten wir eine induzierbare Cre Linie unter dem *Anxa10* Promotor. Die generierte *Anxa10-CreER^{T2}* Linie zeigte ausschließlich im Magen Rekombinationsereignisse und wies keine Beschränkung auf einen bestimmten Zelltyp auf. Die generierte Cre-Linie zeigte jedoch ein ungleichmäßiges Rekombinationsmuster in der Magendrüse auf, d.h. nicht alle Zellen im Magenepithel wurden gleichzeitig rekombiniert. Aufgrund dieser Beobachtung eignet sich diese Maus gut für Krebsmodelle bei denen eine vollständige Transformation des gesamten Epithels nicht erwünscht ist. Für Untersuchungen mit einer vollständigen Rekombination aller Zellen im Epithel eignet sich diese Linie hingegen nicht. Die *Anxa10-CreER^{T2}* Linie wurde sodann zur Modellierung von Magenkrebssubtypen verwendet. Mittels Datenbankrecherchen wurden häufig veränderte Signalwege und Hotspot Mutationen in den verschiedenen Magenkarzinom-Subtypen identifiziert. Wir etablierten ein Mausmodell für den chromosomal instabilen (CIN) Subtypen und zwei Mausmodelle für den genomisch stabilen (GS) Subtypen. Die generierten Modelle ahmten die für den Menschen beschriebenen histologischen Veränderungen nach. Für den CIN Subtypen wurde *Kras*, *Smad4* und *Tp53* Alterationen kombiniert. Die Tumorzellen in diesem Subtyp bildeten Drüsen- und Röhrenstrukturen, welche Ähnlichkeiten mit dem intestinalen Subtyp des Magenkarzinoms im Menschen aufzeigte. Das erste GS Modell (*Kras*, *Cdh1* und *Smad4*) wies eine diffuse Morphologie mit Siegelringzellen auf, womit dieses Modell eine große Ähnlichkeit zum diffusen Subtyp des Magenkarzinoms im Menschen aufzeigte. Das zweite GS Modell (*Kras*, *Cdh1* und *Apc*) wies Tumorzellen mit einer adenomatösen zahnähnlichen Morphologie auf, welche ebenfalls in einem Subtyp des humanen Magenkarzinoms gefunden wurde.

Zusammenfassend zeigt diese Arbeit zum einen, dass Patientenorganoide in der Zukunft als lebende Biomarker fungieren könnten, um ein Therapieansprechen im Patienten vorherzusagen. Zum anderen stellt das neu generierte Magenkrebsmausmodell ein hilfreiches Werkzeug für die weitere Magenkrebsforschung dar.

Summary

Gastric cancer is the second leading cause of cancer related deaths and the fifth most common malignancy worldwide. The prognosis of gastric cancer is often poor. Frequently, the lack of clinical signs lead to a delayed diagnosis with three quarters of patients presenting with non-curable advanced disease. The only curative option is surgery, supported in recent years by perioperative chemotherapy. However, known molecular alterations represent possibilities for targeted therapies to improve overall survival. Nevertheless, biomarkers to predict therapy response are missing, resulting in several failed clinical trials for targeted drugs.

Organoids are a recently developed three-dimensional culture system derived from different sources, i.e. adult tissue stem cells, embryonic stem cells (ESC) or induced pluripotent stem cells (iPSC). While in ESC or iPSC derived organoids a functional niche is present that maintains stem cells, this niche is missing in adult stem cell derived organoids and needs to be replaced by a definite medium containing the relevant growth factors. Organoids have the ability of proliferation, self-renewal and self-organization. They show a comparable functionality of the organs they are derived from. In sum, organoids are valuable tools to study diseases on a patient level.

In this work, we focused on the characterization of gastric cancer by using human and mouse cancer organoids. Firstly, a human gastric cancer organoid biobank was established. The patient derived organoid lines were characterized concerning their molecular profile, treated with classical chemotherapeutics and mutation specific targeting was performed. The generated human cancer organoids showed a high similarity to the tissue they were derived from and allowed a detailed analysis of observed alterations for each individual patient. However, the high number of mutations effected targeted therapies and needed to be interpreted in the whole mutation spectrum of each specific organoid line. In order to establish organoids with defined mutations for in depth analysis of pathway interference, we decided to combine inducible alleles of frequently altered signaling pathways in gastric cancer in mice and derived organoids of the stomach. These organoid lines were further analyzed by their morphology, functionality and drug response. Successful interference with activated pathways demonstrated their potential usefulness as living biomarkers for therapy response testing.

In order to analyze gastric cancer *in vivo* a stomach specific mouse model was established. Intensive literature and database research resulted in the identification of *Annexin10* (*Anxa10*) as potential stomach specific gene which at the same time is expressed in all different cell types of the stomach epithelium. We therefore generated an inducible Cre recombinase mouse line under the *Anxa10* promotor. The *Anxa10*-CreER^{T2} line showed only stomach specific recombination events and no restriction to a specific cell type. Nevertheless, activation of Cre resulted in a patchy recombination pattern throughout the whole gland and

not a uniform recombination in all cells. Due to this patchy expression, the mouse line is an optimal tool for cancer models, where a complete transformation of an organ is not desired. On the other side it is not useful, if a complete knock-out of a certain floxed allele is needed. This new stomach-specific mouse line was then used to model gastric cancer subtypes *in vivo*. Frequently altered pathways and hotspot mutations of each gastric cancer subtype were defined based on the TCGA database. Alterations were mainly found in the following pathways: RTK/RAS, PI3K/AKT, WNT, TGF- β , cell adhesion and chromatin remodelling. We generated and analyzed three different mouse models: one for the chromosomal instability (CIN) subtype and two for the genomically stable (GS) subtype. The different models mimicked very closely the histology of known human gastric cancer subtypes. The intestinal CIN model with mutations in *Kras*, *Smad4* and *Tp53* developed tumors with glandular and tubular structures showing morphologies to human intestinal type gastric cancer. The first GS model with alterations in *Kras*, *Cdh1* and *Smad4* showed cancers with a diffuse tumor cell morphology with the presence of typical signet ring cells. The second GS model with *Kras*, *Cdh1* and *Apc* alterations showed similarities to the adenomatous tooth-like gastric cancer subtype.

Taken together, this study demonstrates that gastric cancer organoids might serve as living biomarkers to predict therapy response and resistance in individual patients. Additionally, the generated gastric cancer mouse model is to our knowledge the first model initiating tumor formation exclusively in the stomach with similar characteristics as described for human gastric cancer. This mouse represents a prime tool for further gastric cancer research.

List of Figures

Figure 1: Morphology of the stomach and gland organization.....	2
Figure 2: TNM classification of gastric cancer.....	5
Figure 3: Flowchart of molecular classification of gastric adenocarcinoma into four subtypes.	6
Figure 4: Key features of gastric cancer subtype.....	7
Figure 5: Pathogenesis of intestinal type gastric cancer.	9
Figure 6: Applications of the organoid technology for studying development, homeostasis and disease.....	15
Figure 7: Exemplary gating strategy for the analysis of EdU positive cells.	32
Figure 8: Exemplary Annexin V-FITC/ PI gating strategy.....	33
Figure 9: Wet-blot Western blot system.....	35
Figure 10: Human gastric cancer organoids.	46
Figure 11: Cancer organoid characterization concerning proliferation..	47
Figure 12: Immunohistochemistry comparison of gastric cancer organoids and derived xenograft tumors to primary cancer tissue.....	48
Figure 13: Gastric cancer organoids showed divergent response to conventional chemotherapy.....	49
Figure 14: Chemotherapy of classical gastric cancer cell lines.	50
Figure 15: Targeting of HER2/neu receptor pathway using trastuzumab.	54
Figure 16: Cell cycle arresting by small molecule targeting.....	55
Figure 17: Process of mouse gastric organoid generation.....	57
Figure 18: Adenoviral infection of normal organoids to generate gastric tumor mouse organoids.	59
Figure 19: Morphologic characterization of mouse gastric tumor organoids.....	60
Figure 20: Gastric cancer characterization of the RTK/RAS activated and diffuse gastric tumor model.	62
Figure 21: Anxa10-CreER ^{T2} mouse-a stomach specific mouse model.....	64
Figure 22: Intestinal GS model.	67
Figure 23: Diffuse GS model.	69
Figure 24: Serrated adenomatous GS model.	71
Figure 25: Gastric cancer organoid models characterized by different morphology and drug response.	73
Figure 26: Characteristics of the generated human gastric cancer biobank.	76
Figure 27: Characteristically features of each gastric cancer subtype.....	80

List of Tables

Table 1: Organoid cultures derived from adult tissue.	12
Table 2: For experiments used devices.....	17
Table 3: Additional material, equipment and used kits.	19
Table 4: Fine chemicals.	20
Table 5: Biochemicals.....	22
Table 6: Used primary antibody with usage dilution, blocking and secondary antibody.	23
Table 7: Used secondary antibody with usage and dilution.....	24
Table 8: Primer sequence for genotyping PCR reactions.....	24
Table 9: Primer sequence for qRT-PCRs.....	25
Table 10: Human gastric cancer 2D cell lines with the corresponding culture medium.....	26
Table 11: Selection medium for adenoviral infected mouse organoids.....	30
Table 12: For in vivo experiments used mice strains.....	42
Table 13: IC50 calculation of gastric cancer organoids and cell lines.....	51
Table 14: Targetable mutations found in DD107 and DD109.	53
Table 15: Gastric cancer subtype modelling using the Anxa10-CreER ^{T2} stomach specific mouse.	65

References

Al-Batran S-E, Hofheinz RD, Pauligk C, Kopp H-G, Haag GM, Luley KB, Meiler J, Homann N, Lorenzen S, Schmalenberg H, Probst S, Koenigsmann M, Egger M, Prasnikař N, Caca K, Trojan J, Martens UM, Block A, Fischbach W, Mahlberg R, Clemens M, Illerhaus G, Zirlik K, Behringer DM, Schmiegel W, Pohl M, Heike M, Ronellenfitch U, Schuler M, Bechstein WO, Königsrainer A, Gaiser T, Schirmacher P, Hozaeel W, Reichart A, Goetze TO, Sievert M, Jäger E, Mönig S, Tannapfel A. 2016. Histopathological regression after neoadjuvant docetaxel, oxaliplatin, fluorouracil, and leucovorin versus epirubicin, cisplatin, and fluorouracil or capecitabine in patients with resectable gastric or gastro-oesophageal junction adenocarcinoma (FLOT4-AIO): results from the phase 2 part of a multicentre, open-label, randomised phase 2/3 trial. *Lancet Oncol*, 17(12):1697–1708 DOI: 10.1016/S1470-2045(16)30531-9.

Alizadeh-Navaei R, Rafiei A, Abedian-Kenari S, Asgarian-Omran H, Valadan R, Hedayatizadeh-Omran A. 2016. Effect of first line gastric cancer chemotherapy regime on the AGS cell line-MTT assay results. *Asian Pacific J Cancer Prev*, 17(1):131–133 DOI: 10.7314/APJCP.2016.17.1.131.

Andersson-Rolf A, Mustata RC, Merenda A, Kim J, Perera S, Grego T, Andrews K, Tremble K, Silva JCR, Fink J, Skarnes WC, Koo B-K. 2017. One-step generation of conditional and reversible gene knockouts. *Nat Methods*, 14(3) DOI: 10.1038/nmeth.4156.

Arnold K, Sarkar A, Yram MA, Polo JM, Bronson R, Sengupta S, Seandel M, Geijsen N, Hochedlinger K. 2011. Sox2 + adult stem and progenitor cells are important for tissue regeneration and survival of mice. *Cell Stem Cell*, 9(4):317–329 DOI: 10.1016/j.stem.2011.09.001.

Arnold M, Soerjomataram I, Ferlay J, Forman D. 2015. Global incidence of oesophageal cancer by histological subtype in 2012. *Gut*, 64(3):381 LP – 387 DOI: 10.1136/gutjnl-2014-308124.

Asioli S, Maletta F, Verdun Di Cantogno L, Satolli MA, Schena M, Pecchioni C, Botta C, Chiusa L, Molinaro L, Conti L, Viale G, Ingravallo G, Maiorano E, Sapino A. 2012. Approaching heterogeneity of human epidermal growth factor receptor 2 in surgical specimens of gastric cancer. *Hum Pathol*, 43(11):2070–2079 DOI: 10.1016/j.humpath.2012.02.017.

Bang Y-J, Van Cutsem E, Feyereislova A, Chung HC, Shen L, Sawaki A, Lordick F, Ohtsu A, Omuro Y, Satoh T, Aprile G, Kulikov E, Hill J, Lehle M, Rüschoff J, Kang Y-K. 2010.

Trastuzumab in combination with chemotherapy versus chemotherapy alone for treatment of HER2-positive advanced gastric or gastro-oesophageal junction cancer (ToGA): a phase 3, open-label, randomised controlled trial. *Lancet*, 376(9742):687–697 DOI: 10.1016/S0140-6736(10)61121-X.

Barber M, Fitzgerald RC, Caldas C. 2006. Familial gastric cancer – aetiology and pathogenesis. *Best Pract Res Clin Gastroenterol*, 20(4):721–734 DOI: <https://doi.org/10.1016/j.bpg.2006.03.014>.

Barker N, Huch M, Kujala P, van de Wetering M, Snippert HJ, van Es JH, Sato T, Stange DE, Begthel H, van den Born M, Danenberg E, van den Brink S, Korving J, Abo A, Peters PJ, Wright N, Poulsom R, Clevers H. 2010. Lgr5+ve Stem Cells Drive Self-Renewal in the Stomach and Build Long-Lived Gastric Units In Vitro. *Cell Stem Cell*, 6(1):25–36 DOI: 10.1016/j.stem.2009.11.013.

Barker N, Ridgway RA, van Es JH, van de Wetering M, Begthel H, van den Born M, Danenberg E, Clarke AR, Sansom OJ, Clevers H. 2009. Crypt stem cells as the cells-of-origin of intestinal cancer. *Nature*, 457(7229):608–611 DOI: 10.1038/nature07602.

Bartfeld S, Bayram T, Van De Wetering M, Huch M, Begthel H, Kujala P, Vries R, Peters PJ, Clevers H. 2015. In vitro expansion of human gastric epithelial stem cells and their responses to bacterial infection. *Gastroenterology*, 148(1):126-136.e6 DOI: 10.1053/j.gastro.2014.09.042.

Becker K, Langer R, Reim D, Novotny A, Meyer zum Buschenfelde C, Engel J, Friess H, Hofler H. 2011. Significance of histopathological tumor regression after neoadjuvant chemotherapy in gastric adenocarcinomas: a summary of 480 cases. *Ann Surg*, 253(5):934–939 DOI: 10.1097/SLA.0b013e318216f449.

Bjerknes M, Cheng H. 2006. [14] - Intestinal Epithelial Stem Cells and Progenitors. In: Klimanskaya I, Lanza RBT-M in E (eds) *Adult Stem Cells*. Academic Press, pp. 337–383 DOI: [https://doi.org/10.1016/S0076-6879\(06\)19014-X](https://doi.org/10.1016/S0076-6879(06)19014-X).

Bjerknes M, Cheng H. 2002. Multipotential stem cells in adult mouse gastric epithelium. *Am J Physiol Liver Physiol*, 283(3):G767–G777 DOI: 10.1152/ajpgi.00415.2001.

Boj SF, Hwang C II, Baker LA, Chio IIC, Engle DD, Corbo V, Jager M, Ponz-Sarvisé M, Tiriác H, Spector MS, Gračanin A, Oni T, Yu KH, Van Boxtel R, Huch M, Rivera KD, Wilson JP, Feigin ME, Öhlund D, Handly-Santana A, Ardito-Abraham CM, Ludwig M, Elyada E, Alagesan B, Biffi G, Yordanov GN, Delcuze B, Creighton B, Wright K, Park Y, Morsink FHM, Molenaar

IQ, Borel Rinkes IH, Cuppen E, Hao Y, Jin Y, Nijman IJ, Iacobuzio-Donahue C, Leach SD, Pappin DJ, Hammell M, Klimstra DS, Basturk O, Hruban RH, Offerhaus GJ, Vries RGJ, Clevers H, Tuveson DA. 2015. Organoid models of human and mouse ductal pancreatic cancer. *Cell*, 160(1–2):324–338 DOI: 10.1016/j.cell.2014.12.021.

Boretto M, Cox B, Noben M, Hendriks N, Fassbender A, Roose H, Amant F, Timmerman D, Tomassetti C, Vanhie A, Meuleman C, Ferrante M, Vankelecom H. 2017. Development of organoids from mouse and human endometrium showing endometrial epithelium physiology and long-term expandability. *Development*, 144(10):1775–1786 DOI: 10.1242/dev.148478.

Bosman F, Carneiro F, Hruban R, Theise N. 2010. WHO Classification of Tumors of the Digestive System.

Boussadia O, Kutsch S, Hierholzer A, Delmas V, Kemler R. 2002. E-cadherin is a survival factor for the lactating mouse mammary gland. *Mech Dev*, 115(1–2):53–62 DOI: 10.1016/S0925-4773(02)00090-4.

Broda TR, McCracken KW, Wells JM. 2019. Generation of human antral and fundic gastric organoids from pluripotent stem cells. *Nat Protoc*, 14(1):28–50 DOI: 10.1038/s41596-018-0080-z.

Broutier L, Mastrogiovanni G, Verstegen MMA, Francies HE, Gavarró LM, Bradshaw CR, Allen GE, Arnes-Benito R, Sidorova O, Gaspersz MP, Georgakopoulos N, Koo B-K, Dietmann S, Davies SE, Praseedom RK, Lieshout R, IJzermans JNM, Wigmore SJ, Saeb-Parsy K, Garnett MJ, van der Laan LJW, Huch M. 2017. Human primary liver cancer–derived organoid cultures for disease modeling and drug screening. *Nat Med*, 23:1424 DOI: 10.1038/nm.4438.

Cao W, Liu J, Wang L, Li M, Verstegen MMA, Yin Y, Ma B, Chen K, Bolkestein M, Sprengers D, van der Laan LJW, Doukas M, Kwekkeboom J, Smits R, Peppelenbosch MP, Pan Q. 2018. Modeling liver cancer and therapy responsiveness using organoids derived from primary mouse liver tumors. *Carcinogenesis*, 40(1):145–154 DOI: 10.1093/carcin/bgy129.

Cerami E, Gao J, Dogrusoz U, Gross BE, Onur S, Larsson E, Antipin Y, Reva B, Goldberg AP, Sander C. 2014. The cBio Cancer Genomics Portal: An Open Platform for Exploring Multidimensional Cancer Genomics Data. *Cancer Discov*, 2(5):401–404 DOI: 10.1158/2159-8290.CD-12-0095.The.

Chakrabarti J, Holokai L, Syu L, Steele N, Chang J, Dlugosz A, Zavros Y. 2018. Mouse-Derived Gastric Organoid and Immune Cell Co-culture for the Study of the Tumor Microenvironment. In: Baratta M (ed) *Epithelial Cell Culture: Methods and Protocols*. Springer New York, New York, NY, pp. 157–168 DOI: 10.1007/978-1-4939-8600-2_16.

Choi E, Roland JT, Barlow BJ, O'Neal R, Rich AE, Nam KT, Shi C, Goldenring JR. 2014. Cell lineage distribution atlas of the human stomach reveals heterogeneous gland populations in the gastric antrum. *Gut*, 63(11):1711–1720 DOI: 10.1136/gutjnl-2013-305964.

Clevers H. 2016. Modeling Development and Disease with Organoids. *Cell*, 165(7):1586–1597 DOI: 10.1016/j.cell.2016.05.082.

Cunningham D, Allum WH, Stenning SP, Thompson JN, Van de Velde CJ, Nicolson M, Scarffe JH, Lofts FJ, Falk SJ, Iveson TJ, Smith DB, Langley RE, Verma M, Weeden S, Chua YJ, Participants MT. 2006. Perioperative chemotherapy versus surgery alone for resectable gastroesophageal cancer. *N Engl J Med*, 355(1):11–20 DOI: 10.1056/NEJMoa055531.

Dekkers JF, Whittle JR, Vaillant F, Chen H-R, Dawson C, Liu K, Geurts M, Herold MJ, Clevers H, Lindeman GJ, Visvader JE. 2019. Modeling breast cancer using CRISPR/Cas9-mediated engineering of human breast organoids. *JNCI J Natl Cancer Inst* DOI: 10.1093/jnci/djz196.

Demitrack ES, Gifford GB, Keeley TM, Carulli AJ, VanDussen KL, Thomas D, Giordano TJ, Liu Z, Kopan R, Samuelson LC. 2015. Notch signaling regulates gastric antral LGR5 stem cell function. *EMBO J*, 34(20):1–15 DOI: 10.15252/embj.201490583.

Dignass AU, Sturm A. 2001. Peptide growth factors in the intestine. *Eur J Gastroenterol Hepatol*, 13(7):763–770 DOI: 10.1097/00042737-200107000-00002.

Dijkstra KK, Cattaneo CM, Weeber F, Chalabi M, van de Haar J, Fanchi LF, Slagter M, van der Velden DL, Kaing S, Kelderman S, van Rooij N, van Leerdam ME, Depla A, Smit EF, Hartemink KJ, de Groot R, Wolkers MC, Sachs N, Snaebjornsson P, Monkhorst K, Haanen J, Clevers H, Schumacher TN, Voest EE. 2018. Generation of Tumor-Reactive T Cells by Co-culture of Peripheral Blood Lymphocytes and Tumor Organoids. *Cell*, 174(6):1586-1598.e12 DOI: 10.1016/j.cell.2018.07.009.

Drost J, van Jaarsveld RH, Ponsioen B, Zimmerlin C, van Boxtel R, Buijs A, Sachs N, Overmeer RM, Offerhaus GJ, Begthel H, Korving J, van de Wetering M, Schwank G, Logtenberg M, Cuppen E, Snippert HJ, Medema JP, Kops GJPL, Clevers H. 2015. Sequential cancer mutations in cultured human intestinal stem cells. *Nature*, 521:43 DOI: doi.org/10.1038/nature14415.

Evans GS, Flint N, Somers AS, Eyden B, Potten CS. 1992. The development of a method for the preparation of rat intestinal epithelial cell primary cultures. *J Cell Sci*, 101(1):219–231.

Farley FW, Soriano P, Steffen LS, Dymecki SM. 2000. Widespread recombinase expression using FLPeR (Flipper) mice. *genesis*, 28(3- 4):106–110 DOI: 10.1002/1526-

968X(200011/12)28:3/4<106::AID-GENE30>3.0.CO;2-T.

Fatehullah A, Tan SH, Barker N. 2016. Organoids as an in vitro model of human development and disease. *Nat Cell Biol*, 18(3):246–54 DOI: 10.1038/ncb3312.

Ferlay J, Soerjomataram I, Dikshit R, Eser S, Mathers C, Rebelo M, Parkin DM, Forman D, Bray F. 2015. Cancer incidence and mortality worldwide: Sources, methods and major patterns in GLOBOCAN 2012. *Int J Cancer*, 136(5):E359–E386 DOI: 10.1002/ijc.29210.

Florou D, Patsis C, Ardavanis A, Scorilas A. 2013. Effect of doxorubicin, oxaliplatin, and methotrexate administration on the transcriptional activity of BCL-2 family gene members in stomach cancer cells. *Cancer Biol Ther*, 14(7):587–596 DOI: 10.4161/cbt.24591.

Friedrich G, Soriano P. 1991. Promoter traps in embryonic stem cells: A genetic screen to identify and mutate developmental genes in mice. *Genes Dev*, 5(9):1513–1523 DOI: 10.1101/gad.5.9.1513.

Fuchs CS, Tomasek J, Yong CJ, Dumitru F, Passalacqua R, Goswami C, Safran H, Dos Santos LV, Aprile G, Ferry DR, Melichar B, Tehfe M, Topuzov E, Zalcborg JR, Chau I, Campbell W, Sivanandan C, Pikiel J, Koshiji M, Hsu Y, Liepa AM, Gao L, Schwartz JD, Tabernero J. 2014. Ramucirumab monotherapy for previously treated advanced gastric or gastro-oesophageal junction adenocarcinoma (REGARD): An international, randomised, multicentre, placebo-controlled, phase 3 trial. *Lancet*, 383(9911):31–39 DOI: 10.1016/S0140-6736(13)61719-5.

Fumagalli A, Drost J, Suijkerbuijk SJE, van Boxtel R, de Ligt J, Offerhaus GJ, Begthel H, Beerling E, Tan EH, Sansom OJ, Cuppen E, Clevers H, van Rheenen J. 2017. Genetic dissection of colorectal cancer progression by orthotopic transplantation of engineered cancer organoids. *Proc Natl Acad Sci*, 114(12):E2357 LP-E2364 DOI: 10.1073/pnas.1701219114.

Gao Dong, Vela I, Sboner A, Iaquinta PJ, Karthaus WR, Gopalan A, Dowling C, Wanjala JN, Undvall EA, Arora VK, Wongvipat J, Kossai M, Ramazanoglu S, Barboza LP, Di W, Cao Z, Zhang QF, Sirota I, Ran L, Macdonald TY, Beltran H, Mosquera JM, Touijer KA, Scardino PT, Laudone VP, Curtis KR, Rathkopf DE, Morris MJ, Danila DC, Slovin SF, Solomon SB, Eastham JA, Chi P, Carver B, Rubin MA, Scher HI, Clevers H, Sawyers CL, Chen Y. 2014. Organoid cultures derived from patients with advanced prostate cancer. *Cell*, 159(1):176–187 DOI: 10.1016/j.cell.2014.08.016.

Gao Jianjiong, Aksoy BA, Dogrusoz U, Dresdner G, Gross B, Sumer SO, Sun Y, Jacobsen A, Sinha R, Larsson E, Ethan C, Sander C, Schultz N. 2014. Integrative analysis of complex

cancer genomics and clinical profiles using cBioPortal. *Sci Signal*, 6(269):1–34 DOI: 10.1126/scisignal.2004088.

Gao M, Lin M, Rao M, Thompson H, Hirai K, Choi M, Georgakis G V, Sasson AR, Bucobo JC, Tzimas D, D'Souza LS, Buscaglia JM, Davis J, Shroyer KR, Li J, Powers S, Kim J. 2018. Development of Patient-Derived Gastric Cancer Organoids from Endoscopic Biopsies and Surgical Tissues. *Ann Surg Oncol*, 25(9):2767–2775 DOI: 10.1245/s10434-018-6662-8.

Gao X, Tate P, Hu P, Tjian R, Skarnes WC, Wang Z. 2008. ES cell pluripotency and germ-layer formation require the SWI / SNF chromatin remodeling component BAF250a. *Proc Natl Acad Sci U S A*, 105(18):6656–6661 DOI: 10.1073/pnas.0801802105.

Global Burden of Disease Cancer Collaboration. 2015. The global burden of cancer 2013. *JAMA Oncol*, 1(4):505–527 DOI: 10.1001/jamaoncol.2015.0735.

Hanahan D, Weinberg RA. 2011. Hallmarks of cancer: The next generation. *Cell*, 144(5):646–674 DOI: 10.1016/j.cell.2011.02.013.

Hanahan D, Weinberg RA. 2000. The Hallmarks of Cancer. *Cell*, 100(1):57–70 DOI: 10.1016/S0092-8674(00)81683-9.

Haramis A-PG, Begthel H, van den Born M, van Es J, Jonkheer S, Offerhaus GJA, Clevers H. 2004. De Novo Crypt Formation and Juvenile Polyposis on BMP Inhibition in Mouse Intestine. *Science (80-)*, 303(5664):1684 LP – 1686 DOI: 10.1126/science.1093587.

Hayakawa Y, Ariyama H, Stancikova J, Sakitani K, Asfaha S, Renz BW, Dubeykovskaya ZA, Shibata W, Wang H, Westphalen CB, Chen X, Takemoto Y, Kim W, Khurana SS, Tailor Y, Nagar K, Tomita H, Hara A, Sepulveda AR, Setlik W, Gershon MD, Saha S, Ding L, Shen Z, Fox JG, Friedman RA, Konieczny SF, Worthley DL, Korinek V, Wang TC. 2015. Mist1 Expressing Gastric Stem Cells Maintain the Normal and Neoplastic Gastric Epithelium and Are Supported by a Perivascular Stem Cell Niche. *Cancer Cell*, 28(6):800–814 DOI: 10.1016/j.ccell.2015.10.003.

He XC, Zhang J, Tong W-G, Tawfik O, Ross J, Scoville DH, Tian Q, Zeng X, He X, Wiedemann LM, Mishina Y, Li L. 2004. BMP signaling inhibits intestinal stem cell self-renewal through suppression of Wnt– β -catenin signaling. *Nat Genet*, 36(10):1117–1121 DOI: 10.1038/ng1430.

Hofmann C, Obermeier F, Artinger M, Hausmann M, Falk W, Schoelmerich J, Rogler G, Grossmann J. 2007. Cell-Cell Contacts Prevent Anoikis in Primary Human Colonic Epithelial Cells. *Gastroenterology*, 132(2):587–600 DOI: 10.1053/j.gastro.2006.11.017.

Hu B, Hajj N El, Sittler S, Lammert N, Barnes R, Meloni-Ehrig A. 2012. Gastric cancer: Classification, histology and application of molecular pathology. *J Gastrointest Oncol*, 3(3):251–261 DOI: 10.3978/j.issn.2078-6891.2012.021.

Hu H, Gehart H, Artegiani B, López-Iglesias C, Dekkers F, Basak O, van Es J, Chuva de Sousa Lopes SM, Begthel H, Korving J, van den Born M, Zou C, Quirk C, Chiriboga L, Rice CM, Ma S, Rios A, Peters PJ, de Jong YP, Clevers H. 2018. Long-Term Expansion of Functional Mouse and Human Hepatocytes as 3D Organoids. *Cell*, 175(6):1591-1606.e19 DOI: <https://doi.org/10.1016/j.cell.2018.11.013>.

Huang S, Ye H, Guo W, Dong X, Wu N, Zhang X, Huang Z. 2015. CDK4/6 inhibitor suppresses gastric cancer with CDKN2A mutation. *Int J Clin Exp Med*, 8(7):11692–11700.

Hubert CG, Rivera M, Spangler LC, Wu Q, Mack SC, Prager BC, Couce M, McLendon RE, Sloan AE, Rich JN. 2016. A Three-Dimensional Organoid Culture System Derived from Human Glioblastomas Recapitulates the Hypoxic Gradients and Cancer Stem Cell Heterogeneity of Tumors Found *In Vivo&/em>*; *Cancer Res*, 76(8):2465 LP – 2477 DOI: 10.1158/0008-5472.CAN-15-2402.

Huch M, Boj SF, Clevers H. 2013. Lgr5+ liver stem cells, hepatic organoids and regenerative medicine. *Regen Med*, 8(4):385–387 DOI: 10.2217/rme.13.39.

Huch M, Bonfanti P, Boj SF, Sato T, Loomans CJM, van de Wetering M, Sojoodi M, Li VSW, Schuijers J, Gračanin A, Ringnalda F, Begthel H, Hamer K, Mulder J, van Es JH, de Koning E, Vries RGJ, Heimberg H, Clevers H. 2013. Unlimited in vitro expansion of adult bi-potent pancreas progenitors through the Lgr5/R-spondin axis. *EMBO J*, 32(20):2708–2721 DOI: 10.1038/emboj.2013.204.

Huch M, Gehart H, van Boxtel R, Hamer K, Blokzijl F, Verstegen MMA, Ellis E, van Wenum M, Fuchs SA, de Ligt J, van de Wetering M, Sasaki N, Boers SJ, Kemperman H, de Jonge J, Ijzermans JNM, Nieuwenhuis EES, Hoekstra R, Strom S, Vries RRG, van der Laan LJW, Cuppen E, Clevers H. 2015. Long-Term Culture of Genome-Stable Bipotent Stem Cells from Adult Human Liver. *Cell*, 160(1):299–312 DOI: 10.1016/j.cell.2014.11.050.

Hunt RH, Camilleri M, Crowe SE, El-Omar EM, Fox JG, Kuipers EJ, Malfertheiner P, McColl KEL, Pritchard DM, Rugge M, Sonnenberg A, Sugano K, Tack J. 2015. The stomach in health and disease. *Gut*, 64(10):1650 LP – 1668 DOI: 10.1136/gutjnl-2014-307595.

Isaacson J, Cattanch B. 1962. Two new “hairless” mutants - Sha and Hfh11. *Mouse New Lett*, 27:31.

Jackson EL, Willis N, Mercer K, Bronson RT, Crowley D, Montoya R, Jacks T, Tuveson DA. 2001. Analysis of lung tumor initiation and progression using conditional expression of oncogenic K-ras. *Genes Dev*, 15(24):3243–3248 DOI: 10.1101/gad.943001.

Jung P, Sato T, Merlos-Suárez A, Barriga FM, Iglesias M, Rossell D, Auer H, Gallardo M, Blasco MA, Sancho E, Clevers H, Batlle E. 2011. Isolation and in vitro expansion of human colonic stem cells. *Nat Med*, 17(10):1225–1227 DOI: 10.1038/nm.2470.

Karam SM. 1999. Lineage commitment and maturation of epithelial cells in the gut. *Front Biosci*, 4(1):286–298 DOI: 10.2741/Karam.

Karam SM, Leblond CP. 1993a. Dynamics of epithelial cells in the corpus of the mouse stomach. I. Identification of proliferative cell types and pinpointing of the stem cell. *Anat Rec*, 236(2):259–279 DOI: 10.1002/ar.1092360202.

Karam SM, Leblond CP. 1993b. Dynamics of epithelial cells in the corpus of the mouse stomach. II. Outward migration of pit cells. *Anat Rec*, 236(2):280–296 DOI: 10.1002/ar.1092360203.

Karam SM, Leblond CP. 1993c. Dynamics of epithelial cells in the corpus of the mouse stomach. III. Inward migration of neck cells followed by progressive transformation into zymogenic cells. *Anat Rec*, 236(2):297–313 DOI: 10.1002/ar.1092360204.

Karam SM, Leblond CP. 1993d. Dynamics of epithelial cells in the corpus of the mouse stomach. V. Behavior of entero-endocrine and caveolated cells: General conclusions on cell kinetics in the oxyntic epithelium. *Anat Rec*, 236(2):333–340 DOI: 10.1002/ar.1092360206.

Karam SM, Leblond CP. 1992. Identifying and counting epithelial cell types in the “corpus” of the mouse stomach. *Anat Rec*, 232(2):231–246 DOI: 10.1002/ar.1092320208.

Karthus WR, Iaquina PJ, Drost J, Gračanin A, Van Boxtel R, Wongvipat J, Dowling CM, Gao D, Begthel H, Sachs N, Vries RGJ, Cuppen E, Chen Y, Sawyers CL, Clevers HC. 2014. Identification of multipotent luminal progenitor cells in human prostate organoid cultures. *Cell*, 159(1):163–175 DOI: 10.1016/j.cell.2014.08.017.

Kavuri SM, Jain N, Galimi F, Cottino F, Leto SM, Migliardi G, Searleman AC, Shen W, Monsey J, Trusolino L, Jacobs SA, Bertotti A, Bose R. 2015. HER2 activating mutations are targets for colorectal cancer treatment. *Cancer Discov*, 5(8):832–841 DOI: 10.1158/2159-8290.CD-14-1211.

Kessler M, Hoffmann K, Brinkmann V, Thieck O, Jackisch S, Toelle B, Berger H, Mollenkopf

H-J, Mangler M, Sehouli J, Fotopoulou C, Meyer TF. 2015. The Notch and Wnt pathways regulate stemness and differentiation in human fallopian tube organoids. *Nat Commun*, 6:8989 DOI: 10.1038/ncomms9989.

Kim K-A, Kakitani M, Zhao J, Oshima T, Tang T, Binnerts M, Liu Y, Boyle B, Park E, Emtage P, Funk WD, Tomizuka K. 2005. Mitogenic Influence of Human R-Spondin1 on the Intestinal Epithelium. *Science* (80-), 309(5738):1256 LP – 1259 DOI: 10.1126/science.1112521.

Kim T-H, Shivdasani RA. 2016. Stomach development, stem cells and disease. *Development*, 143(4):554–565 DOI: 10.1242/dev.124891.

Kinoshita H, Hayakawa Y, Koike K. 2017. Metaplasia in the stomach—precursor of gastric Cancer? *Int J Mol Sci*, 18(10) DOI: 10.3390/ijms18102063.

Kinoshita H, Hayakawa Y, Konishi M, Hata M, Tsuboi M, Hayata Y, Hikiba Y, Ihara S, Nakagawa H, Ikenoue T, Ushiku T, Fukayama M, Hirata Y, Koike K. 2018. Three types of metaplasia models through Kras activation, Pten deletion, or Cdh1 deletion in the gastric epithelium. *J Pathol*, 247(1):35–47 DOI: 10.1002/path.5163.

Koelz H. 1992. Gastric acids in vertebrates. *Scand J Gastroenterol Suppl*, 193:2–6 DOI: 10.3109/00365529209095998.

Korinek V, Barker N, Moerer P, van Donselaar E, Huls G, Peters PJ, Clevers H. 1998. Depletion of epithelial stem-cell compartments in the small intestine of mice lacking Tcf-4. *Nat Genet*, 19(4):379–383 DOI: 10.1038/1270.

Kuhnert F, Davis CR, Wang H-T, Chu P, Lee M, Yuan J, Nusse R, Kuo CJ. 2004. Essential requirement for Wnt signaling in proliferation of adult small intestine and colon revealed by adenoviral expression of Dickkopf-1. *Proc Natl Acad Sci*, 101(1):266 LP – 271 DOI: 10.1073/pnas.2536800100.

Kuraguchi M, Wang XP, Bronson RT, Rothenberg R, Ohene-Baah NY, Lund JJ, Kucherlapati M, Maas RL, Kucherlapati R. 2006. Adenomatous polyposis coli (APC) is required for normal development of skin and thymus. *PLoS Genet*, 2(9):1362–1374 DOI: 10.1371/journal.pgen.0020146.

Kwon GS, Viotti M, Hadjantonakis A-K. 2008. The Endoderm of the Mouse Embryo Arises by Dynamic Widespread Intercalation of Embryonic and Extraembryonic Lineages. *Dev Cell*, 15(4):509–520 DOI: 10.1016/j.devcel.2008.07.017.

Lancaster MA, Huch M. 2019. Disease modelling in human organoids. *Dis Model Mech*,

12(7):dmm039347 DOI: 10.1242/dmm.039347.

de Lau W, Barker N, Low TY, Koo B-K, Li VSW, Teunissen H, Kujala P, Haegebarth A, Peters PJ, van de Wetering M, Stange DE, van Es JE, Guardavaccaro D, Schasfoort RBM, Mohri Y, Nishimori K, Mohammed S, Heck AJR, Clevers H. 2011. Lgr5 homologues associate with Wnt receptors and mediate R-spondin signalling. *Nature*, 476(7360):293–297 DOI: 10.1038/nature10337.

Lauren P. 1965. The two histological main types of gastric carcinoma: diffuse and so-called intestinal-type carcinoma. *Acta Pathol Microbiol Scand*, 64:31–49 DOI: 10.1002/1097-0142(197706)39:6<2475::AID-CNCR2820390626>3.0.CO;2-L.

Lawson KA, Meneses JJ, Pedersen RA. 1986. Cell fate and cell lineage in the endoderm of the presomite mouse embryo, studied with an intracellular tracer. *Dev Biol*, 115(2):325–339 DOI: 10.1016/0012-1606(86)90253-8.

Lee CS, Sund NJ, Behr R, Herrera PL, Kaestner KH. 2005. Foxa2 is required for the differentiation of pancreatic α -cells. *Dev Biol*, 278(2):484–495 DOI: 10.1016/j.ydbio.2004.10.012.

Lee ER, Trasler J, Dwivedi S, Leblond CP. 1982. Division of the mouse gastric mucosa into zymogenic and mucous regions on the basis of gland features. *Am J Anat*, 164(3):187–207 DOI: 10.1002/aja.1001640302.

Lee J-H, Bhang DH, Beede A, Huang TL, Stripp BR, Bloch KD, Wagers AJ, Tseng Y-H, Ryeom S, Kim CF. 2014. Lung stem cell differentiation in mice directed by endothelial cells via a BMP4-NFATc1-thrombospondin-1 axis. *Cell*, 156(3):440–455 DOI: 10.1016/j.cell.2013.12.039.

Lee J, Snyder ER, Liu Y, Gu X, Wang J, Flowers BM, Kim YJ, Park S, Szot GL, Hruban RH, Longacre TA, Kim SK. 2017. Reconstituting development of pancreatic intraepithelial neoplasia from primary human pancreas duct cells. *Nat Commun*, 8(1):14686 DOI: 10.1038/ncomms14686.

Lee Jun H, Chang ĀKK, Yoon ĀC, Tang ĀLH, Strong VE, Yoon SS. 2018. Lauren Histologic Type Is the Most Important Factor Associated With Pattern of Recurrence Following Resection of Gastric Adenocarcinoma. , 267(1):105–113 DOI: 10.1097/SLA.0000000000002040.

Lee Suk Hyung, Hu W, Matulay JT, Silva M V, Owczarek TB, Kim K, Chua CW, Barlow LJ, Kandoth C, Williams AB, Bergren SK, Pietzak EJ, Anderson CB, Benson MC, Coleman JA,

Taylor BS, Abate-Shen C, McKiernan JM, Al-Ahmadie H, Solit DB, Shen MM. 2018. Tumor Evolution and Drug Response in Patient-Derived Organoid Models of Bladder Cancer. *Cell*, 173(2):515–528 DOI: 10.1016/j.cell.2018.03.017.

Leushacke M, Ng A, Galle J, Loeffler M, Barker N. 2013. Lgr5+ Gastric Stem Cells Divide Symmetrically to Effect Epithelial Homeostasis in the Pylorus. *Cell Rep*, 5(2):349–356 DOI: 10.1016/j.celrep.2013.09.025.

Li X, Francies HE, Secrier M, Perner J, Miremadi A, Galeano-Dalmau N, Barendt WJ, Letchford L, Leyden GM, Goffin EK, Barthorpe A, Lightfoot H, Chen E, Gilbert J, Noorani A, Devonshire G, Bower L, Grantham A, MacRae S, Grehan N, Wedge DC, Fitzgerald RC, Garnett MJ. 2018. Organoid cultures recapitulate esophageal adenocarcinoma heterogeneity providing a model for clonality studies and precision therapeutics. *Nat Commun*, 9(1):2983 DOI: 10.1038/s41467-018-05190-9.

Li X, Nadauld L, Ootani A, Corney DC, Pai RK, Gevaert O, Cantrell MA, Rack PG, Neal JT, Chan CWM, Yeung T, Gong X, Yuan J, Wilhelmy J, Robine S, Attardi LD, Plevritis SK, Hung KE, Chen CZ, Ji HP, Kuo CJ. 2014. Oncogenic transformation of diverse gastrointestinal tissues in primary organoid culture. *Nat Med*, 20(7):769–777 DOI: 10.1038/nm.3585.

Linnemann JR, Miura H, Meixner LK, Irmeler M, Kloos UJ, Hirschi B, Bartsch HS, Sass S, Beckers J, Theis FJ, Gabka C, Sotlar K, Scheel CH. 2015. Quantification of regenerative potential in primary human mammary epithelial cells. *Development*, 142(18):3239–3251 DOI: 10.1242/dev.123554.

Lochhead P, El-Omar EM. 2008. Gastric cancer. *Br Med Bull*, 85(1):87–100 DOI: 10.1093/bmb/ldn007.

Longacre TA, Fenoglio-Preiser CM. 1990. Mixed hyperplastic adenomatous polyps/serrated adenomas. A distinct form of colorectal neoplasia. *American J Surg Pathol*, 14(6):524–37 DOI: 10.1097/00000478-199006000-00003.

Lordick F, Janjigian YY. 2016. Clinical impact of tumour biology in the management of gastroesophageal cancer. *Nat Rev Clin Oncol*, 13(6):348–360 DOI: 10.1038/nrclinonc.2016.15.

Maimets M, Rocchi C, Bron R, Pringle S, Kuipers J, Giepmans BNG, Vries RGJ, Clevers H, de Haan G, van Os R, Coppes RP. 2016. Long-Term In Vitro Expansion of Salivary Gland Stem Cells Driven by Wnt Signals. *Stem Cell Reports*, 6(1):150–162 DOI: <https://doi.org/10.1016/j.stemcr.2015.11.009>.

Matano M, Date S, Shimokawa M, Takano A, Fujii M, Ohta Y, Watanabe T, Kanai T, Sato T. 2015. Modeling colorectal cancer using CRISPR-Cas9-mediated engineering of human intestinal organoids. *Nat Med*, 21(3):256–62 DOI: 10.1038/nm.3802.

McColl KEL, Going JJ. 2010. Aetiology and classification of adenocarcinoma of the gastro-oesophageal junction/cardia. *Gut*, 59(3):282 LP – 284 DOI: 10.1136/gut.2009.186825.

McCracken KW, Catá EM, Crawford CM, Sinagoga KL, Schumacher M, Rockich BE, Tsai Y-H, Mayhew CN, Spence JR, Zavros Y, Wells JM. 2014. Modelling human development and disease in pluripotent stem-cell-derived gastric organoids. *Nature*, 516:400 DOI: 10.1038/nature13863.

Means AL, Xu Y, Zhao A, Ray KC, Gu G. 2008. A CK19CreERT knockin mouse line allows for conditional DNA recombination in epithelial cells in multiple endodermal organs. *Genesis*, 46(6):318–323 DOI: 10.1002/dvg.20397.

Merker SR, Weitz J, Stange DE. 2016. Gastrointestinal organoids: How they gut it out. *Dev Biol*, 420:239–250 DOI: 10.1016/j.ydbio.2016.08.010.

Mills JC, Shivdasani RA. 2011. Gastric epithelial stem cells. *Gastroenterology*, 140(2):412–424 DOI: 10.1053/j.gastro.2010.12.001.

Mullenders J, de Jongh E, Brousalı A, Roosen M, Blom JPA, Begthel H, Korving J, Jonges T, Kranenburg O, Meijer R, Clevers HC. 2019a. Mouse and human urothelial cancer organoids: A tool for bladder cancer research. *Proc Natl Acad Sci*, 116(10):4567 LP – 4574 DOI: 10.1073/pnas.1803595116.

Mullenders J, de Jongh E, Brousalı A, Roosen M, Blom JPA, Begthel H, Korving J, Jonges T, Kranenburg O, Meijer R, Clevers HC. 2019b. Mouse and human urothelial cancer organoids: A tool for bladder cancer research. *Proc Natl Acad Sci*, 116(10):4567 LP – 4574 DOI: 10.1073/pnas.1803595116.

Nanki K, Toshimitsu K, Takano A, Fujii M, Shimokawa M, Ohta Y, Matano M, Seino T, Nishikori S, Ishikawa K, Kawasaki K, Togasaki K, Takahashi S, Sukawa Y, Ishida H, Sugimoto S, Kawakubo H, Kim J, Kitagawa Y, Sekine S, Koo B-K, Kanai T, Sato T. 2018. Divergent Routes toward Wnt and R-spondin Niche Independency during Human Gastric Carcinogenesis. *Cell*, 174(4):856-869.e17 DOI: 10.1016/j.cell.2018.07.027.

Noguchi TK, Ninomiya N, Sekine M, Komazaki S, Wang P-C, Asashima M, Kurisaki A. 2015. Generation of stomach tissue from mouse embryonic stem cells. *Nat Cell Biol*, 17(8):984–93 DOI: 10.1038/ncb3200.

Nuciforo S, Fofana I, Matter MS, Blumer T, Calabrese D, Boldanova T, Piscuoglio S, Wieland S, Ringnalda F, Schwank G, Terracciano LM, Ng CKY, Heim MH. 2018. Organoid Models of Human Liver Cancers Derived from Tumor Needle Biopsies. *Cell Rep*, 24(5):1363–1376 DOI: <https://doi.org/10.1016/j.celrep.2018.07.001>.

Olive KP, Tuveson DA, Ruhe ZC, Yin B, Willis NA, Bronson RT, Crowley D, Jacks T. 2004. Mutant *p53* Gain of Function in Two Mouse Models of Li-Fraumeni Syndrome. *Cell*, 119(6):847–860 DOI: 10.1016/j.cell.2004.11.004.

Ootani A, Li X, Sangiorgi E, Ho QT, Ueno H, Toda S, Sugihara H, Fujimoto K, Weissman IL, Capecchi MR, Kuo CJ. 2009. Sustained in vitro intestinal epithelial culture within a Wnt-dependent stem cell niche. *Nat Med*, 15:701 DOI: 10.1038/nm.1951.

Parkin DM, Läärä E, Muir CS. 1988. Estimates of the worldwide frequency of sixteen major cancers in 1980. *Int J Cancer*, 41(2):184–197 DOI: 10.1002/ijc.2910410205.

Paterson AL, Shannon NB, Lao-Sirieix P, Ong C-AJ, Peters CJ, O'Donovan M, Fitzgerald RC. 2013. A systematic approach to therapeutic target selection in oesophago-gastric cancer. *Gut*, 62(10):1415 LP – 1424 DOI: 10.1136/gutjnl-2012-302039.

Peleteiro B, Bastos A, Ferro A, Lunet N. 2014. Prevalence of Helicobacter pylori Infection Worldwide: A Systematic Review of Studies with National Coverage. *Dig Dis Sci*, 59(8):1698–1709 DOI: 10.1007/s10620-014-3063-0.

Peng WC, Logan CY, Fish M, Anbarchian T, Aguisanda F, Álvarez-Varela A, Wu P, Jin Y, Zhu J, Li B, Grompe M, Wang B, Nusse R. 2018. Inflammatory Cytokine TNF α Promotes the Long-Term Expansion of Primary Hepatocytes in 3D Culture. *Cell*, 175(6):1607-1619.e15 DOI: <https://doi.org/10.1016/j.cell.2018.11.012>.

Pinto D, Gregorieff A, Begthel H, Clevers H. 2003. Canonical Wnt signals are essential for homeostasis of the intestinal epithelium. *Genes Dev*, 17(14):1709–1713 DOI: 10.1101/gad.267103.

Polkowski W, van Sandick JW, Offerhaus GJA, ten Kate FJW, Mulder J, Obertop H, van Lanschot JJB. 1999. Prognostic Value of Laurén Classification and c-erbB-2 Oncogene Overexpression in Adenocarcinoma of the Esophagus and Gastroesophageal Junction. *Ann Surg Oncol*, 6(3):290–297 DOI: 10.1007/s10434-999-0290-2.

Pompaiyah M, Bartfeld S. 2017. Molecular Pathogenesis and Signal Transduction by Helicobacter pylori. *Cell Mic*, 400:149–168 DOI: 10.1007/978-3-319-50520-6.

Pringle S, Maimets M, van der Zwaag M, Stokman MA, van Gosliga D, Zwart E, Witjes MJH, de Haan G, van Os R, Coppes RP. 2016. Human Salivary Gland Stem Cells Functionally Restore Radiation Damaged Salivary Glands. *Stem Cells*, 34(3):640–652 DOI: 10.1002/stem.2278.

Quante M, Marrache F, Goldenring JR, Wang TC. 2010. TFF2 mRNA transcript expression marks a gland progenitor cell of the gastric oxyntic mucosa. *Gastroenterology*, 139(6):2018–2027.e2 DOI: 10.1053/j.gastro.2010.08.003.

Roman AKS, Shivdasani RA. 2011. Boundaries, junctions and transitions in the gastrointestinal tract. *Exp Cell Res*, 317(19):2711–2718 DOI: <https://doi.org/10.1016/j.yexcr.2011.07.011>.

Rubio CA. 2001. Serrated neoplasia of the stomach: a new entity. *J Clin Pathol*, 54(11):849–853 DOI: 10.1136/jcp.54.11.849.

Sachs N, Papaspyropoulos A, Zomer-van Ommen DD, Heo I, Böttinger L, Klay D, Weeber F, Huelsz-Prince G, Iakobachvili N, Amatngalim GD, de Ligt J, van Hoeck A, Proost N, Viveen MC, Lyubimova A, Teeven L, Derakhshan S, Korving J, Begthel H, Dekkers JF, Kumawat K, Ramos E, van Oosterhout MF, Offerhaus GJ, Wiener DJ, Olimpio EP, Dijkstra KK, Smit EF, van der Linden M, Jaksani S, van de Ven M, Jonkers J, Rios AC, Voest EE, van Moorsel CH, van der Ent CK, Cuppen E, van Oudenaarden A, Coenjaerts FE, Meyaard L, Bont LJ, Peters PJ, Tans SJ, van Zon JS, Boj SF, Vries RG, Beekman JM, Clevers H. 2019. Long-term expanding human airway organoids for disease modeling. *EMBO J*, 38(4):e100300 DOI: 10.15252/embj.2018100300.

Sasaki T, Giltay R, Talts U, Timpl R, Talts JF. 2002. Expression and distribution of laminin $\alpha 1$ and $\alpha 2$ chains in embryonic and adult mouse tissues: An immunochemical approach. *Exp Cell Res*, 275(2):185–199 DOI: 10.1006/excr.2002.5499.

Sato T, van Es JH, Snippert HJ, Stange DE, Vries RG, van den Born M, Barker N, Shroyer NF, van de Wetering M, Clevers H. 2011. Paneth cells constitute the niche for Lgr5 stem cells in intestinal crypts. *Nature*, 469(7330):415–418 DOI: 10.1038/nature09637.

Sato T, Stange DE, Ferrante M, Vries RGJ, Van Es JH, Van Den Brink S, Van Houdt WJ, Pronk A, Van Gorp J, Siersema PD, Clevers H. 2011. Long-term expansion of epithelial organoids from human colon, adenoma, adenocarcinoma, and Barrett's epithelium. *Gastroenterology*, 141(5):1762–1772 DOI: 10.1053/j.gastro.2011.07.050.

Sato T, Vries RG, Snippert HJ, van de Wetering M, Barker N, Stange DE, van Es JH, Abo A,

Kujala P, Peters PJ, Clevers H. 2009. Single Lgr5 stem cells build crypt-villus structures in vitro without a mesenchymal niche. *Nature*, 459(7244):262–5 DOI: 10.1038/nature07935.

Satoki S, Yoshihiro H, Kosuke S, Shinzo Y, Takako S, Ryota N, Hirotsugu W, Shuntaro Y, Atsuo Y, Yutaka Y, Tetsuo U, Masashi F, Kazuhiko K. 2015. Distribution of intestinal metaplasia as a predictor of gastric cancer development. *J Gastroenterol Hepatol*, 30(8):1260–1264 DOI: 10.1111/jgh.12946.

Schepers A, Clevers H. 2012. Wnt signaling, stem cells, and cancer of the gastrointestinal tract. *Cold Spring Harb Perspect Biol*, 4(4):a007989–a007989 DOI: 10.1101/cshperspect.a007989.

Schepers AG, Snippert HJ, Stange DE, van den Born M, van Es JH, van de Wetering M, Clevers H. 2012. Lineage tracing reveals Lgr5+ stem cell activity in mouse intestinal adenomas. *Science (80-)*, 337(6095):730 LP – 735 DOI: 10.1126/science.1224676.

Schlaermann P, Toelle B, Berger H, Schmidt SC, Glanemann M, Ordemann J, Bartfeld S, Mollenkopf HJ, Meyer TF. 2016. A novel human gastric primary cell culture system for modelling *Helicobacter pylori* infection in vitro. *Gut*, 65(2):202 LP – 213 DOI: 10.1136/gutjnl-2014-307949.

Schumacher MA, Aihara E, Feng R, Engevik A, Shroyer NF, Ottemann KM, Worrell RT, Montrose MH, Shivdasani RA, Zavros Y. 2015. The use of murine-derived fundic organoids in studies of gastric physiology. *J Physiol*, 593(8):1809–1827 DOI: 10.1113/jphysiol.2014.283028.

Schweiger PJ, Clement DL, Page ME, Schepeler T, Zou X, Sirokmány G, Watt FM, Jensen KB. 2018. Lrig1 marks a population of gastric epithelial cells capable of long-term tissue maintenance and growth in vitro. *Sci Rep*, 8(1):15255 DOI: 10.1038/s41598-018-33578-6.

Seidlitz T, Merker SR, Rothe A, Zakrzewski F, von Neubeck C, Grützmann K, Sommer U, Schweitzer C, Schölch S, Uhlemann H, Gaebler A-M, Werner K, Krause M, Baretton GB, Welsch T, Koo B-K, Aust DE, Klink B, Weitz J, Stange DE. 2019a. Human gastric cancer modelling using organoids. *Gut*, 68(2):207–217 DOI: 10.1136/gutjnl-2017-314549.

Seidlitz T, Chen Y-T, Uhlemann H, Schölch S, Kochall S, Merker SR, Klimova A, Hennig A, Schweitzer C, Pape K, Baretton GB, Welsch T, Aust DE, Weitz J, Koo B-K, Stange DE. 2019b. Mouse Models of Human Gastric Cancer Subtypes with Stomach-Specific CreERT2-Mediated Pathway Alterations. *Gastroenterology*, 157(6):1599–1614 DOI: 10.1053/j.gastro.2019.09.026.

Seino T, Kawasaki S, Shimokawa M, Tamagawa H, Toshimitsu K, Fujii M, Ohta Y, Matano M, Nanki K, Kawasaki K, Takahashi S, Sugimoto S, Iwasaki E, Takagi J, Itoi T, Kitago M, Kitagawa Y, Kanai T, Sato T. 2018. Human Pancreatic Tumor Organoids Reveal Loss of Stem Cell Niche Factor Dependence during Disease Progression. *Cell Stem Cell*, 22(3):454-467.e6 DOI: <https://doi.org/10.1016/j.stem.2017.12.009>.

Shamir ER, Ewald AJ. 2014. Three-dimensional organotypic culture: experimental models of mammalian biology and disease. *Nat Rev Mol Cell Biol*, 15(10):647–64 DOI: [10.1038/nrm3873](https://doi.org/10.1038/nrm3873).

Stange DE, Koo BK, Huch M, Sibbel G, Basak O, Lyubimova A, Kujala P, Bartfeld S, Koster J, Geahlen JH, Peters PJ, Van Es JH, Van De Wetering M, Mills JC, Clevers H. 2013. Differentiated Trophoblast cells act as reserve stem cells to generate all lineages of the stomach epithelium. *Cell*, 155(2):357–368 DOI: [10.1016/j.cell.2013.09.008](https://doi.org/10.1016/j.cell.2013.09.008).

Tam PPL, Beddington RS. 1987. The formation of mesodermal tissues in the mouse embryo during gastrulation and early organogenesis. *Development*, 99(1):109–126 DOI: [10.1242/dev.00176](https://doi.org/10.1242/dev.00176).

Tan P, Yeoh KG. 2015. Genetics and Molecular Pathogenesis of Gastric Adenocarcinoma. *Gastroenterology*, 149(5):1153–1162 DOI: [10.1053/j.gastro.2015.05.059](https://doi.org/10.1053/j.gastro.2015.05.059).

The Cancer Genome Atlas Research Network. 2014. Comprehensive molecular characterization of gastric adenocarcinoma. *Nature*, 513(7517):202–209 DOI: [10.1038/nature13480](https://doi.org/10.1038/nature13480).

Thiem S, Eissmann MF, Elzer J, Jonas A, Putoczki TL, Poh A, Nguyen P, Preaudet A, Flanagan D, Vincan E, Waring P, Buchert M, Jarnicki A, Ernst M. 2016. Stomach-specific activation of oncogenic KRAS and STAT3-dependent inflammation cooperatively promote gastric tumorigenesis in a preclinical model. *Cancer Research*, 76(8):2277-2287 DOI: [10.1158/0008-5472.CAN-15-3089](https://doi.org/10.1158/0008-5472.CAN-15-3089).

Tikoo A, Roh V, Montgomery KG, Ivetic I, Waring P, Pelzer R, Hare L, Shackleton M, Humbert P, Phillips WA. 2012. Physiological Levels of Pik3ca H1047R Mutation in the Mouse Mammary Gland Results in Ductal Hyperplasia and Formation of ER a -Positive Tumors. *J Biol Chem*, 287(5):1–13 DOI: [10.1371/journal.pone.0036924](https://doi.org/10.1371/journal.pone.0036924).

Tiriac H, Belleau P, Engle DD, Plenker D, Deschênes A, Somerville T, Froeling FEM, Burkhart RA, Denroche RE, Jang G-H, Miyabayashi K, Young CM, Patel H, Ma M, LaComb JF, Palmaira RLD, Javed AA, Huynh JA, Johnson M, Arora K, Robine N, Shah M, Sanghvi R, Goetz AB,

Lowder CY, Martello L, Driehuis E, Lecomte N, Askan G, Iacobuzio-Donahue CA, Clevers H, Wood LD, Hruban RH, Thompson ED, Aguirre AJ, Wolpin BM, Sasson A, Kim J, Wu M, Bucobo JC, Allen PJ, Sejpal D V, Nealon W, Sullivan JD, Winter JM, Gimotty PA, Grem JL, DiMaio DJ, Buscaglia JM, Grandgenett PM, Brody JR, Hollingsworth MA, Kane GM, Notta F, Kim EJ, Crawford JM, Devoe CE, Ocean A, Wolfgang CL, Yu KH, Li E, Vakoc CR, Hubert B, Fischer SE, Wilson JM, Moffitt RA, Knox JJ, Krasnitz A, Gallinger S, Tuveson DA. 2018. Organoid profiling identifies common responders to chemotherapy in pancreatic cancer. *Cancer Discov*, 8(9):1112–1129 DOI: 10.1158/2159-8290.CD-18-0349.

Turco MY, Gardner L, Hughes J, Cindrova-Davies T, Gomez MJ, Farrell L, Hollinshead M, Marsh SGE, Brosens JJ, Critchley HO, Simons BD, Hemberger M, Koo B-K, Moffett A, Burton GJ. 2017. Long-term, hormone-responsive organoid cultures of human endometrium in a chemically defined medium. *Nat Cell Biol*, 19(5):568–577 DOI: 10.1038/ncb3516.

Turco MY, Gardner L, Kay RG, Hamilton RS, Prater M, Hollinshead MS, McWhinnie A, Esposito L, Fernando R, Skelton H, Reimann F, Gribble FM, Sharkey A, Marsh SGE, O’Rahilly S, Hemberger M, Burton GJ, Moffett A. 2018. Trophoblast organoids as a model for maternal–fetal interactions during human placentation. *Nature*, 564(7735):263–267 DOI: 10.1038/s41586-018-0753-3.

Uemura N, Okamoto S, Yamamoto S, Matsumura N, Yamaguchi S, Yamakido M, Taniyama K, Sasaki N, Schlemper RJ. 2001. Helicobacter pylori Infection and the Development of Gastric Cancer. *N Engl J Med*, 345(11):784–789 DOI: 10.1056/NEJMoa001999.

Union for International Cancer Control. 1982. TNM-Atlas: Illustrated Guide to the Classification of Malignant Tumours. 1st ed. Spiessl B, Scheibe O, Wagner G (eds) Springer Berlin Heidelberg GmbH.

Union for International Cancer Control. 2017. TNM Classification of Malignant Tumours. 8th ed. Brierley JD, Gospodarowicz MK, Wittekind C (eds) WILEY Blackwell, Weinheim.

Vidal et al. 2009. High preoperative serum vascular endothelial growth factor levels predict poor clinical outcome after curative resection of gastric cancer. *BJS*, 96(12):1443–1451 DOI: 10.1002/bjs.6780.

Vlachogiannis G, Hedayat S, Vatsiou A, Jamin Y, Fernández-mateos J, Khan K, Lampis A, Eason K, Huntingford I, Burke R, Rata M, Koh D, Tunariu N, Collins D, Hulkki-wilson S, Ragulan C, Spiteri I, Moorcraft SY, Chau I, Rao S, Watkins D, Fotiadis N, Bali M, Darvish-damavandi M, Lote H, Eltahir Z, Smyth EC, Begum R, Clarke PA, Hahne JC, Dowsett M, Bono J De, Workman P, Sadanandam A, Fassan M, Sansom OJ, Eccles S, Starling N, Braconi C,

Sottoriva A, Robinson SP, Cunningham D, Valeri N. 2018. Patient-derived organoids model treatment response of metastatic gastrointestinal cancers. , 926(February):920–926 DOI: 10.1126/science.aao2774.

Weinreich J, Archid R, Bajaeifer K, Hack A, Königsrainer A, Schott TC. 2014. Growth and Chemosensitivity of Gastric Adenocarcinoma and Non-Malignant Cell Lines in Response to Novel Anti-Cancer Drug Combinations. *Chemotherapy*, 60(5–6):346–352 DOI: 10.1159/000438943.

Werner K, Weitz J, Stange DE. 2016. Organoids as Model Systems for Gastrointestinal Diseases: Tissue Engineering Meets Genetic Engineering. *Curr Pathobiol Rep*, 4(1):1–9 DOI: 10.1007/s40139-016-0100-z.

Van De Wetering M, Francies HE, Francis JM, Bounova G, Iorio F, Pronk A, Van Houdt W, Van Gorp J, Taylor-Weiner A, Kester L, McLaren-Douglas A, Blokker J, Jaksani S, Bartfeld S, Volckman R, Van Sluis P, Li VSW, Seepo S, Sekhar Pedamallu C, Cibulskis K, Carter SL, McKenna A, Lawrence MS, Lichtenstein L, Stewart C, Koster J, Versteeg R, Van Oudenaarden A, Saez-Rodriguez J, Vries RGJ, Getz G, Wessels L, Stratton MR, McDermott U, Meyerson M, Garnett MJ, Clevers H. 2015. Prospective derivation of a living organoid biobank of colorectal cancer patients. *Cell*, 161(4):933–945 DOI: 10.1016/j.cell.2015.03.053.

Willet SG, Mills JC. 2016. Stomach Organ and Cell Lineage Differentiation: From Embryogenesis to Adult Homeostasis. *Cmgh*, 2(5):546–559 DOI: 10.1016/j.jcmgh.2016.05.006.

Wroblewski LE, Piazuolo MB, Chaturvedi R, Schumacher M, Aihara E, Feng R, Noto JM, Delgado A, Israel DA, Zavros Y, Montrose MH, Shroyer N, Correa P, Wilson KT, Peek RM. 2015. *Helicobacter pylori* targets cancer-associated apical-junctional constituents in gastroids and gastric epithelial cells. *Gut*, 64(5):720–30 DOI: 10.1136/gutjnl-2014-307650.

Xiao Y, Cuiling L, Pedro-Luis H, Chu-Xia D. 2002. Generation of Smad4/Dpc4 conditional knockout mice. *Genesis*, 32(2):80–81 DOI: 10.1002/gene.10029.

Xin L, Lukacs RU, Lawson DA, Cheng D, Witte ON. 2007. Self-Renewal and Multilineage Differentiation In Vitro from Murine Prostate Stem Cells. *Stem Cells*, 25(11):2760–2769 DOI: 10.1634/stemcells.2007-0355.

Xu ZY, Tang JN, Xie HX, Du YA, Huang L, Yu PF, Cheng XD. 2015. 5-Fluorouracil Chemotherapy of Gastric Cancer Generates Residual Cells With Properties of Cancer Stem Cells. *Int J Biol Sci*, 11(3):284–294 DOI: 10.7150/ijbs.10248.

Yan HHN, Siu HC, Law S, Ho SL, Yue SSK, Tsui WY, Chan D, Chan AS, Ma S, Lam KO, Bartfeld S, Man AHY, Lee BCH, Chan ASY, Wong JWH, Cheng PSW, Chan AKW, Zhang J, Shi J, Fan X, Kwong DLW, Mak TW, Yuen ST, Clevers H, Leung SY. 2018. A Comprehensive Human Gastric Cancer Organoid Biobank Captures Tumor Subtype Heterogeneity and Enables Therapeutic Screening. *Cell Stem Cell*, 23(6):882–897 DOI: 10.1016/j.stem.2018.09.016.

Ychou M, Boige V, Pignon JP, Conroy T, Bouch?? O, Lebreton G, Ducourtieux M, Bedenne L, Fabre JM, Saint-Aubert B, Gen??ve J, Lasser P, Rougier P. 2011. Perioperative chemotherapy compared with surgery alone for resectable gastroesophageal adenocarcinoma: An FNCLCC and FFCD multicenter phase III trial. *J Clin Oncol*, 29(13):1715–1721 DOI: 10.1200/JCO.2010.33.0597.

Yuan T-M, Liang R-Y, Chueh PJ, Chuang S-M. 2015. Role of ribophorin II in the response to anticancer drugs in gastric cancer cell lines. *Oncol Lett*, 9(4):1861–1868 DOI: 10.3892/ol.2015.2900.

Zhang J, Zhang ZB, Gao H, Zhang D, Wang WL. 2009. Down-Regulation of SHH/BMP4 Signalling in Human Anorectal Malformations. *J Int Med Res*, 37(6):1842–1850 DOI: 10.1177/147323000903700620.

Zhao G-F, Zhao S, Liu J-J, Wu J-C, He H-Y, Ding X-Q, Yu X-W, Huang K-Q, Li Z-J, Zheng H-C. 2017. Cytokeratin 19 promoter directs the expression of Cre recombinase in various epithelia of transgenic mice. *Oncotarget*, 8(11):18303–18311 DOI: 10.18632/oncotarget.15435.

Zhao Z, Hou N, Sun Y, Teng Y, Yang X. 2010. Atp4b promoter directs the expression of Cre recombinase in gastric parietal cells of transgenic mice. *J Genet Genomics*, 37(9):647–652 DOI: 10.1016/S1673-8527(09)60083-7.

Zhao Z, Sun Y, Hou N, Teng Y, Wang Y, Yang X. 2009. Capn8 promoter directs the expression of Cre recombinase in gastric pit cells of transgenic mice. *Genesis*, 47(10):674–679 DOI: 10.1002/dvg.20552.

Appendix

Appendix Table 1: Clinical data of patient derived organoids (Seidlitz et al., 2019a).

Patient ID	Sex	Age at diagnosis	Diagnosis	TNM classification (UICC stage)	Organoid tissue of origin	Histology (Lauren classification)	Neoadjuvant chemotherapy	Tumor regression (Becker et al., 2011)
DD107*	Male	49	<i>Stomach corpus carcinoma</i>	<i>pT3, pN2, pM0 (IIIa)</i>	<i>Stomach corpus</i>	<i>intestinal</i>	<i>ECF</i>	<i>3</i>
DD109*	Male	56	<i>Adenocarcinoma of esophagogastric junction (AEGI)</i>	<i>pT2, pN1, pM1 (IV)</i>	<i>Lung metastasis</i>	<i>diffuse</i>	-	-
DD143	Female	61	<i>Adenocarcinoma of esophagogastric junction (AEGII)</i>	pT3, pN1, pM0 (IIb)	Esophago-gastric junction	intestinal	FLOT	3
DD155	Male	56	<i>Adenocarcinoma of esophagogastric junction (AEGI)</i>	pT2, pN1, pM1 (IV)	Esophago-gastric junction	diffuse	-	-
DD156	Female	80	Stomach corpus carcinoma	pT3, pN0, pM0 (IIa)	Stomach corpus	mixed-type	-	-

DD191*	Female	66	Adenocarcinoma of esophagogastric junction (AEGII)	pT3, pN1, pM0 (IIb)	Esophago-gastric junction	intestinal	FLOT	3
DD194	Female	46	Stomach corpus carcinoma	pT4a, pN3, pM1 (IV)	Stomach corpus	diffuse	FLOT	ns
DD209	Female	60	Adenocarcinoma of esophagogastric junction (AEGII)	pT3, pN1, pM0 (IIb)	Esophago-gastric junction	diffuse	FLOT	3
DD211	Male	66	Stomach antrum carcinoma	pT3, pN1, pM0 (IIb)	Stomach antrum	intestinal	ECF	3
DD218	Female	50	Adenocarcinoma of esophagogastric junction (AEGII)	pT3, pN3, M0 (IIIb)	Esophago-gastric junction	intestinal	-	-
DD241	Male	78	Adenocarcinoma of esophagogastric junction (AEGI)	pT3, pN0, pM0 (IIa)	Esophago-gastric junction	mixed-type	ECF	1
DD256	Male	88	Adenocarcinoma of esophagogastric junction (AEGII)	pT3, pN1, pM0 (IIa)	Esophago-gastric junction	intestinal	-	-
DD257	Female	80	Stomach carcinoma	pT3, pN1, pM0 (IIb)	Stomach	mixed-type	-	-
DD260	Male	64	Stomach carcinoma	pT3, pN1, pM1 (IV)	Stomach	diffuse	Cisplatin/Capeci tabine	2

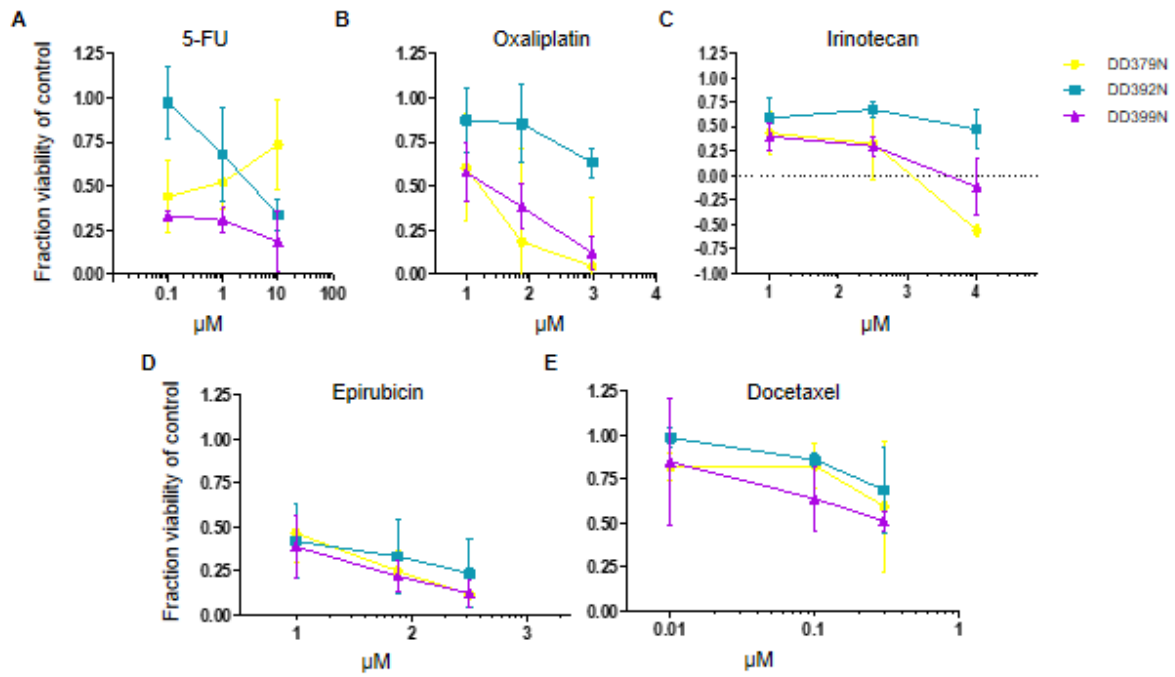
DD261	Male	60	Stomach antrum carcinoma	pT3, pN3, pM1 (IV)	Stomach antrum	diffuse	FLOT	2
DD265	Male	78	Adenocarcinoma of esophagogastric junction (AEGII)	pT3, pN2, pM0 (IIIa)	Esophago-gastric junction	diffuse	-	-
DD271	Male	81	Adenocarcinoma of esophagogastric junction (AEGIII)	pT3, pN1, pM1 (IIb)	Esophago-gastric junction	intestinal	-	-
DD282*	Female	81	Stomach antrum carcinoma	pT3, pN0, pM0 (IIa)	Stomach antrum	intestinal	-	-
DD316	Female	58	Adenocarcinoma of esophagogastric junction (AEGIII)	pT4b, pN1, pM0 (IIb)	Esophago-gastric junction	intestinal	yes, ns	3
DD323	Female	78	Adenocarcinoma of esophagogastric junction (AEGIII)	pT4a, pN1, pM0 (IIIa)	Esophago-gastric junction	diffuse	-	-

ECF: Epirubicin/ Cisplatin/ Fluoruracil

FLOT: Fluoruracil/ Leucovorin/ Oxaliplatin/ Docetaxel

ns: not specified

* further analyzed



Appendix Figure 1: Gastric normal organoids show divergent response to conventional chemotherapy. (A-E) Cell viability assay after 5-FU, oxaliplatin, irinotecan, epirubicin and docetaxel. Analysis for oxaliplatin, irinotecan, epirubicin and docetaxel was performed after 24 h incubation time whereas 5-FU was incubated for 72 h. Values were normalized to untreated control organoids of the same patient (n=3) (Seidlitz et al., 2019a).

Anlage 1: Erklärung zur Eröffnung des Promotionsverfahrens [Formblatt 1.2.1]

Anlage 2: Erklärung zur Einhaltung rechtlicher Vorschriften [Formblatt 1.1]